Forschungszentrum Karlsruhe
in der Helmholtz-Gemeinschaft

Wissenschaftliche Berichte
FZKA 6945
SAM-ECOSTAR-D45

Melt Cooling by Bottom Flooding:The Experiments CometPC-H4 and -H5

CONTRACT FIKS – CT1999 - 00003

EX-VESSEL CORE MELT STABILIZATION RESEARCH

**H. Alsmeyer, T. Cron, G. Merkel,
S. Schmidt-Stiefel, W. Tromm, T. Wenz**

**Institut für Kern- und Energietechnik
Programm Nukleare Sicherheitsforschung**

März 2004

Forschungszentrum Karlsruhe

in der Helmholtz-Gemeinschaft

Wissenschaftliche Berichte

FZKA 6945
SAM-ECOSTAR-D45

Melt Cooling by Bottom Flooding: The Experiments CometPC-H4 and -H5

CONTRACT FIKS-CT1999-00003

EX-VESSEL CORE MELT STABILIZATION RESEARCH

H. Alsmeyer, T. Cron, G. Merkel, S. Schmidt-Stiefel, W. Tromm, T. Wenz

Institut für Kern- und Energietechnik
Programm Nukleare Sicherheitsforschung

Forschungszentrum Karlsruhe GmbH, Karlsruhe
2004

Acknowledgment

This work was partly funded by the European Commission in the Fifth Framework Programme under the ECOSTAR Contract FIKS-CT1999-00003.

Impressum der Print-Ausgabe:

Als Manuskript gedruckt

Forschungszentrum Karlsruhe GmbH
Postfach 3640, 76021 Karlsruhe

Mitglied der Hermann von Helmholtz-Gemeinschaft
Deutscher Forschungszentren (HGF)

ISSN 0947-8620

Abstract

The large-scale experiments CometPC-H4 and -H5 investigate cooling of simulated corium melts by flooding the melt from the bottom through layers of porous, water filled concrete. Both experiments use 800 kg of oxidic and metallic melts, initial temperature from 1800 to 1900°C, with simulation of nuclear decay heat by inductive heating with 300 KW typical. The experiments are performed in a cylindrical geometry to allow flooding from the bottom or/and from the sidewalls after erosion of the layers of sacrificial concrete, which cover the porous concrete.

In the experiment CometPC-H4, lateral erosion was faster than expected with the consequence that passive flooding started from the sidewalls. Sideward erosion was safely stopped by the lateral water inflow, but the surface of the melt was flooded and a permanent surface crust formed before onset of flooding from the bottom. This resulted in a typical top flooding situation, in that the surface crust prevented efficient melt fragmentation. Therefore, upward heat removal was not sufficient and downward erosion of the bottom concrete continued. After further erosion of the sacrificial concrete layer at the bottom, the melt contacted the porous, water filled concrete layer. Passive injection of coolant water into the bottom of the melt increased the steam pressure and broke up the surface crust, through which part of the residual liquid melt was ejected into the overlaying coolant water. Although coolability was improved, parts of the melt locally continued downward erosion, which finally interrupted the internal heating of the melt after 3000 s.

With this experience, the subsequent experiment CometPC-H5 was designed with adequate thickness of the sacrificial concrete layers to start melt flooding from the bottom. The experiment showed the typical bottom-flooding situation with fast melt cooling and formation of a porous melt structure. However, during the further course of the test, some residual liquid melt fraction impeded the water inflow. Subsequent increase of the water pressure by the operator broke up the blockage and generated a coolable situation. Successful cooling was then demonstrated until 1 hour, when heating of the melt was terminated.

With the background of all relevant CometPC tests it is concluded, that this cooling concept has a high potential and that the water filled porous concrete layer is a reliable barrier. However, porosity of the melt during flooding and solidification should be improved by conceptual modifications, which inject the coolant water more homogeneously.

Kühlung der Schmelze durch Flutung von unten: die Experimente CometPC-H4 und -H5

Zusammenfassung

Die großskaligen Experimente CometPC-H4 und -H5 untersuchen die Kühlbarkeit simulierter Kernschmelzen durch Flutung von unten, die durch Wasserzutritt aus einer porösen, wasserführenden Betonschicht erfolgt. Beide Experimente verwenden 800 kg Metall- plus Oxid-Schmelze mit Anfangstemperaturen von 1800 bis 1900°C und simulieren die nukleare Nachwärme durch induktive Beheizung mit typisch 300 KW. Die Experimente wurden in zylindrischer Geometrie ausgeführt und erlauben damit die Flutung der Schmelze von unten und von der Seite, nachdem die Schichten von Opferbeton erodierte wurden, die den porösen Beton zunächst abdecken.

Im Experiment CometPC-H4 war die seitliche Erosion schneller als erwartet, wodurch die passive Flutung von der Seite her einsetzte. Das seitliche Eindringen der Schmelze wurde dadurch sicher gestoppt. Es wurde jedoch die Oberfläche der Schmelze überflutet, und es bildete sich eine stabile Oberflächenkruste aus, bevor die Flutung der Schmelze von unten einsetzte. Dies erzeugte die typische Situation der „Flutung von oben“, bei der die Oberflächenkruste eine wirksame Fragmentierung der Schmelze verhindert. Daher war die Wärmeabfuhr nach oben nicht ausreichend, und die Erosion des Betons am Boden ging weiter. Nach weiterer Erosion der Beton-Opferschicht erreichte die Schmelze die wasserführende, poröse Betonschicht. Der passive Zutritt des Kühlwassers in die Unterseite der Schmelze erhöhte den Druck durch Verdampfung, wodurch die Kruste an der Oberfläche aufgebrochen und ein Teil der noch flüssigen Schmelze in die obenliegende Wasserschicht ausgetragen wurde. Obwohl dadurch die Kühlbarkeit verbessert wurde, drangen lokal noch flüssige Teile der Schmelze weiter nach unten vor und führten schließlich nach 3000 s zur Unterbrechung der Beheizung der Schmelze.

Aufbauend auf dieser Erfahrung wurde das nachfolgende Experiment CometPC-H5 durch Wahl der Dicke der Beton-Opferschichten so ausgelegt, dass die Flutung von unten her beginnt. Das Experiment zeigt entsprechend die typischen Vorgänge der „Flutung von unten“ mit schneller Abkühlung der Schmelze und Ausbildung einer porösen Struktur. Jedoch wurde während des weiteren Verlaufs die Wasserzufuhr durch Verlagerung eines noch flüssigen Schmelzebereichs behindert. Die Erhöhung des Wasserdrucks durch den Operator beseitigte die Blockade und erzeugte eine kühlbare Konfiguration. Die erfolgreiche Kühlung wurde bis zum Abschalten der Beheizung nach einer Stunde nachgewiesen.

Auf der Basis aller relevanten CometPC-Experimente wird geschlossen, dass dieses Kühlkonzept ein hohes Potential hat und dass der wasserführende, poröse Beton eine zuverlässige Barriere darstellt. Es sollte jedoch die Porosität der Schmelze während der Flutung und Erstarrung verbessert werden durch Änderungen am Konzept, die einen gleichmäßigeren Wasserzutritt ermöglichen.

TABLE OF CONTENTS

LIST OF TABLES

LIST OF FIGURES

1 Introduction

1.1 Background

Ex-vessel melt cooling is one of the demanding challenges which is essential to stabilize and terminate a core melt accident if the melt should penetrate the reactor pressure vessel. Resolving the coolability issue does not only require the removal of the sensible and the latent heat of the corium, but also of the fission product decay heat, which is a long lasting source of internal heat generation. Different options of direct contact of melt and coolant water are considered in various research institutions to resolve the coolability issue. Such investigations are also part of the ECOSTAR programme.

The COMET core cooling concept for ex-vessel melt cooling is based on bottom flooding: After erosion of a sacrificial concrete layer, the melt is passively flooded from the bottom by passive injection of coolant water. The water is forced up through the melt, the resulting evaporation process of the coolant water breaks up the melt and creates a porous, permeable structure of the melt from which the heat is easily extracted. Therefore, the porous melt solidifies within less than one hour typical and is permanently flooded by water.

The actual variant of the COMET cooling concept under investigation uses a layer of porous, water filled concrete from which the water is injected to the bottom of the melt after erosion of the sacrificial concrete layer atop. This variant, called CometPC concept (= Comet Porous Concrete), is presently investigated in large-scale experiments with respect to its efficacy and robustness.

The present report describes the experiments CometPC-H4 and CometPC-H5. These experiments were performed, together with CometPC-H3 [1], as contribution to the international ECOSTAR Project, which is partly funded by the European Commission in the 5th Framework Programme.

1.2 Objectives

The experiments CometPC-H4 and -H5 are designed as large-scale coolability tests with metal plus oxide melts that simulate the corium melt. The high initial temperature of the melt together with the simulation of the nuclear decay heat throughout the test allows an adequate representation of the corium melt. Sustained simulation of the decay heat during the main phases of the experiments is necessary to allow the study of short and long-term heat transfer processes from the melt and to investigate reliable arrest of the melt. The main objectives are: Arrest of the melt, that is stop of the basement erosion, heat removal from the melt through efficient evaporation of the coolant water, fast solidification of the melt to exclude long term release of radioactive fission products, and exclusion of major thermochemical attack of important containment structures through the melt. Avoidance of major basement erosion during the long term release of nuclear decay heat is necessary to maintain containment integrity in a core melt accident.

The preceding experiment CometPC-H3 was performed as a 1-dimensional experiment, using sidewalls of inert ceramic. This represented, in a 1 to 1 scale with realistic heat flux densities and melt heights, a circular section of 92 cm diameter of the larger, horizontal cooling device that could be located under the pressure vessel, either in the reactor cavity or in a special spreading compartment. To complete the test series, two further experiments, which are described in this report, investigate the cooling process in a large cylindrical test device. In addition to the cooling process for the horizontal layered melt these tests are designed to study also the influence of the vertical sidewalls with respect to cooling and stability of the sidewalls. Therefore, the tests shall deliver the necessary information for the safe functioning and design of the vertical and horizontal boundaries of the cooling device. The height of the simulated corium melt, the simulated internal decay power density and consequently the heat flux densities are typical for the considered accident conditions.

The experiments study all sequences of melt cooling and stabilization, representing all important heat transfer and cooling processes, from onset of concrete erosion over start of flooding and cooling to final melt solidification and long term heat removal.

2 Test Facility

2.1 Experimental Concept

Figure 2-1 shows the principal concept of the cooling device, based on bottom water injection from the porous concrete layer. The coolant water is supplied from the side to the high porosity concrete layer, which guaranties homogeneous water distribution under the large cooling device. The low porosity concrete layer allows, by its specifically designed, higher flow resistance, the controlled coolant injection into the corium melt, after the melt has eroded the sacrificial concrete layer atop.

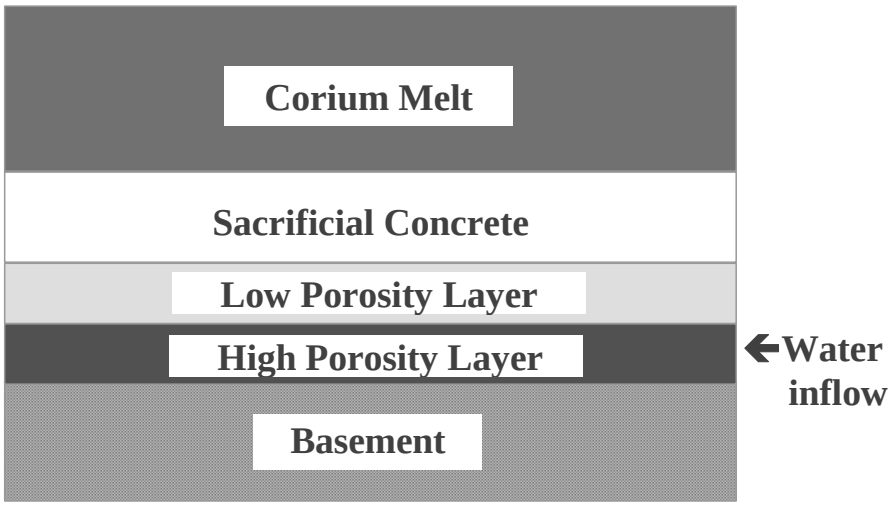

Figure 2-1 CometPC-Concept of melt cooling by water injection to the bottom of the melt

The basic experimental set-up realised in the two experiments CometPC-H4 and -H5 with cylindrical cooling geometry, is shown in Figure 2-2. The cooling device with the outer diameter of 1.1 m is placed at the bottom of the test rig on top of the induction coil which delivers the simulated decay heat by electrical heating. The inner part of the coolant device is made from sacrificial concrete, which is backed up to the bottom and the sidewalls by the intermediate layers of porous, water filled concrete. Water is supplied to the porous concrete layers from the side of the test rig. The cylindrical sidewalls above the coolant device are formed by MgO ceramic rings, which prevent attack of the upper test rig.

The simulated corium melt is generated externally by a thermite reaction with an initial temperature of about 1900°C and is poured onto the cooling device through a lid in the hood of the crucible. This defines the experimental time zero, when the first phase of dry erosion of the sacrificial concrete layer begins. This phase is followed by passive onset of flooding, melt fragmentation, cooling and finally complete solidification. During all these processes, heating takes place through the induction coil, which is located under the cooling device.

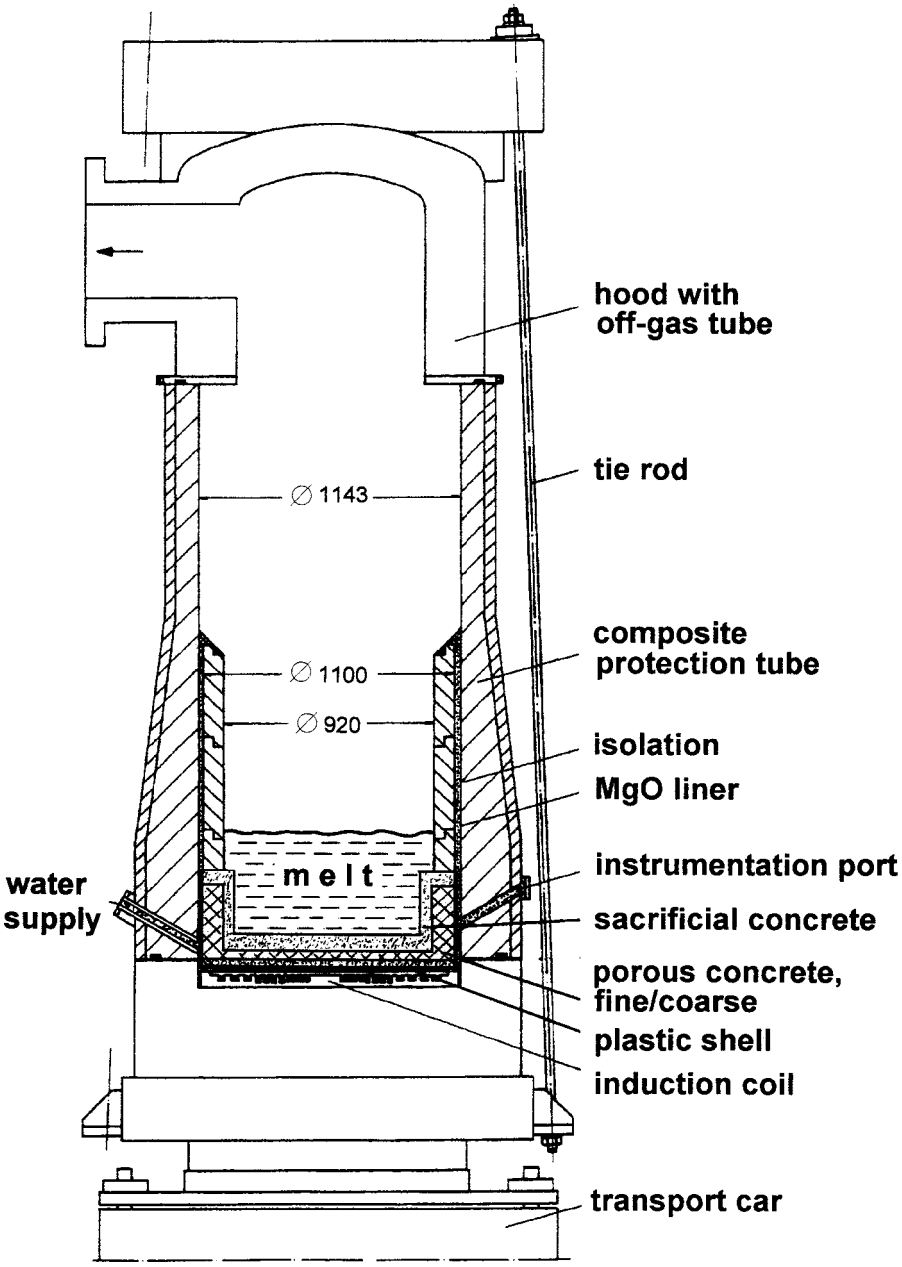

Figure 2-2 Schematic of the CometPC cooling tests in cylindrical geometry

All gases, which are generated during these processes, are collected in the free volume of the crucible, which is inerted by a defined argon cover gas flow, and are fed through the off-gas tube to the open atmosphere. In this off-gas tube, the characteristics if the gas with respect to temperature, composition and flow rate are measured on-line. This includes also the steam that is produced during the flooding process and during long-term cooling.

The outer crucible is designed to withstand higher pressure pulses if they should occur. The test assembly is located on a transport car to allow installation and disassembly of the test rig. Figure 2-3 shows the test apparatus as part of the general installation.

The next paragraphs describe important details of the test facility.

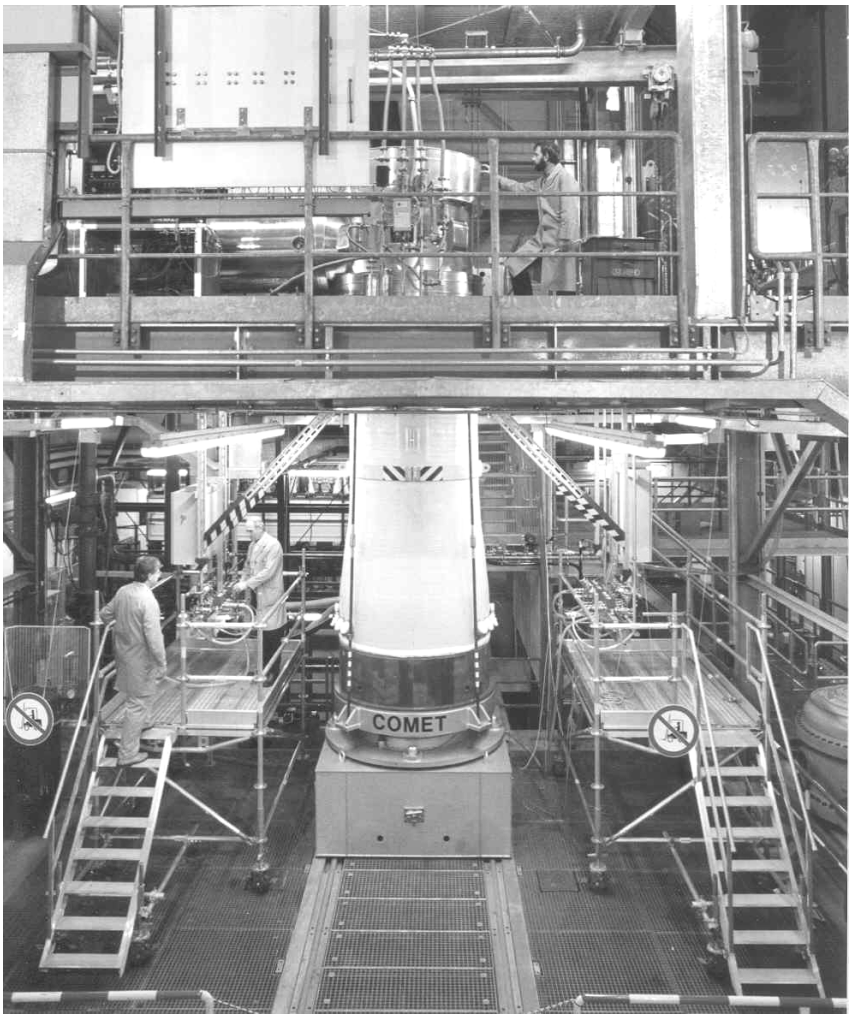

Figure 2-3 View of the COMET Facility

2.2 Melt and Melt Generation

The simulated corium melt is generated by a thermite reaction in the external thermite reaction vessel located above the test vessel. The basis for this reaction is the commercial thermite powder R70/SSH (Elektro -Thermit GmbH & Co KG, Essen, Germany), that produces liquid Al_2O_3 plus Fe by the strongly exothermic thermite reaction

$$Al + Fe_2O_3 \Rightarrow Al_2O_3 + 2\ Fe + h_{chem} \ ,$$

where h_{chem} is the chemical reaction enthalpy. To lower the freezing temperature and to increase the freezing range of the resulting oxide melt in accordance with the real corium melt, about 30 % of burned lime CaO is added to the thermite powder, which leads to the formation of a two component Al_2O_3 – CaO oxide melt mixture.

In addition, Ni pellets are mixed to the thermite powder, to produce a two component Fe/Ni – metal melt. The Ni fraction is necessary to influence the inductive coupling of the metal melt to the induction coil: For temperatures below the Curie temperature of 774°C, pure iron

would change from paramagnetic to ferromagnetic behaviour. Consequently, inductive heating, which simulates the decay heat, would concentrate in the colder portions of the ferromagnetic iron “melt”, leading to a strongly non-homogeneous simulation of decay heating. The addition of 15 % Ni to the Fe melt reduces the transition to ferromagnetism to 400°C, and thus allows further induction heating of the solidifying metal melt.

To compensate for the energy to heat the high masses of additional CaO and Ni, the thermite mixture is preheated to about 200°C by electrical heater rods in the thermite reaction vessel, before ignition of the thermite. The resulting temperature of the melt at pouring is 1900°C. The time between ignition and pour is 90 s. As thermite burn is completed after 25 s, the residual time is sufficient that the metal phase segregates completely to the bottom of the reaction vessel, covered by the pure oxide melt.

800 kg of melt are poured through a lid in the hood of the test vessel. This is about 400 kg metal melt, followed by some 400 kg oxide melt, controlled by an on-line weighing system. The residual oxide melt in experiment CometPC-H5 is discharged to a slag container.

The calculated densities of the melts are 6470 kg/m^3 for the metal phase and 2670 kg/m^3 for the oxide phase. Therefore, the oxide phase is on top of the metal phase, as expected in the reactor situation after dilution of the oxide melt by eroded concrete.

2.3 Crucible and Cooling Device

The test crucible, as shown in Figure 2-2 and further described in section 3 and 4, is equipped with the cooling device, the induction coil for decay heat simulation, water supply, and all necessary instrumentation. The crucible is gas tight, so that all gases, released during concrete erosion and during cooling of the melt, are collected in the upper free volume of the crucible and transferred through the hood and the off-gas tube to the open atmosphere. Before start of the melt pour, the atmospheric gases are replaced by argon cover gas to exclude any burn in the crucible or in the off-gas tube. Only during pour of the melt from 0 s to about 50 s, leakage of gases through the temporarily open lid does occur.

The following elements are essential for the crucible and cooling device:

- The support structure, which includes the water-cooled induction coil, is located on the transport car. As all other components, which are close to the induction coil, the structure is fabricated from non-metallic materials. The upper free surface of the induction coil is covered by a 6 mm silicone foil, which protects the coil against any water that could be released during the cooling process atop. The induction coil is connected to the electrical induction circuit and to a specific water-cooling system.
- To minimise inductive losses, the cooling device is directly positioned on the silicone foil above the induction coil. This concept relies on the efficacy of bottom flooding and cooling, as the minimum distance between hot melt and induction coil is about 15 cm only
- Cylindrical rings of MgO oxide, 920 mm inner diameter, 90 mm thick, are placed above the cooling device and form the upper radial confinement of the melt. As MgO is sufficiently stable, the melt can only attack the structures below. The gap between the

MgO rings and the protection tube is filled with dry quartz sand for thermal insulation.

- The composite protection tube is formed by an inner structure of refractory concrete, and an outer shell of gas tight, high temperature epoxy liner
- The upper hood is a steel structure with inner ceramic liner. It is connected to the off-gas tube.
- 4 tie rods tighten upper and lower parts of the crucible, and maintain its integrity if inner mechanical loads should act on the structures.
- 4 redundant water supply lines are connected to the coolant device to supply the coolant water for bottom flooding.
- 2 instrumentation ports are used for thermocouple and glass fibre instrumentation of the cooling device. The outer sections of the ports are filled with water to keep the outer instrumentation lines cold (avoid heat-up by the electro-magnetic stray field).

2.4 Water Supply

The coolant water for passive bottom flooding of the melt is supplied from a water tank, which is located about 2 m above the inner bottom surface of the cooling device. The effective overpressure of the coolant water is 0.1 bar, which is the specified overpressure for the actual test, and takes into account the hydrostatic pressure of the 35 cm respectively 50 cm high melt. The water level in the water tank is kept constant by level control and refill of fresh water from the building supply system. The temperature of the water is 20°C.

During the normal test sequence, no operator actions are taken to control or modify the coolant water flow. Thus, the coolant flow is a result of the initial water pressure and of the flow conditions, which develop during the test.

In case, however, of unexpected events or to replace or discharge the water from the crucible, the operator has several possibilities to modify the water flow. He can interrupt the bottom water flow and discharge the accumulated water into an external water tank. In addition, a spray system can be activated from the top of the crucible, which brings coolant water to the surface of the melt. These options are used after end of the experiments to remove water from the test vessel.

2.5 Off-Gas System

The off-gas system, which is connected to the crucible hood, consists of a horizontal connecting tube, 1 m long, with a ceramic liner of 40 cm inner diameter, a vessel to retain any melt which could be ejected from the test vessel, and an 11 m long horizontal steel tube of 50 cm inner diameter, exhausting the gas flow to the atmosphere outside of the building.

The large flow diameter of the off-gas system excludes pressure build-up in the test vessel even for high gas rates. The off-gas system is preheated to 110 °C before and during the experiment to exclude condensation of steam, thus allowing measurement of the vapour

flow. The end of the off-gas tube is nearly closed by a paper diaphragm, which allows argon inertisation before start of the test. The diaphragm is expelled by the first hot gases produced during pour of the melt. Off-gas analysis is performed by instrumentation located in the long off-gas tube.

At the end of the off-gas tube, a heater plug ignites the off-gas if the concentration of burnable gases is sufficient. A standing flame usually characterizes the first phase of dry concrete erosion.

2.6 Decay Heat Simulation

Decay heat is simulated in the melt by induction heating which couples to the metallic fraction of the melt. The horizontal induction coil, located under the cooling insert, forms the resonance circuit together with a set of 27 large high voltage capacitors, driven by a 1 kHz power supply.

The maximum inductor voltage is 2600 V, the maximum current 12000 A. The rated upper heating power for a non-magnetic (paramagnetic) melt is 400 kW.

The heating power deposited in the melt is determined online by the measured actual total power from which the losses by ohmic resistance and by the electromagnetic stray field are subtracted. These losses were determined in separate system tests, depending on voltage and currents of the induction circuit. In addition, a complete balance of all electric cooling circuits confirms the validity of this approach.

During the experiment, the inductive power is adjusted by control of the inductor voltage. This is performed manually by the operator, based on the displayed actual power history. The net heating power strongly varies with the coupling efficiency between induction coil and metal melt. There are mainly three reasons that influence the electromagnetic coupling:

(1) Agitation and the variation of void in the melt: For higher void, the efficiency of coupling is reduced. Strong high frequency power oscillations are characteristic for the early MCCI processes and during onset of bottom flooding. Solidification of the melt, in whatever structure, leads to more stable coupling.

(2) The reduced distance between melt and induction coil, which is a consequence of concrete erosion, improves the coupling.

(3) The electrical properties of the metal melt change with temperature. The most important property for the actual melt is the magnetic permeability, which for the Fe-Ni melt strongly increases below the Curie temperature, i. e. below 400°C. This will occur after solidification and further quenching of the “melt” or parts of the melt, resulting in a higher efficiency of heating.

For the present test, the induction coil is started 4 minutes before pour of the melt. The decay power will increase from about 150 kW at start of the test to 300 kW after onset of cooling, which is in accordance with the decay power density.

2.7 Instrumentation and Data Acquisition

The Comet facility is equipped with a multitude of instrumentation to monitor and control the experiment and to collect data for subsequent evaluation. Besides registration on chart recorders and printers, all data are stored and displayed on a PC data acquisition system.

More than 100 measurement signals are collected to characterise the following information:

1. Electrical induction heating: Gross power, net power, various voltages and currents, inductor frequency, control temperatures and coolant flows
2. Generation and pour of the thermite melt: Mass of melt in the thermite reaction vessel and during pour of the melt, temperature of melt during pour, signals to control the pour
3. CometPC cooling device: Temperature and erosion profile of the sacrificial concrete layer and of the porous concrete layers, temperature in the structures nearby, glass fibre instrumentation as ultimate safety signal in case of extreme melt penetration
4. Coolant flow to the cooling device: Water flow rate, water pressure (including possible pressure pulses), height of water level during flooding
5. Upper crucible hood: Temperatures and pressures in the gas room, control and rate of the argon cover gas flow
6. Off-gas system: Gas flow, temperature, and pressure; gas composition by on-line quadrupole mass spectrometry and aerosol density by transmission of laser beam
7. Control signals and conditions of the experimental hall

The temperature of the melt during the interaction and cooling phase cannot be measured because of the chemically aggressive melt. In previous experiments, the lifetime even of PtRh10-Pt (type S) thermocouples was not sufficient to detect a reliable temperature of the melt.

Several video systems are used to observe the experiment, including two video installations, which are directed from the crucible hood onto the surface of the melt. These systems are especially useful to observe all processes, which are related to melt fragmentation, flooding, and cooling.

The following sections 3 and 4 give the specific details of experiments CometPC-H4 and -H5, respectively.

3 Experiment CometPC-H4

3.1 Details of Cooling Device and Melt Generation

3.1.1 Cooling Device

Figure 3-1 gives the details of the cooling device as prepared for experiment CometPC-H4.

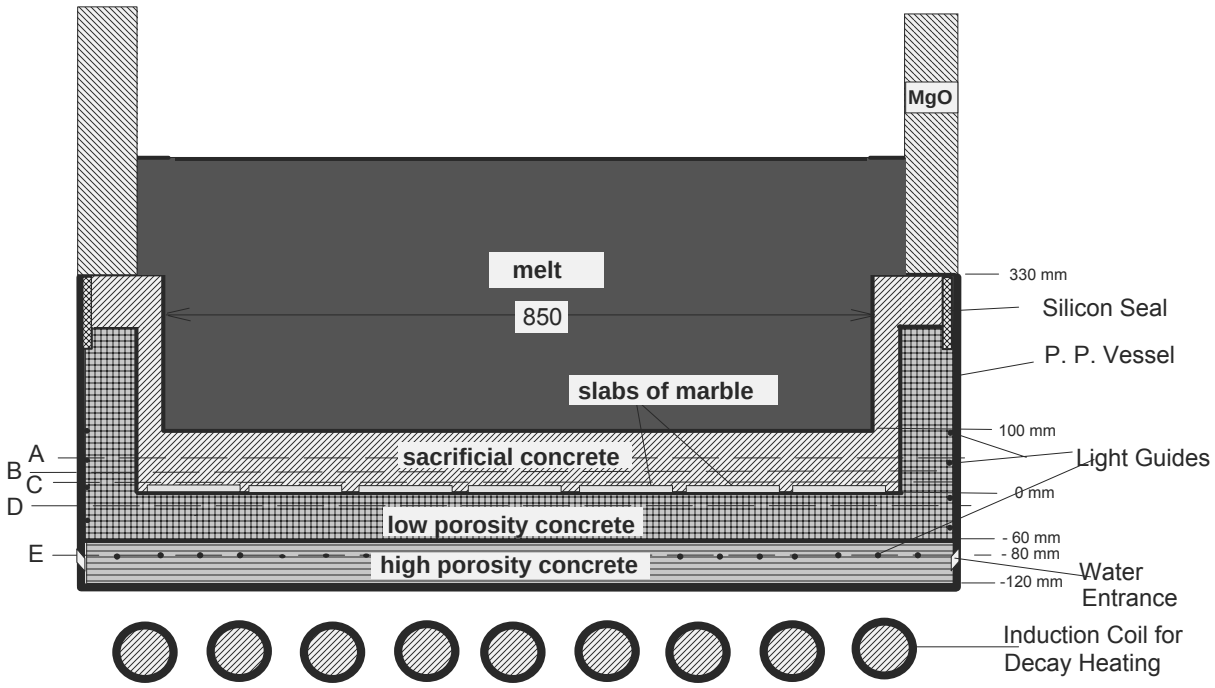

Figure 3-1 CometPC-H4: Details of the cooling device

To save space and to allow a wide cooling surface, the outer watertight shell of the device is formed by 15 mm thick polypropylene casing. This replaces the shell of structural concrete that was used in previous tests, but relies heavily on the efficacy of the cooling process in that no temperatures above 150°C are allowed for the polypropylene vessel, in spite of the small distance to the hot melt. The horizontal layer of high porosity concrete, located at the bottom of the polypropylene shell, is 60 mm thick, and receives water through 4 supply lines from the side. The low porosity concrete layer atop is 60 m thick in the central horizontal part and 70 mm thick in the vertical cylinder wall. Horizontal and vertical section of the fine porosity concrete liner are not separated with respect to the coolant water flow, i. e. all water is supplied through the high porosity layer. To improve water supply to the porous sidewalls, 12 vertical tubes are embedded in the porous concrete close to the polypropylene vessel wall transferring water from the bottom layer to the upper sidewalls.

The innermost sacrificial concrete layer is 100 mm thick at the bottom and 40 mm thick at the sidewalls. It is fabricated with aggregates of broken borosilicate glass with the following composition: SiO_2 62,5 %, B_2O_3 > 6 %, Al_2O_3 > 5 %, Na_2O 14,5 %, CaO 6 %, MgO 3,5 %, TiO_2 < 1 %, Fe_2O_3 < 1 %, K_2O >1 %, other impurities <0,5 %. This glass, when melted and

mixed to the simulated or real corium melt, reduces its viscosity and thus favours the spreading process. In addition, the boron as strong neutron absorber eliminates criticality problems.

Thin slabs of marble ($CaCO_3$) separate sacrificial concrete and the low porosity concrete and exclude blockage of the upper layer of low porosity concrete, when during preparation of the cooling device, the liquid sacrificial concrete layer is poured onto the device. When attacked by the hot melt, the marble slabs fail mechanically and give way to the coolant water flow.

Ceramic rings of MgO are placed on top of the coolant device to exclude attack of the outer protection tube. Figure 2-2 shows the cooling device installed in the test rig.

The initial diameter of the inner test volume is 850 mm. The height of the porous sidewalls is sufficient to contain all the metal melt, from which the main downward and sideward concrete erosion is expected. The height of the oxide melt extends over the cooling device into the area of ceramic rings.

Instrumentation in the cooling device consists of thermocouples embedded in the different concrete layers (partly indicated by the levels A – E), and of light guides in bottom and side walls which act as safety instrumentation.

The maximum coolant water flow in case of complete opening of the fine porous concrete surface was estimated to be 3 l/s.

3.1.2 Melt Generation

The following Table 3-1 shows the composition of the thermite powder and the resulting melt composition.

Table 3-1: Composition of the thermite powder and of the resulting melts in CometPC-H4

Constituent	kg
Initial composition:	
Thermite powder R 70/SSH	618.2
CaO	216.4
Ni	60.0
total	894.6
Generated melt (initial T 1800°C):	
Oxide: 56.2 % Al_2O_3 + 43.8 % CaO	494.6
Metal: 85.0 % Fe + 15.0 % Ni	400.0
total	894.6

The thermite mixture was preheated to 250°C over a period of 2 days to increase the initial temperature of the thermite melt. From the generated melt, the 400 kg metal melt plus 400 kg oxide melt are poured into the cooling device, the residual oxide melt is poured into a slag container. The resulting initial heights are 109 mm for the metal melt and 243 mm for the oxide melt, without void by the percolating gases. The corresponding total melt height is 353 mm.

No simulated fission products were added to the melt.

3.2 Test Procedure

The conduct of the experiment was planned as given in Table 3-2. The estimated time for start of flooding was based on prediction of downward melt propagation and is subject to uncertainties in the propagation process, such as local effects etc. Indeed it turned out, that substantial deviations in start of flooding, cooling and melt solidification occurred, predominantly because of onset of flooding from the sidewalls.

Table 3-2: Planned conduct of the CometPC-H4 experiment

Time, s	Event
until –240	Facility prepared, argon inertisation completed, induction coil operating, coolant water supply connected with 0.1 bar overpressure
-90	Ignition of thermite powder, allow separation of metal and oxide phases
0	Start of melt pour (duration ~ 40 s), onset of dry erosion of sacrificial concrete layer, continuous decay heating with about 150 kW
200	activate flow meters in off-gas tube after decrease of first intense gas release
about 600	Onset of passive flooding from bottom layer expected after erosion of sacrificial concrete layer; heating power increases by downward propagation of the melt to about 300 kW, operator controls decay power level to 300 kW until end of heated test. Observation of melt fragmentation, cooling, and solidification
about 2000	Complete melt solidification expected, further heating with 300 kW to observe stability of long-term cooling over further 1800 s
about 3800	End of heated test, decay power off
post test	Cool down and release of water from flooded and solidified melt, inspection and conservation of test vessel for further dismantling

The realized experimental conduct is provided in Table 3-3.

Table 3-3: Realized conduct of the CometPC-H4 experiment

Time, s	Event
until -90	Test preparation as planned, induction coil operating
-90	Ignition of thermite powder, thermite burn completed after 30 s, separation of metal and lighter oxide phases
0 →160	Pour of melt: 400 kg metal + 400 kg oxide melt with 1800°C, completed after 42 s. Onset of dry erosion of sacrificial concrete layer, initial downward erosion rate about 0.2 mm/s, averaged over bottom surface. Simulated decay heat about 100 kW. Hydrogen flame at end of off-gas line until onset of flooding at 166 s. Aerosol formation due to concrete erosion give diffuse view of the melt surface until onset of flooding
164 →166	Flowmeter shows start of passive coolant water injection
166 →260	Camera shows flooding from vertical sidewall in north, produces mild local ejection of oxide melt, but only little melt fragmentation. At 260 s, first crust on upper melt surface visible in North. Flow rate of coolant water 1.2. l/s
260→350	Crust growth proceeds. At 290 s, water flow from northern cylinder wall to melt surface visible. At 320 s melt surface completely covered by boiling water and mostly encrusted. Downward erosion continues and seems unaffected by the upper cooling process, reaches 50 mm at 400 s. Decay power in the melt is some 200 kW.
350→430	In the west of upper crust, 1 hole remains, which produces moderate volcanic eruptions of oxide melt under water until 430 s. Only mild interactions of melt and water occur.
430→1181	Further erosion of bottom sacrificial concrete layer without any melt ejection through the top surface crust, which is completely stable under layer of boiling water. Detected melt front at 1050 s is 20 mm above porous concrete layer at bottom of coolant device.
1181→1197	Melt contacts the water filled porous bottom layer. Strong steam production, vigorous volcanic ejection of some 30 % of the oxide melt through central hole in the top crust with fast quenching and porous solidification. Melt ejection ends as melt and crust separate. Pronounced spike of steam flow through off-gas tube with entrained water.
1230→1270	Again ejection of some melt, as seen by hot particles in the water. However, significantly less melt transfer than in the previous ejection.
1270→2955	Slow boiling from the melt surface, significantly below the decay power in the melt, which is maintained near 300 kW as planned. No further volcanic eruptions occur. Downward propagation of the melt into porous, water filled concrete layer continues, especially in north-west, as no major cooling processes are effective. Thermocouples in north-west show melt propagation to –50 mm into fine-porous concrete layer at 2900 s. Ongoing oscillations of the net induced power indicates, that parts of the melt are still liquid.

2995	Light guide, which is located at –80 mm in the porous concrete layer, interrupted by melt. Automatic safety signal switches-off the induction heating. Parts of the melt were not arrested in the porous layer.
2995→4000	Melt without simulated decay heat cooled and quenched by continuous water supply. Melt solidifies without further downward propagation. The plastic shell of the cooling device and the test facility remain intact.
post test	Accumulated coolant water drained out. Test vessel prepared for disassembly and further analysis.

The actual sequence of the CometPC-H4 cooling test substantially differs from the expected sequence. The main reason is the occurred change in the flooding and fragmentation process, which results in significantly less cooling efficiency and in ongoing downward propagation of parts of the not sufficiently cooled melt. This is briefly described below.

Melt generation and pour of the melt were as planned. Figure 3-2 shows the reaction period of the thermite (from –90 to –70 s) and the pour starting at time zero. Thermite burn was completed 20 s after the ignition (at -70 s, indicated by the end of oscillations of the weighing system), which is a short reaction time. The subsequent time of 70 s is sufficient to allow complete segregation of metal and oxide phases. Note that the thermite weight has a constant offset of about –70 kg.

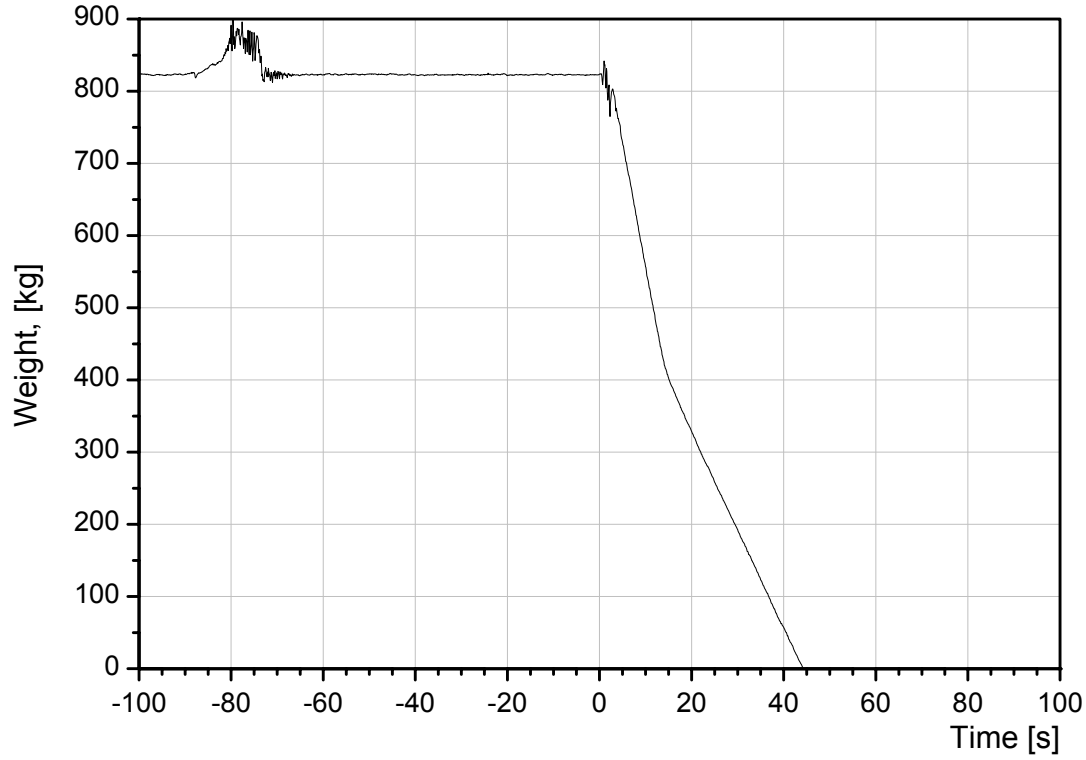

Figure 3-2 CometPC-H4: Weight of thermite vessel during thermite burn and melt release

Pour of 800 kg melt into the test vessel, starting at time zero (defines t = 0 s), is completed after 42 s. At that time, the remaining 95 kg oxide melt is transferred to the slag wagon. The clear change of the slop in Figure 3-2 indicates the transition from heavier metal to the lighter oxide flow. It corresponds to the 400 kg metal weight and shows that metal and oxide melts are fully separated. The crucible hood is closed upon completion of the pour after 60 s, so that all gases are directed through the off-gas line. However, a small leakage of gases may have taken place, because some scattered melt prevented complete closure of the lid.

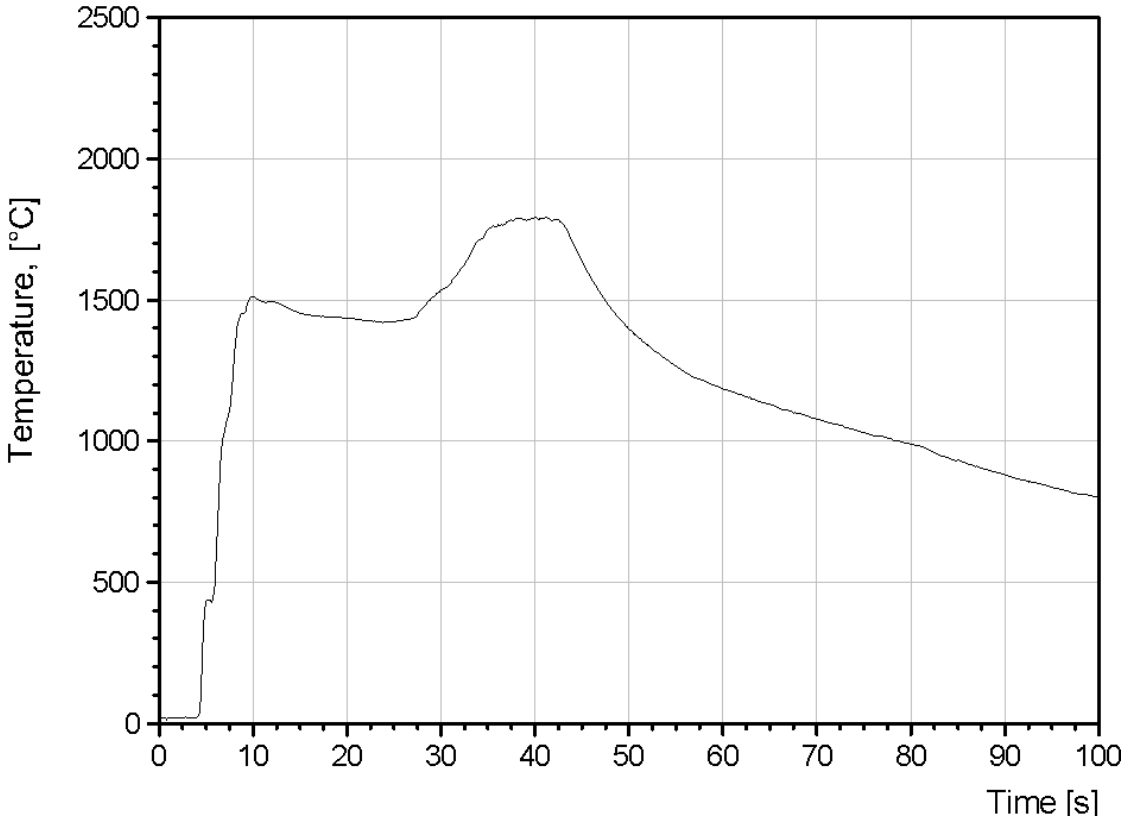

Figure 3-3 CometPC-H4: Initial temperature of melt measured in the spout

The initial temperature of the melt was measured in the spout, as given in Figure 3-3. The W/Re thermocouple detects the expected 1800°C level after some delay during release of the oxide melt at about 40 s. Some crust near the tip of the thermocouple may have prevented faster response.

As derived from visual observations and the different measurements, the erosion and cooling process is characterized by the following phases:

1. From 0 – 166 s: Dry erosion of the sacrificial concrete layer with release of steam (partly reduced to hydrogen) and aerosols from decomposing concrete. The initial downward erosion may have proceeded 30 to 40 mm (see Figure 3-17). Assuming the same sideward erosion process, the sacrificial concrete layer at the cylinder wall is melted away, so that coolant water flow from the side may start.
2. From 166 – 350 s: Water is passively injected to the melt from the side predominantly through the northern sidewall, with about 1 l/s. This has only local effect on melt fragmentation and cooling. Water flows to the surface of the melt and covers the melt surface, which forms a thin crust, while the bulk of the melt remains at high

temperatures. Downward propagation of the sacrificial concrete continues (still 60 mm sacrificial concrete remaining at the bottom), whereas sideward propagation is stopped by contact with the porous, water filled concrete surface.

3. From 350 – 430 s: Melt has formed a closed surface crust under the water layer, anchored to the sidewalls of the crucible. Only one central hole for gas release remaining, which develops as the vent of a volcano, through which oxide melt is transferred to the top water layer during a period of 40 s. The melt is driven by gas release from decomposing concrete. Melt ejection ends when melt and top crust near the vent separate, that is some void exists under the central crust. Downward melt propagation continues.
4. From 430 – 1181 s: The surface crust and boiling water atop are stable. Heat removal by steam release drops below simulated decay power level. Simulated decay power sufficient to further erode the remaining bottom sacrificial concrete layer. Probably no water penetrating downwards through the vent of the volcano.
5. From 1181 – 1197 s: After erosion of the bottom sacrificial concrete layer, melt contacts porous, water filled concrete layer at the bottom and bottom water injection starts. Fast evaporation in the enclosed melt expels part of the oxide melt through the vent of the volcano. Vigorous interaction, but no explosive events. Expulsion ends when about 30 % of the oxide melt are released.
6. From 1197 – 2995 s: Melt ejection did not significantly improve the coolability. Decay power removed by vapour flow drops again below decay level. Consequently, parts of the melt continue to erode the porous, water filled concrete layer. A fragmentation and sufficient stabilisation of the residual melt does not occur, although the water might enter now also from the bottom.
7. 2995 s: The melt contacts locally the safety instrumentation at –80 mm in the porous, water filled concrete layer. Sufficient melt coolability was not achieved.

The outer structure of the cooling device remained completely intact, as it was in sufficient contact with the coolant water.

The following sections discuss important experimental details of CometPC-H4, as available from different measurements.

3.3 Detailed Test Results

3.3.1 Simulated Decay Power

Figure 3-4 through 3-6 show the characteristics of induction heating from start of melt pour (time 0) until 4000 s for the net power, the voltage supplied to the induction coil, and the efficiency of heating, which is defined as the net power to the melt divided by the total electric power delivered to the induction system. Heating efficiency is equivalent to the inductive coupling of the melt to the electromagnetic field.

The voltage of the induction coil is under control of the operator, who adjusts the voltage to achieve the net power input to the melt (decay power) according to the test plan. The operator uses on-line information about the total power and the net power to the melt.

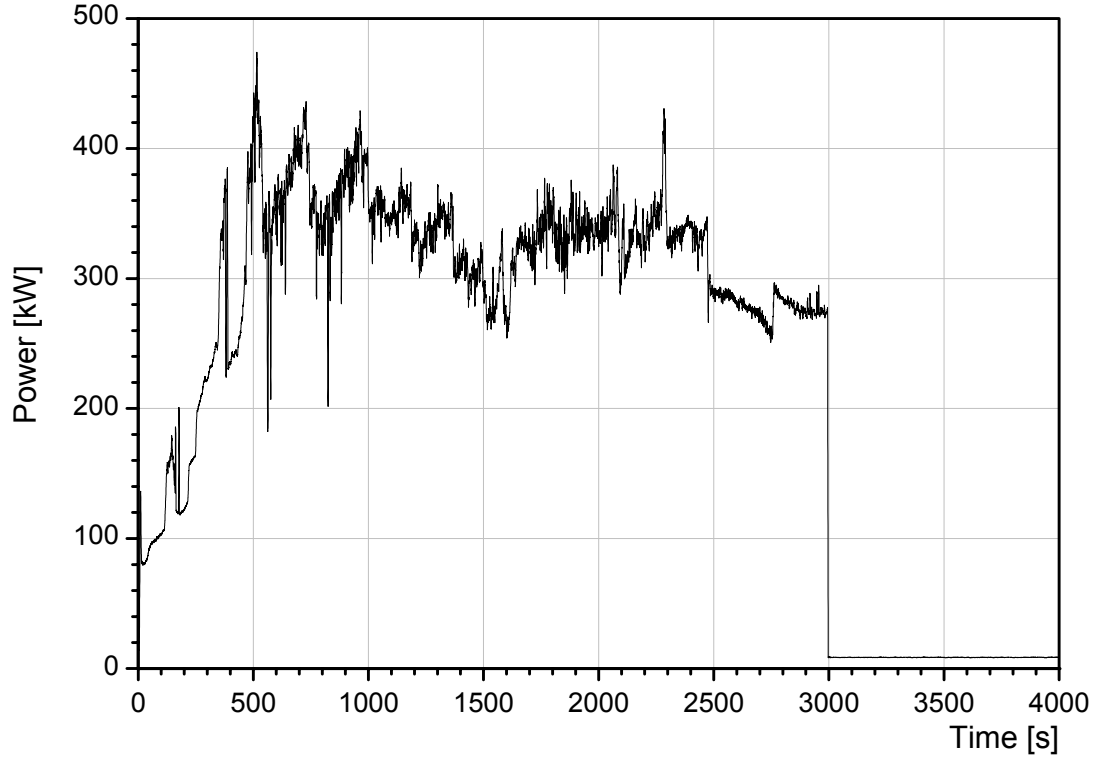

Figure 3-4 CometPC-H4:Simulated decay heat by induction heating of the melt (net power)

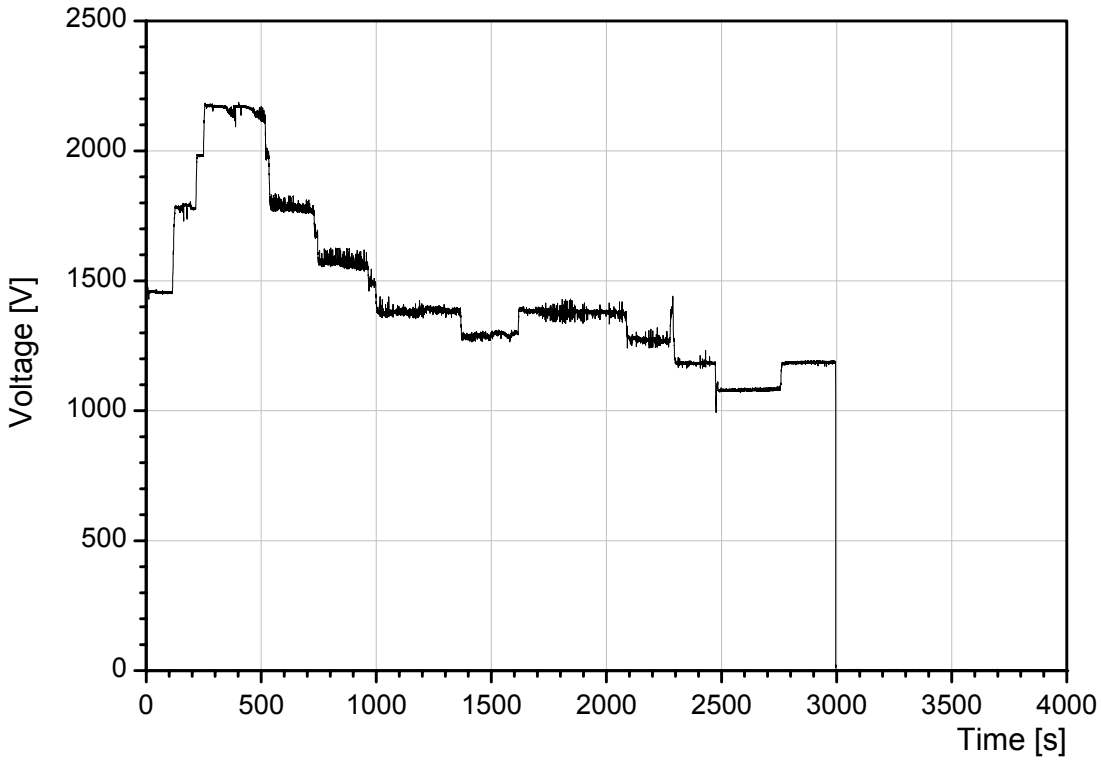

Figure 3-5 CometPC-H4: Voltage of induction coil

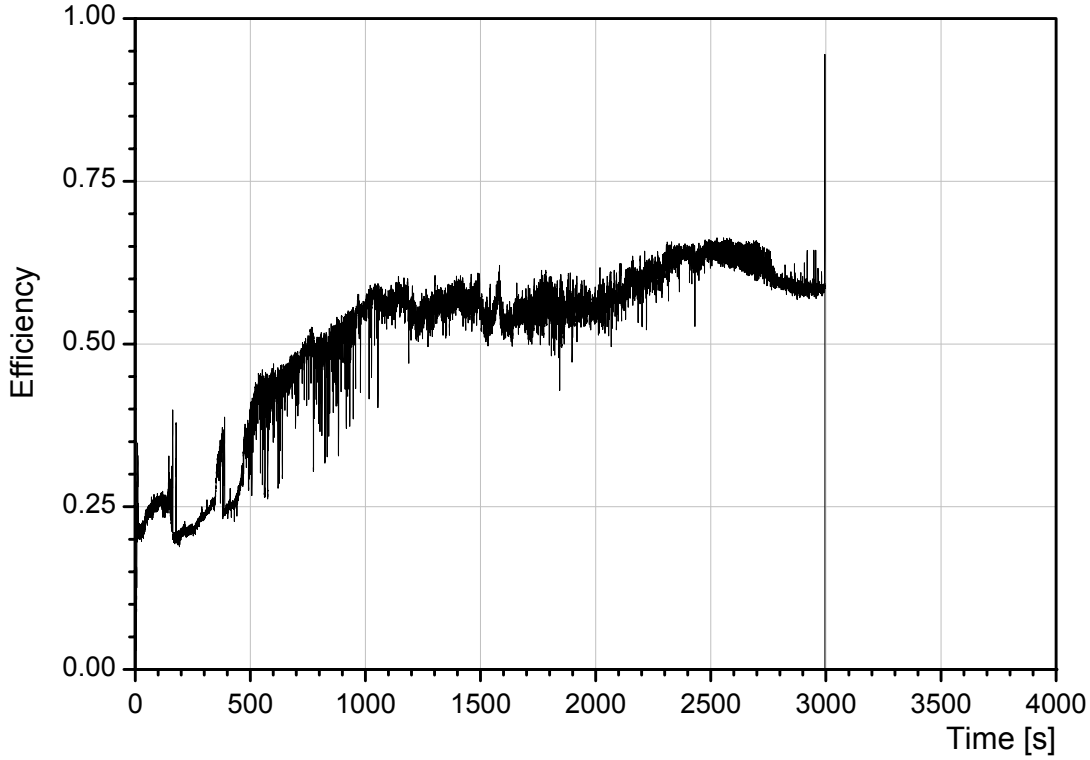

Figure 3-6 CometPC-H4: Efficiency of induction heating

At time zero, the induction coil is operated with a voltage 1.5 kV, which is expected to heat the melt with about 150 kW. The initial larger distance of the melt to the induction coil and the smaller diameter of the melt (as compared to the previous experiment CoemtPC-H3) results, however, in a lower heating efficiency and the operator increases within 200 s the inductor voltage in 3 steps to 2.2 kV, which brings the power to the 300 kW level. The strong oscillations which occur in power and heating efficiency until 500 s are characteristic for the agitated metal melt. No major influence on power input is seen by the sideward water inflow which starts at 166 s. From 500 until end of heating the power level is 300 to 400 kW. The heating efficiency increases mainly from 500 to 1050 s. This is due to the fact that the metal melt continuously erodes the sacrificial concrete layer at the bottom and thus comes closer to the induction coil. The operator therefore reduces the inductor voltage in several steps. The high frequency oscillations, which are visible in the power trace indicate that parts of the metal melt are still being agitated by gases. On the other side, the high heating efficiency of more than 55 % may indicate that parts of the metal have formed ferromagnetic crusts.

The strong volcanic eruption, which occurs between 1181 to 1197 s due to contact with the bottom coolant water from the porous concrete layer has nearly no effect on the power input and heating efficiency. This is consistent with the post-test observation, that only oxide melt was ejected.

Later in the test, from 2000 to 3000 s, during slow local propagation of the metal melt, the high frequency power oscillations decrease. This may indicate further solidification of the steel melt, but does not result in the final stop of downward propagation. Finally, the safety signal automatically switches-off the induction heating at 2995 s.

3.3.2 Coolant Water Flow

Figure 3-7 through 3-9 show the coolant water flow to the melt as the sum of sideward and bottom water flow, the approximate water level in the crucible (measured in the isolation gap behind the MgO liner), and the water pressure in the supply lines, respectively.

Figure 3-7 clearly shows the onset of passive flooding, which occurs from the northern section of the sidewall at 165 s. This (unexpected) early coolant flow from the sidewall increases to a maximum rate of 1.2 litre water/s at 300 s. As concrete erosion is predominantly through the metal phase of the melt, water ingression is expected to occur near the lower edge of the vertical cylinder wall. Increase of the water flow and the post test sectioning of the cooling device (Figure 3-18) shows that water ingress was sufficiently homogeneous to arrest the melt at the inner cylinder wall. A part of the water is evaporated, cools and solidifies the melt near the inner cylinder wall without major fragmentation, the remaining water penetrates near the wall to the surface of the melt and finally floods the melt surface at 320 s. The decrease of the water flow rate starting at 350 s is mainly due to the accumulation of a water layer on the crusted melt surface, resulting in a continuous reduction of the driving water pressure. The volcanic eruptions which occur in the period from 390 to 430 s and which are driven by the gases from concrete erosion at the bottom, have no effect on the lateral inflow of the coolant water.

A pronounced increase of the coolant flow rate is visible at 1180 s . This is the start of bottom water injection, when the melt after continuous downward erosion contacts the water filled porous concrete layer, leading to the vigorous volcanic melt ejection. The bottom coolant flow as derived from the increase of the flow rate is however small, some 0.12 litre/s, and probably indicates local bottom cooling only. In case of complete evaporation the bottom coolant flow could remove about 300 KW, which roughly corresponds to the simulated decay at that time of the test. As, however, the bottom water flow is not sufficiently homogeneous, complete stop of the melt is not assured. The long term water injection from bottom and sidewall after continuous decrease of the flow rate approaches 0.3 litre/s at 2800 s. (The ripple of the flow curve that is seen in Figure 3-7, is due to some oscillations of the level of the water supply tank related to the automatic refill action.)

At 2900 s we observe a distinct drop of the water flow rate, which is attributed to the stop of bottom flow by some blockage formation near the lower interface. The remaining water flow from 2900 to 3670 s may be reduced to the lateral inflow only. The slow localized downward erosion, which is detected by the thermocouples (see Figure 3-18) is continuing and leads to the interruption of the safety light guide at 2995 s, and induction heating is ended. Water flow during this period, however, remains unaffected. From 3670 to 3725 s the operator takes control over the water management and increases the water pressure to stop any potential, residual downward erosion and to protect the induction heating system. Further operator actions are taken after 4000 s to cool the water and to release the water from the test vessel.

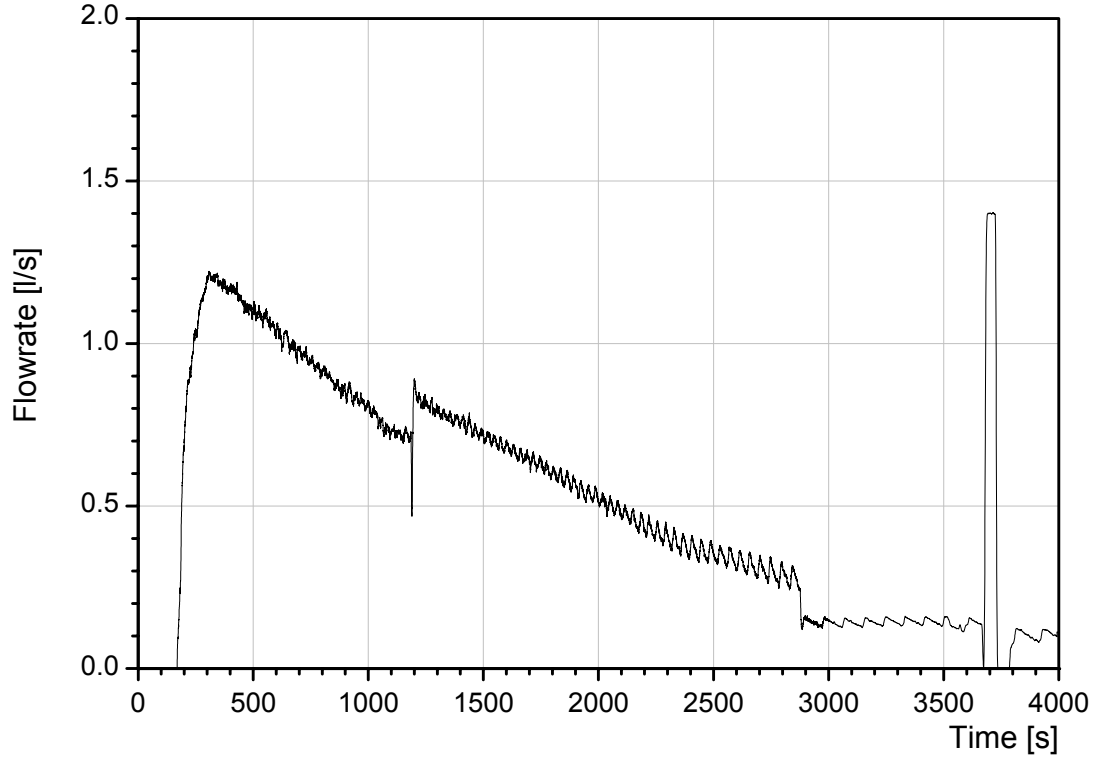

Figure 3-7 CometPC-H4:Coolant water flow to the melt

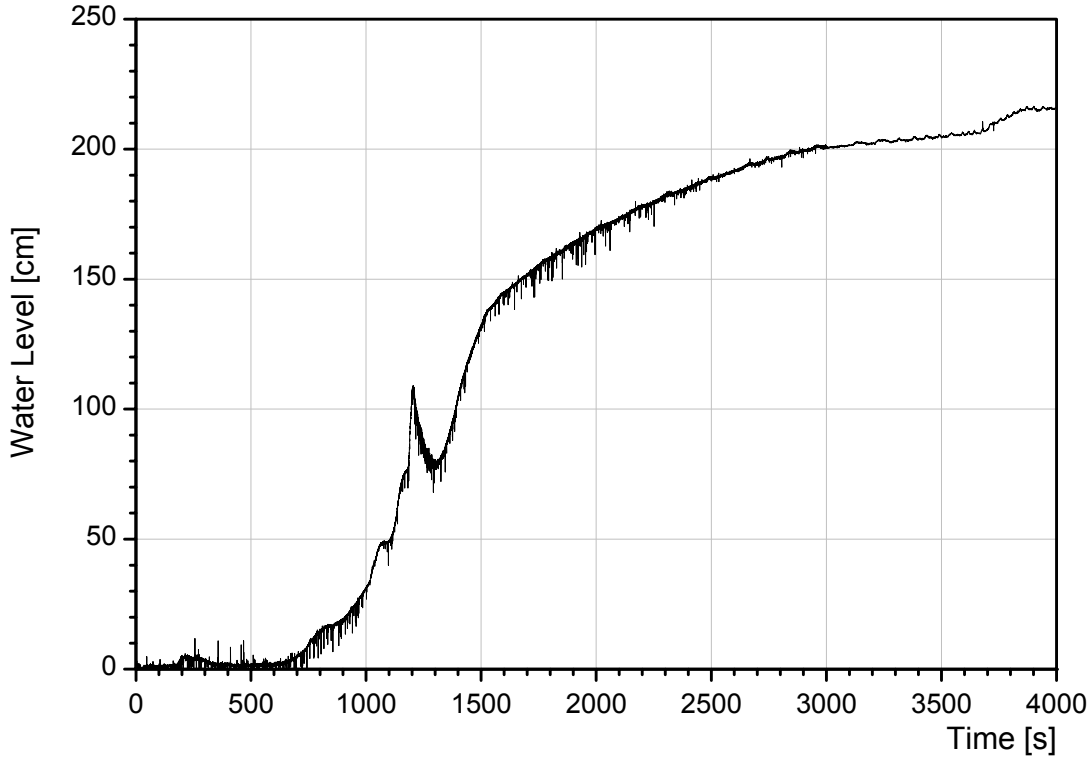

Figure 3-8 CometPC-H4: Approximate water level measured in the isolation gap

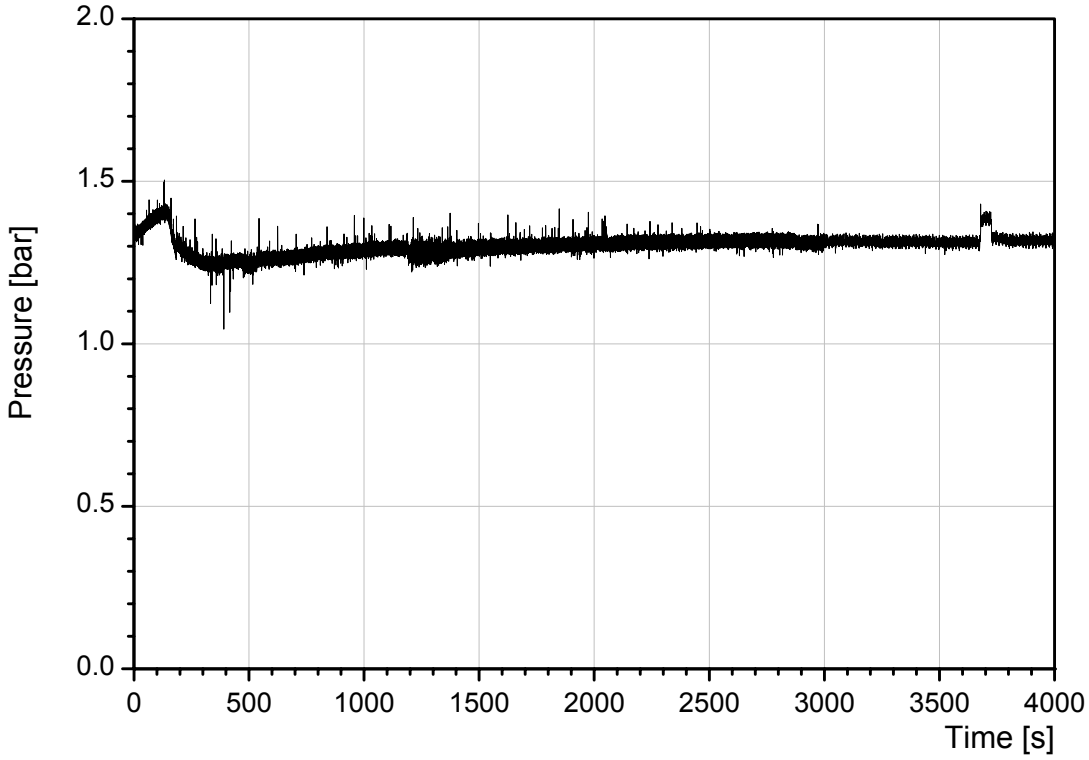

Figure 3-9 CometPC-H4: Coolant water pressure in supply lines

The approximate water level is given in Figure 3-8. This water level is measured in the isolation gap behind the MgO liner (see Figure 2.2) and therefore detects the central water height with a certain delay, especially in the early test phase after 350 s, when leakage from the central crucible to the isolation gap is small. Until 350 s, the water level is zero. At 350 s, the water covers the melt surface (level height some 60 cm) and then the central water level rises to 130 cm at 1500 s. After 1500 s, the measured level agrees with the central water level, indicating that the melt surface is covered by a water layer of 80 cm or more.

Figure 3-9 gives the absolute water pressure in the coolant supply lines near the water filled porous concrete layer, resulting from the height of the water supply tank. Certain pressure losses in the supply lines reduce the measured static pressure, depending on the flow velocity. The water overpressure is 0.1 bar over the hydrostatic pressure of the melt. The long term pressure variations are due to the change of the water flow rate. The small spikes are due to “noise” from induction heating. The increase of “noise” after 1180 s over some 100 s is caused by the strong melt eruption, which, however, has only minor effect on the water pressure. Also visible is the operator initiated transient pressure increase at 3670 s after end of the test.

3.3.3 Heat removal by coolant evaporation

With start of melt cooling by onset of passive flooding, a large amount of steam is generated, which is released through the off-gas tube. In the off-gas tube, gas velocity and gas temperature are measured simultaneously, which, after subtraction of the argon cover gas flow, and referred to the measured gas temperature in the hood of the crucible, allow calculation of the enthalpy flux with the steam flow. This heat flux is a good approximation of the heat flux that is extracted from the melt by evaporation of the bottom coolant flow.

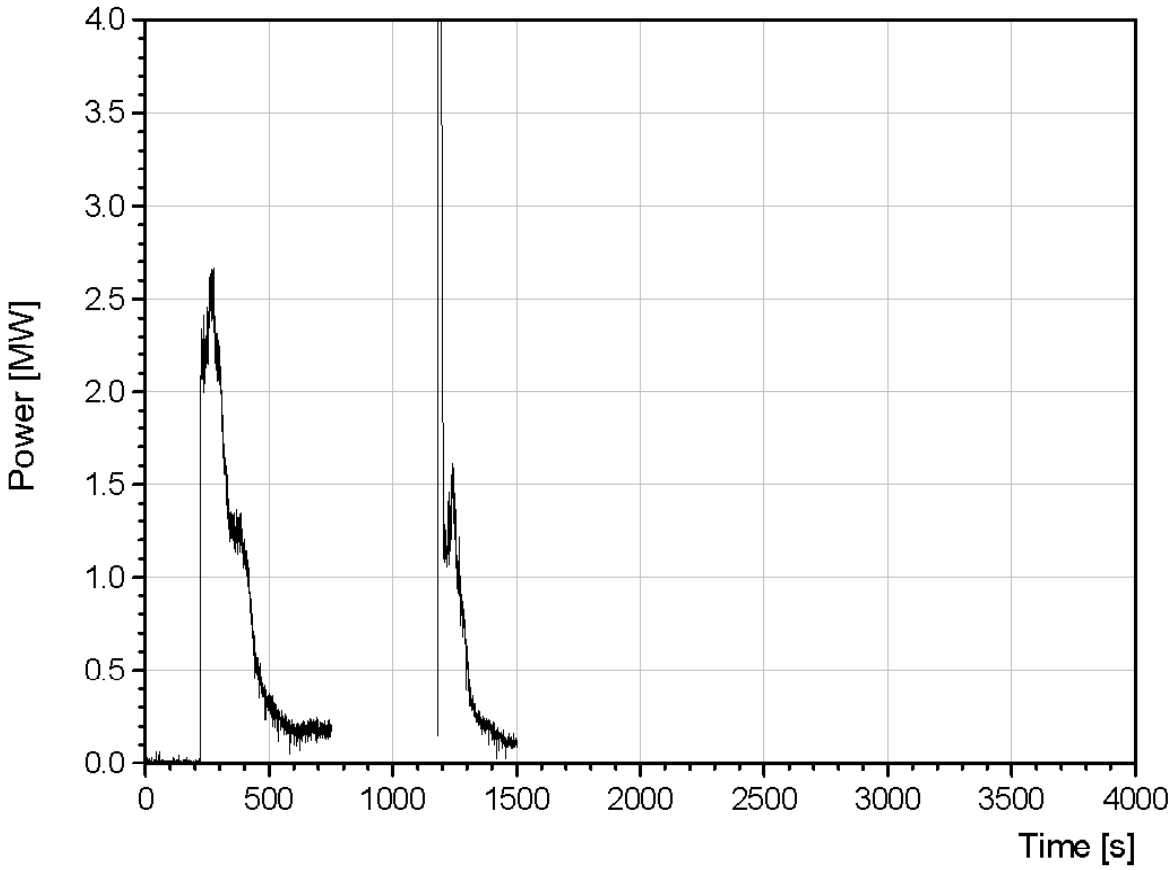

Figure 3-10 CometPC-H4: Power extracted by evaporation of coolant water (derived from turbine flow measurements)

Figure 3-10 gives the measured cooling power, which until 1180 s is the result of evaporation of the coolant flow from the sidewall, which starts at 165 s. The corresponding measuring devices in the off-gas line are activated at 240 s. Until 300 s, the majority of the injected water is evaporated. Thereafter, the extracted power reduces drastically, which indicates that those regions of the melt which are in direct contact with the coolant water, such as the upper melt surface and those regions of the melt which are in contact with the inner cylinder wall, are cooled. At 320 s, the video observation shows that the melt is covered by boiling water on the thin surface crust. The energy that is extracted by the first cooling peak in the period from 240 to 500 s in Figure 3-10, is 380 MJ. With the assumption, that the fraction of

the melt that is cooled is 50 weight % metal and 50 weight % oxide, the cooled melt fraction is estimated with 270 kg, which is 1/3 of the initial melt mass[1)]. At 500 s, the bulk of the melt is still at high temperature and partly liquid (indicated e.g. by a short period of volcanic melt ejection). But further heat extraction until 1180 s is small, namely in the order of 200 KW, as the stable surface crust excludes an efficient heat removal.

In the period from 750 to 1181 s and from 1500 to the end of the test, partial condensation of the steam flow does not allow estimation of the power in the off-gas.

The second peak, starting at 1181 s is caused by onset of bottom flooding and characterises the vigorous melt ejection into the water overlayer. The integrated power of the second peak from 1181 to 1400 s is 190 MJ, which corresponds to the thermal energy of 103 kg oxide melt [1)]. This agrees with the mass of the porous particle bed found in post test analysis.

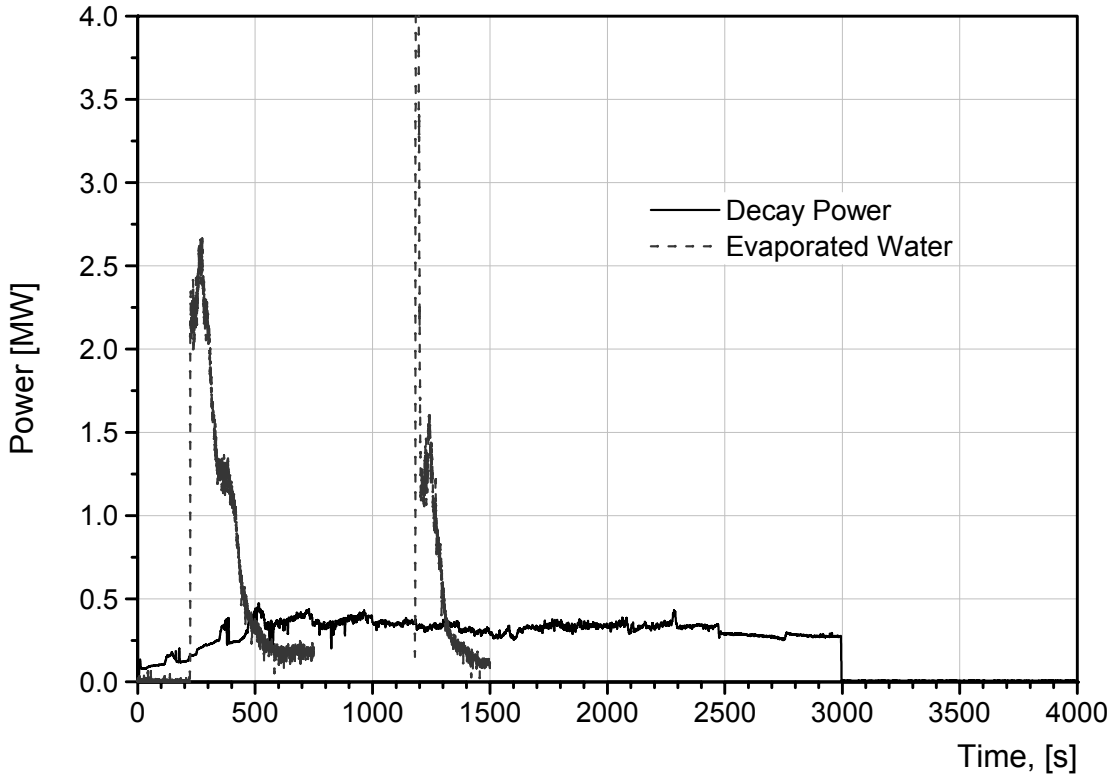

Figure 3-11 CometPC-H4: Simulated decay power and power extracted by evaporation

Figure 3-11 compares the simulated decay power in the melt and the power measured in the steam flow from Figure 3-10. In spite of some uncertainties in determining the power in the off-gas flow it is evident that, with the exception of the 2 spikes, heat removal is smaller than the energy input. Therefore, local downward concrete erosion is continuing, although sufficient coolant water is available above the melt surface.

[1)] The enthalpy difference of the oxide from 1500 to 100°C is 1851 J/g, of the metal 987 J/g, calculated with GEMINI [2]

3.3.4 Gas Release

This section describes the gas flow during the test, measured in the hood of the crucible and in the off-gas line, which connects the crucible with the open atmosphere.

The gas pressure in the hood is given in Figure 3-12, showing a practically constant atmospheric pressure. Some very small oscillations are detected after 165 s when passive flooding starts. A small pressure spike of 0.1 bar occurs at 1181 s when the melt contacts the porous bottom layer and oxide melt is ejected into the upper water layer.

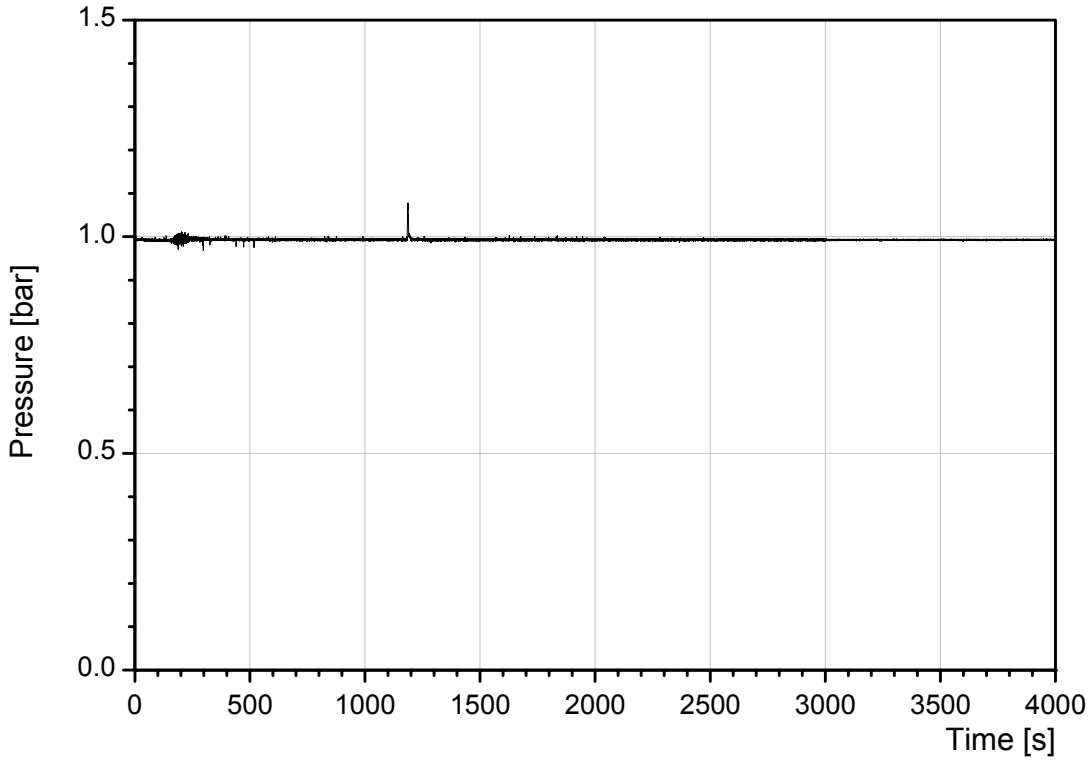

Figure 3-12 CometPC-H4: Gas pressure in the hood of the crucible

The off-gas temperature in the crucible hood is given in Figure 3-13, measured by a thermocouple protruding into the gas volume. This temperature is used to determine the enthalpy of the steam flow after onset of bottom flooding as discussed in section 3.3.3.

When the melt is poured into the crucible, the off-gas temperature rises up to 420°C, and then reduces to about 300°C during the first phase of dry concrete erosion. These temperatures are of course lower than at the melt surface , because the gases deposit part of their energy to the colder structures of the upper crucible. With onset of sideward flooding at 165 s, a substantial steam rate is produced, and the gas temperature rises again to nearly 500°C. After formation of the surface crust and its quenching the temperature comes close to 100°C, indicating boiling of the saturated water layer.

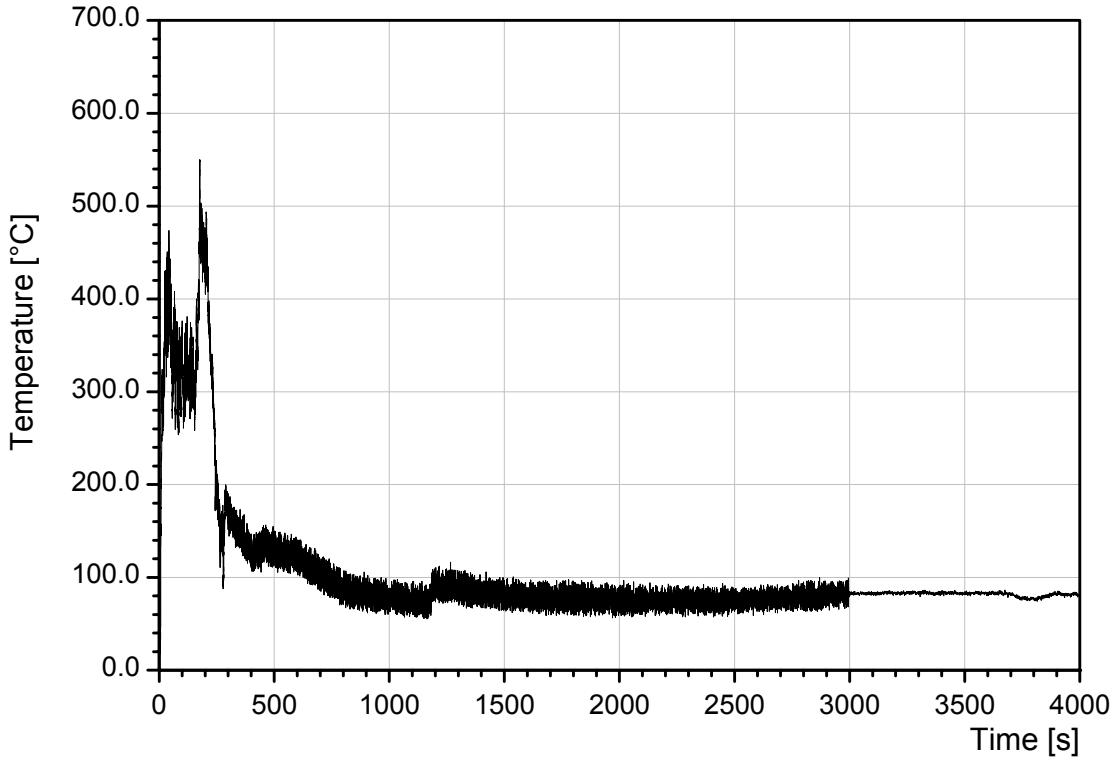

Figure 3-13 CometPC-H4: Gas temperature in the hood of the crucible

A small increase of the gas temperature is seen at 1181 s, when part of the oxide melt is ejected into the upper water layer, which at this time is some 50 cm high. Because of the very effective quenching process the steam temperature is close to 100°C. The slight drop of the gas temperature below 100°C later on is due to the ongoing admixture of argon cover gas of room temperature into the upper crucible, and produces mist flow.

Gas composition was measured online by a quadrupole mass spectrometer that detects up to 8 chemical species. Figure 3-14 shows the results for the gases H_2, CH_4, CO, and CO_2. (The steam content could not be detected by this system, because of principal limitations of the spectrometer: As steam would damage the analysis system, steam flow in the analysis system was removed by condensation.) The constant argon cover gas flow is not shown in Figure 3-14, but was used as the reference to determine the release rates of the species based on their measured concentration. The mass spectrometer was calibrated before and after the test with 5 test gases of different compositions. The release rates are given in litre/s at standard gas conditions: 1 l/s corresponds to 1/22.4 mole/s. Note, that due to the long response time of the gas analysis system, the time axis for the gas rates should be shifted by about 30 s to the left side to allow time correlation with processes in the crucible.

The most interesting and most important gas is hydrogen, which is formed by the reduction of steam through iron oxidation. Measurements show a clear hydrogen peak until 400 s, when the melt is covered by the water overlayer. The peak rate is 44 litres/s, which occurs

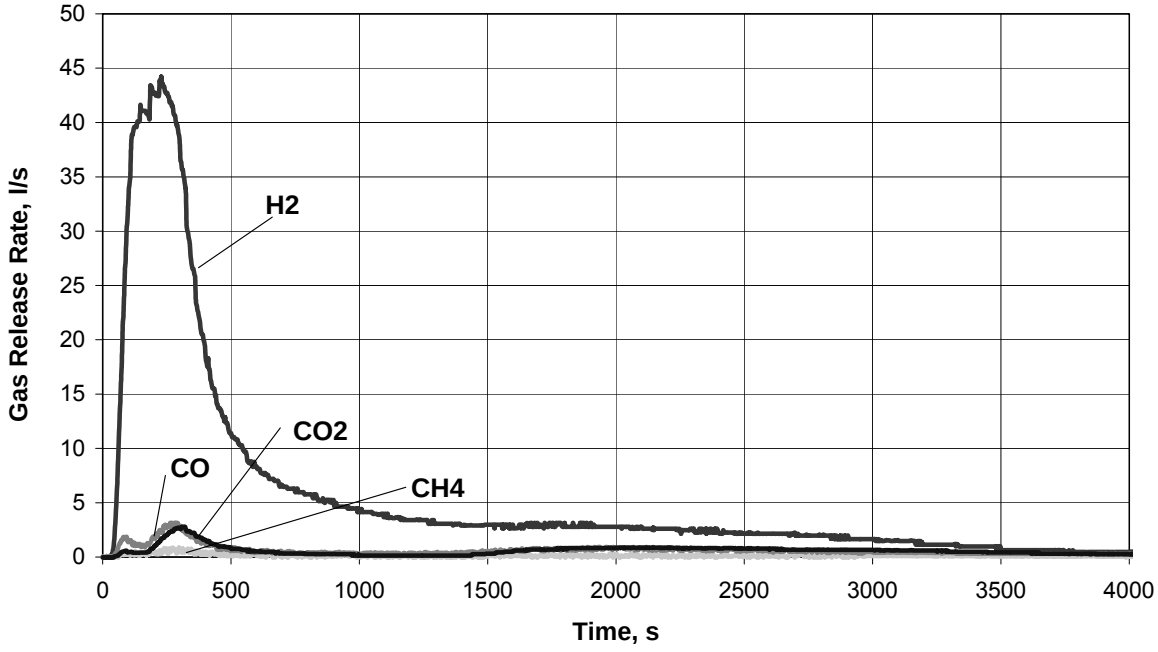

Figure 3-14 CometPC-H4: Release rates of H2, CH4, CO, and CO2 in the off-gas

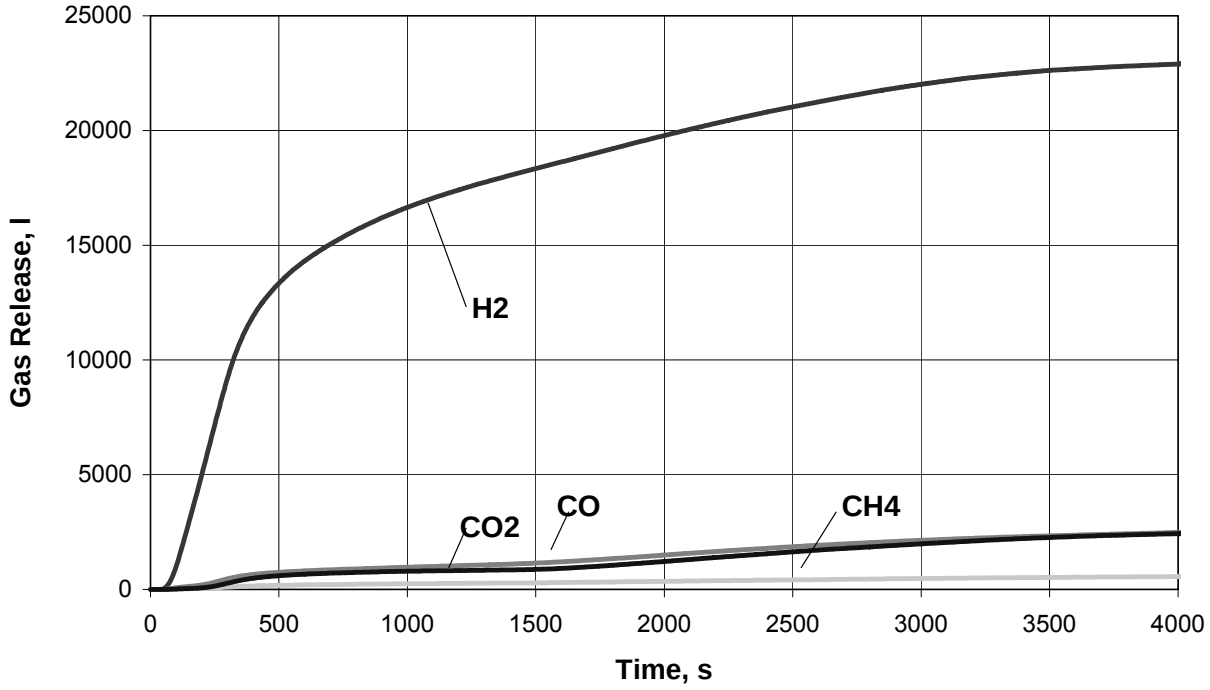

Figure 3-15 CometPC-H4: Integrated gas release of H2, CH4, CO, and CO2 in the off-gas

during the first period of sideward flooding. This rate is nearly a factor 3 of the typical H2 rates found in 1-d experiments, and is due to the additional vertical cylinder walls. In the long term, H2 release goes to nearly zero at end of heating at 3000 s. This reduction is attributed to cool down of the metal phase and its progressive solidification, so that the chemical reaction rate is reduced.

It is remarkable that the no extra hydrogen peak is detected at onset of bottom flooding at 1181 s. This may indicate that the iron fraction of the melt is mostly solidified at that time.

The release rate of the gases CO and CO2 are one order of magnitude below the H2rate, which is typical for siliceous concrete. The release of methane is practically zero. This is an important information because of potential formation of organic iodine in the reactor situation.

Figure 3-15 gives the integrated gas release as determined by integration of Figure 3-14. Some 23000 l of hydrogen (~ 1000 moles H2) are generated during the experiment.

The aerosol concentration was measured in the off-gas by the absorption of a laser beam that passes the off-gas line. The extinction E is defined by the logarithmic ratio of the intensity I/I_0 of the laser beam before and after transmission through the off-gas tube

$$E = \ln (I/I_0)$$

and is in the present application a qualitative information of the aerosol density.

Figure 3-16 shows from 0 to 180 s aerosol release during the first phase of dry concrete erosion. With onset of flooding, aerosol release is drastically reduced, and reaches the minimum value at 260 s, when the coolant water has flooded the melt surface. The low-density aerosol, still detected in the period from 260 to 800 s, is probably due to the ongoing concrete erosion at the bottom of the crucible and the release of the concrete gases through the upper water layer. Volcanic eruptions, that take place from 370-425 s under water, have no visible effect on the aerosol density. The increase of the extinction from 800 s to 1181 s may be attributed to the partial condensation of the steam flow in the off-gas, that limited evaluation of the power in the off-gas (Section 3.3.3) and was measured by the reduced off-gas temperature in Figure 3-13. The vigorous melt ejection that occurs at 1181 s gives a very high extinction, as water droplets, partly produced by steam condensation, absorb the laser beam during the further test .

The reduction of the aerosol production in the present experiment has 3 reasons:

1. The surface crust of the melt stops aerosol release from the hot melt.

2. The water layer on top of the melt traps aerosol particles.

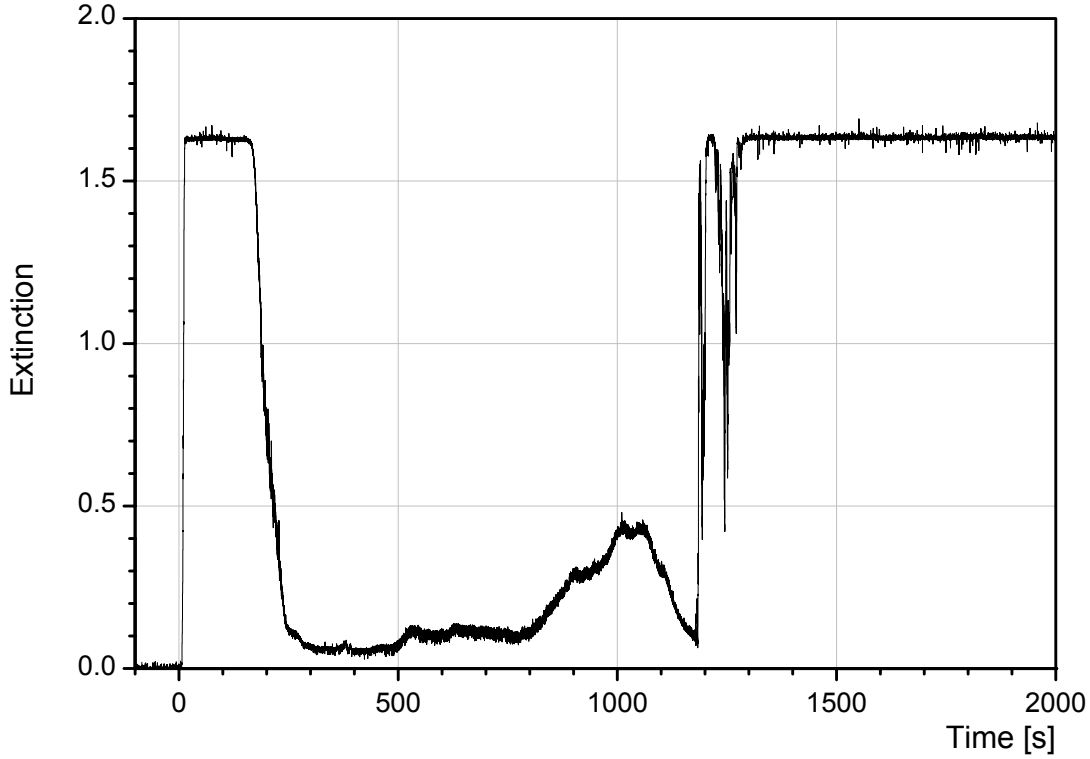

Figure 3-16 CometPC-H4: Extinction of laser beam by aerosols in the off-gas line

3.3.5 Concrete Erosion and Heat Fluxes

The downward erosion of the sacrificial concrete layer was determined from the failure time of a series of thermocouples, which were located in the centreline of the coolant device and in the middle of the 4 quadrants, named NW, SW, SE, and NE, respectively. The position of the thermocouples referred to the upper surface of the porous concrete layer (0 mm), is + 10, + 30, + 50, and + 70 mm, respectively. The top of the sacrificial concrete layer corresponds to + 100 mm. Thermocouples in the porous, water filled concrete layer are located at – 5, – 20, and – 50 mm.

Figure 3-17 shows the measured erosion front in the sacrificial concrete versus time over the period from 0 to 4000 s. At 10 s, the erosion starts at the upper concrete surface (+ 100 mm). For the first 30 mm of concrete erosion, the maximum detected erosion rate is 0.28 mm/s in the centre and north-west of the concrete surface, while the average velocity over this period is about 0.2 mm/s. This high erosion velocity is due to the initial overheat of the melt and exceeds the rate, that corresponds to the simulated decay heat. It is, however, in good agreement with the erosion velocity of 0.17 mm/s measured in the preceding experiment CometPC-H3 over the first 200 s [1].

With decrease of the temperature of the melt, the erosion velocity drops to an average value of 0.04 mm/s near 1000 s. The detected deviations from a flat erosion front until onset of bottom flooding are about 20 mm. The start of sideward flooding at 165 s and of bottom flooding at 1181 s are indicated in Figure 3.17.

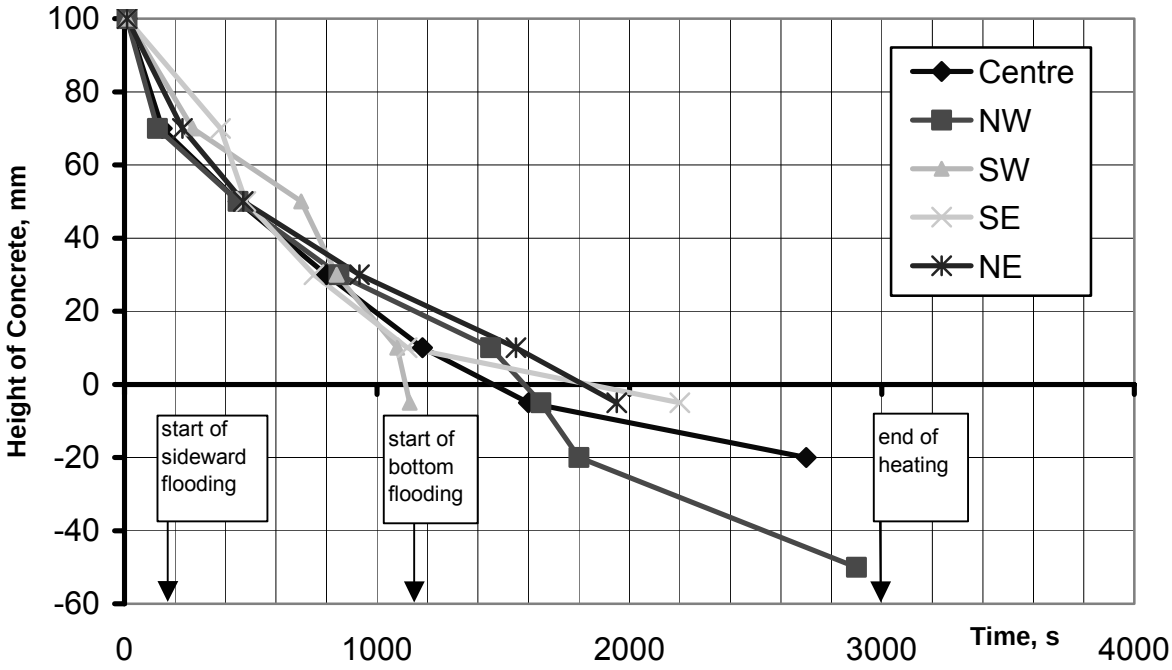

Figure 3-17 CometPC-H4: Erosion front of propagating melt in bottom concrete, based on thermocouple measurements

The downward erosion velocity can be translated to the downward heat flux from the melt, using the properties of the concrete

$$Q_{down} = A \cdot \Delta h_{decomp} \cdot \rho \cdot v \,, \qquad (1)$$

where Q_{down} is the downward heat flux, A the eroded bottom surface (0.57 m^2), Δh_{decomp} the decomposition enthalpy of the sacrificial concrete (2.1 MJ/kg), ρ the density of concrete (2300 kg/m^3), and v the erosion velocity. For a complete energy balance, sideward and upward heat fluxes must also be considered.

For the average initial velocity of 0.2 mm/s until 200 s, the downward heat flux alone is 550 KW from equation (1), which is nearly a factor 2 higher than the simulated decay heat. The consequence is therefore a fast temperature drop of the melt in the early erosion period. This is enhanced by onset of sideward water ingression at 165 s and subsequent top flooding, which extract about 380 MJ by evaporation of the coolant water until 400 s, when a stable surface crust has formed (see chapter 3.3.3).

After 400 s, the temperature of the melt and cooling conditions have stabilized. Heat extraction by evaporation from the side and through the top crust is reduced to about 200 KW (Figure 3-10), which is less than the typical simulated decay power of about 350 KW, and the melt has reached a temperature level close to the solidification temperature. The residual heating power of about 150 KW leads to further, but reduced downward erosion. Indeed, for the period from 400 to 1200 s, Figure 3-17 shows a nearly constant downward erosion rate. From this average late erosion rate of 0.04 mm/s, the downward heat flux

calculated with equation (1) is about 110 KW in good agreement with the estimate above, corresponding to about 30 % of the heating power. Dry concrete erosion into the downward direction therefore continues until the melt contacts the porous concrete layer at 1181 s at position 0 mm, and passive bottom flooding starts.

Bottom flooding leads to an expulsion of about 100 kg oxide melt through a hole in the upper melt crust, but the pre-existing crust excludes sufficient fragmentation of the melt. Figure 3-17 shows a reduction of the downward erosion rate and partial stop of the melt, indicated by the thermocouple behaviour. The erosion in some areas stops between –10 mm and –50 mm, with the exception of the north-west sector, for which the thermocouples show continued erosion and thermocouple failure at –50 mm at 2900 s. Finally, heating and further erosion are stopped by the light guide safety instrumentation, which is hit by the melt at the –80 mm position in the western part of the porous layer at 2955 s.

For the time period from 400 to 1100 s, the following estimates on sideward and upward heat fluxes are made:

As mentioned above, heat extraction by evaporation from the side and through the top crust is about 200 KW (Figure 3-10). Discrimination of sideward and upward heat fluxes from experimental data is however difficult. Because of the large sideward contact area of the melt of 0.93 m^2 (for a collapsed melt height of 0.35 m), the sideward heat flux may be higher than the upward heat flux through 0.57 m^2 only. If the (average) sideward heat flux density were equal to the downward heat flux, the sideward heat flux were 240 KW. This is, however, a too high upper bound, as the upper layer of the melt is oxidic, and its specific heat transfer rate is reduced.

A better estimate is derived from the thickness of the upper melt crust, which is 20 mm as determined from Figure 3-18. The upward heat flux can be calculated assuming direct contact of the melt with the lower side of the crust and boiling water on the upper side, which was the situation in the considered time period. The resulting temperature difference over the crust was about 1400°C, and the thermal conductivity of the slightly porous crust is between 1 and 2 W/m·K. This yields a heat flux density of 70 to 140 KW/m^2, and a total upward heat flux over the area of 0.57 m^2 of 40 to 80 KW. This is about a factor 3 to 1.4 smaller than the downward heat flux of about 110 KW. The total lateral heat flux would then be the difference to 200 KW, which is 160 to 120 KW. The lateral heat flux is completely removed by the evaporating water, without any further concrete attack.

3.4 Post Test Analysis

The apparatus was carefully disassembled in order to document the debris configuration with respect to coolability. The surface of the solidified melt is covered by a 10 to 20 cm high layer of porous oxidic material, which was mostly fused together. This material was clearly ejected by the vigorous expulsion at 2955 s.

Figure 3-18 is a photograph of the vertical section through the solidified melt, with the porous

concrete cooling structure at the bottom and at the lower cylinder walls, the outer polypropylene vessel, and the MgO protection tube atop. The different heights of the cooling device and the collapsed melt heights at start of the test are also given at the right side of the figure. The photo shows the melt in the configuration that was generated by the bottom water ingression at 2955 s, leading to fast pressure increase and oxide melt ejection after break-up of the upper surface crust. This situation remained mainly unchanged until the end of the test, with the exception of some further downward erosion of the porous concrete layer at the bottom. Dominant is the large, voided cavity which extends over the full diameter and which was generated during the melt expulsion. On top of the cavity we see the ejected coarse oxide material. The cavity is formed by a dense upper oxide crust and the densely solidified oxide layer at the bottom. The height of the cavity is 23 cm in the central dome. The upper crust thickness is 20 mm. The inner surface of the crust is smooth, which indicates that the inner crust surface before its solidification was wetted or in contact with a liquid melt layer, which is confirmed also by some solidified droplets at the inner surface. The thickness of the upper crust was used to estimate the upward heat in the previous section. Expulsion of the melt occurred through the central vent at the top of the dome.

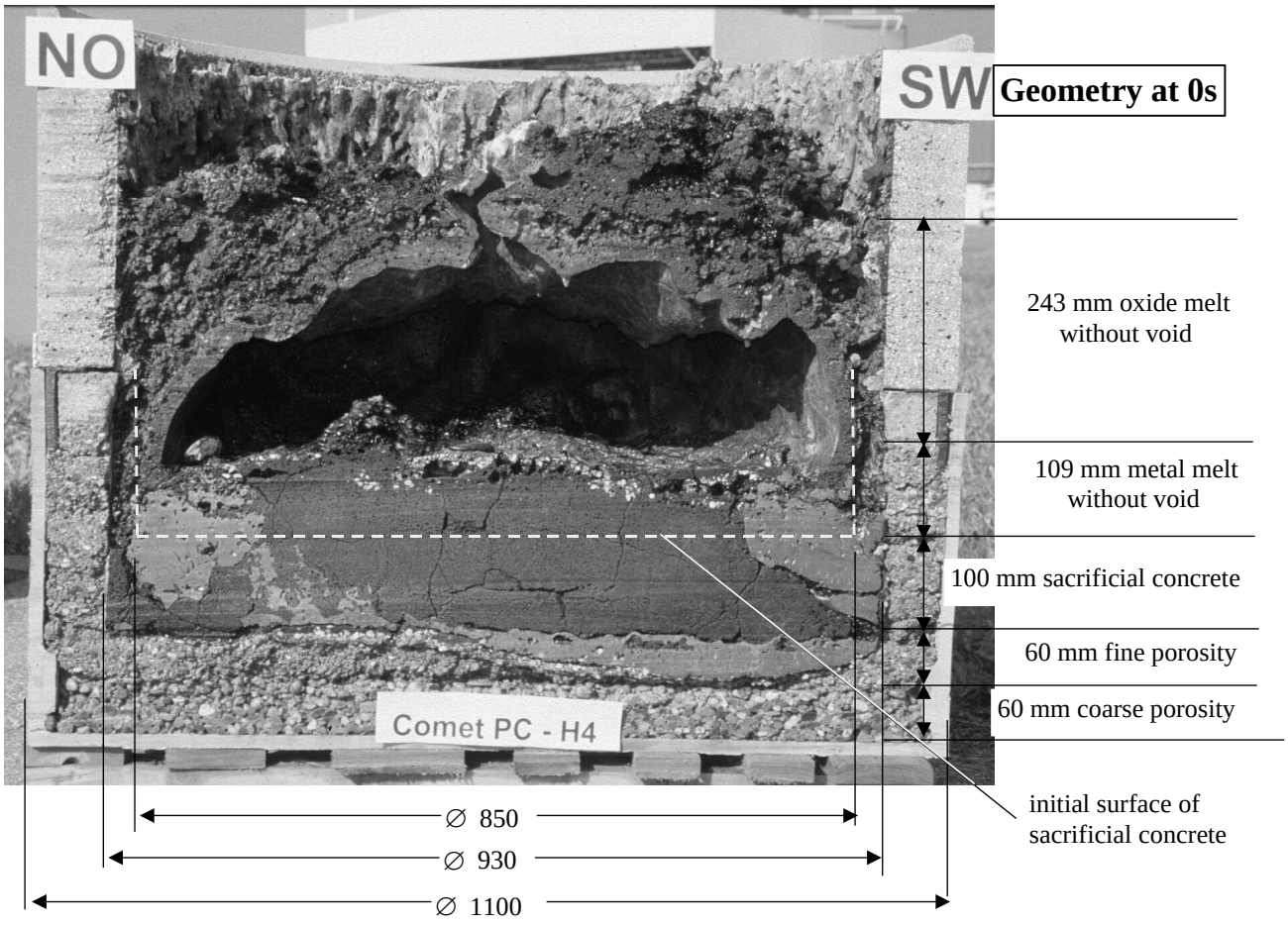

Figure 3-18 CometPC-H4: Solidified melt, sectioned in direction NE to SW

The height of the solidified melt from the bottom of the voided cavity to the porous concrete layer is 22 cm on the left side and 26 cm on the right side, where the welt has eroded part of the porous concrete layer. On the left side, the melt is arrested and solidified at the former interface between the sacrificial concrete layer and the porous concrete layer, which corresponds to position 0 in Figure 3-17, whereas the erosion depth on the right side into the porous concrete layer is 60 mm.

The solidified melt has two phases: Dominating is the dark grey oxide phase. The iron phase is brown and located at the bottom and to a large extend also at the side of the inner crucible. It is remarkable that the melt is solidified without any void, and that there are only very few cracks, which formed during solidification. The inner melt surface shows a layer of white particles, which are not completely melted aggregates of concrete. The compact solidification of the melt indicates, that late in the test, i.e. during melt solidification after end of heating, practically no steam passed through the melt. Steam, generated by evaporation of water from the porous concrete layer at the bottom, has probably bypassed the melt through the sidewalls.

The sacrificial concrete which was located in front of the porous concrete layer is completely eroded and mixed with the initial oxide melt (compare Figure 3-1). The vertical porous cylinder walls are completely stable, whereas parts of the porous concrete layer at the bottom was eroded.

3.5 Conclusions for the actual test CometPC-H4

The experiment CometPC-H4 is a large scale, 3-D cooling test, which investigates cooling of a simulated corium melt by water supply from bottom and sidewalls. The cooling device consisted of a cylindrical vessel with bottom plate, both fabricated from porous, water filled concrete. The inner surfaces were initially protected by a layer of sacrificial, conventional concrete. 800 kg melt were poured into the cooling device and heated with 300 kW over a period of 3000 s to simulate the nuclear decay heat.

As the radial erosion of the sacrificial concrete was higher than expected, flooding started from the side after 180 s instead from the bottom. This flooding stopped radial propagation of the melt, but the flooding mode finally resulted in a typical top flooding scenario. The continuous water flow from the sidewall eventually flooded the surface of the melt after 300 s, and thereby caused the formation of a complete and stable surface crust. This crust prevented fragmentation and efficient cooling of the liquid melt underneath. Therefore downward erosion of the sacrificial concrete layer continued with about 0.04 mm/s until the initiation of bottom flooding, when the melt contacted the lower porous concrete layer after 1180 s. Injection and fast evaporation of the coolant water from the bottom porous concrete layer vigorously ejected about one third of the oxidic melt into the upper water layer over a period of 15 s only, through one central hole in the surface crust. The ejected melt settled on the upper surface crust as a porous layer. The surface crust, although distended by the eruption process, persisted and remained stable, covering the whole melt surface throughout the further test. Because of melt eruption, however, the melt had lost contact to the crust,

which may have further reduced the upward heat flux from the residual melt in the lower crucible. In this respect, this situation is similar to the typical MACE cooling tests with a stable surface crust after top flooding [3].

Subsequent cooling of the remaining melt in the lower crucible by the newly established melt contact to the porous, water filled concrete at the bottom was however incomplete, as parts of the melt continued downward erosion. No further melt ejection occurred, evidently because of the large void between residual melt surface and the top crust. In addition, some of the coolant steam/water flow from the porous bottom layer may have bypassed the melt through the radial porous concrete walls or a radial gap between melt and vertical walls. This resulted in a final, localised downward erosion of the porous concrete until - 80 mm at 2955 s, when the sustained inductive heating was interrupted. - The sectioned crucible shows a very densely solidified melt at the bottom, which penetrated into the porous concrete in south-west, but stopped at the porous concrete interface in north-east. Above the melt exists a large voided cavity with a dense surface crust of about 2 cm and a central vent, and a layer of ejected porous oxide material on top.

The main consequences of the experimental observations are summarized as follows:

- Radial attack of melt is reliably stopped by porous concrete cylinder. The temperatures in the cylinder wall do not exceed 100°C because of the continuous coolant water flow.
- The wrong sequence of flooding, i. e. sideward flooding before bottom flooding, reduces fragmentation and coolability of the melt.
- As expected, radial cooling in connection with surface flooding does not reduce downward penetration, but generates unfavourable conditions for later bottom flooding and cooling by:
  - massive and stable surface crust
  - bypass for coolant steam/water flow from below
- Volcanic eruptions during ongoing concrete erosion before onset of bottom cooling have minor effect on coolability
- Under these conditions, late onset of bottom flooding upon contact of the porous layer after start of lateral flooding is unable to stop and cool the entire melt, in spite of significant ejection of 1/3 of the oxide melt through the central vent in the surface crust, which generated a coolable, porous particle bed on top of surface crust.
- Locally, downward erosion by the residual melt is ongoing into the porous, water-filled concrete layer. Steam/water coolant flow from the bottom my partly bypass the melt through the porous sidewalls. Residual melt at the bottom remains unfragmented and hence uncoolable.
- The radial concrete erosion rate in the first, dry phase of the experiment was close to or slightly higher than the axial erosion rate. The too thin lateral wall thickness of 40 mm in relation to 100 mm axial layer thickness is the reason why the experiment took an other course than expected.

With respect to the coolability issue it is concluded, that

(1) the design of the CometPC cooling concept must guarantee the right sequence of flooding, namely onset of bottom flooding before flooding from the side. This can easily be achieved by adequate thickness of the sacrificial concrete layers at the bottom and side, respectively, and

(2) top flooding alone is unable to cool the melt as a stable surface crust prevents effective melt fragmentation

There are, however, some aspects that make melt cooling in the present experiment more difficult than in the reactor situation. The situation for the present experiment is:

- There is no decay heat simulated in the oxide, with the consequence e.g. of a thicker surface crust.
- Concentration of decay heat in the metal phase requires higher bottom cooling.
- Local accumulations of the metal melt that are closer to the induction coil, are heated with a higher power density than the residual metal. This enhances local penetration and makes cooling more difficult.
- The role of sideward flooding and cooling is reduced for large reactor cavities at least by a factor 6 compared to the present experiment with about 1 m diameter.

The consequences may be that the requirements for the efficiency of bottom flooding of a real corium melt are less demanding and that the present results are too pessimistic. Improvements of the bottom flooding concept are, however, possible and are investigated in the subsequent experiment CometPC-H5.

4 Experiment CometPC-H5

With respect to the general objectives, the experiment CometPC-H5 is identical to the preceding test CometPC-H4. The following modifications are made to achieve better cooling of the melt:

- The thickness of the bottom and lateral layers of sacrificial concrete are changed to start flooding from the bottom before onset of lateral flooding.

- The porous concrete layer of low porosity concrete is fabricated from alumina gravel for higher stability against thermochemical attack from the melt, if attack should occur.

In addition, the height of the melt is increased to 500 mm, in contrast to 350 mm in the preceding test. This increased height is considered as an acceptable level for the application. The necessary details of the set-up and conduct of the test are given below.

4.1 Details of Cooling Device and Melt Generation

4.1.1 Cooling Device

Figure 4-1 gives the details of the cooling device as prepared for experiment CometPC-H5.

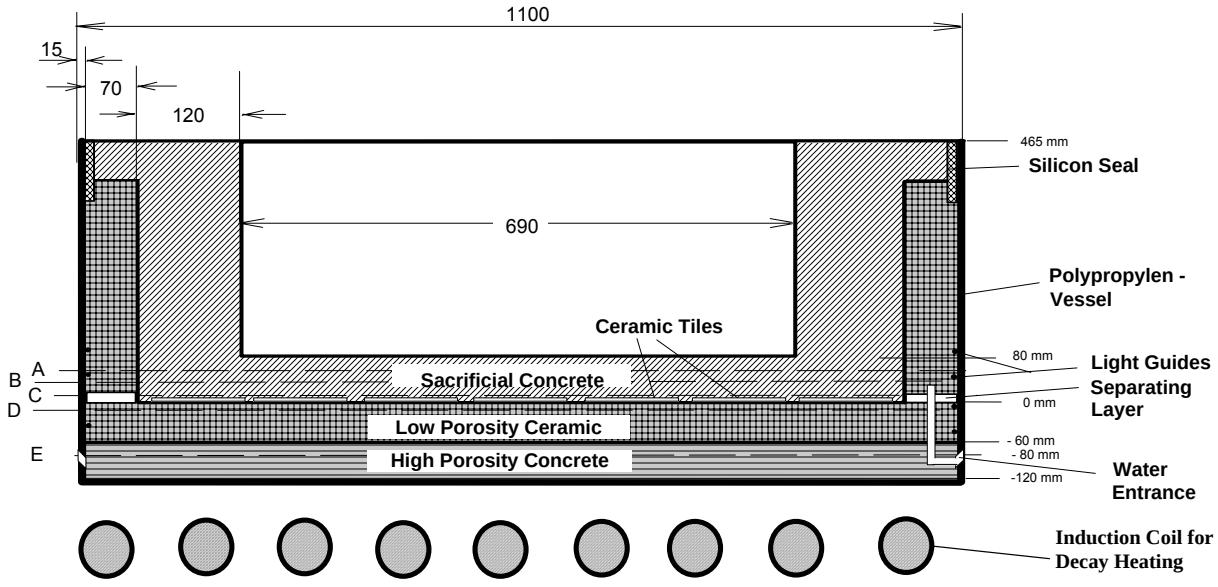

Figure 4-1 CometPC-H5: Details of the cooling device

The outer diameter of the device is defined by the COMET test rig in **Figure 2-2**. To save space and to allow a wide cavity for the melt, the outer watertight shell of the device is formed by a polypropylene casing, which is only 15 mm thick. The selection of this material requires that cooling of the wall and bottom regions is highly effective.

The horizontal layer of high porosity concrete, located at the bottom of the polypropylene shell, is 60 mm thick, and receives water through 2 supply lines from the side. This layer evenly distributes the coolant water under the cooling surface. The low porosity layer atop is 60 mm thick in the horizontal part and 70 mm thick at the vertical cylinder wall. These layers are fabricated from alumina sand and gravel, with the same porosity as the fine porosity concrete layer in CometPC-H4, and will allow and limit the coolant water flow to the melt. Fabricated from Al_2O_3, the layers should however have a higher resistance against thermal melt attack than a porous layer of silica concrete, and thus should give more time for melt fragmentation if the melt should not be stopped above. Horizontal and vertical low porosity layers are separated by a water tight contact zone, to allow and register the separate coolant water flow to each layer. The coolant water for the vertical layer is supplied by 2 specific supply lines, whereas the horizontal layer is fed from the bottom high porosity concrete. The porosity of these layers allows a maximum coolant flow of 3 litre/s from the bottom of the device, if the porous bottom surface were completely unsealed.

The innermost sacrificial concrete layer is 80 mm thick at the bottom and 120 mm thick at the sidewalls, corresponding to the ratio 2:3. It is fabricated with aggregates of broken borosilicate glass with the following composition: SiO_2 62,5 %, B_2O_3 > 6 %, Al_2O_3 > 5 %, Na_2O 14,5 %, CaO 6 %, MgO 3,5 %, TiO_2 < 1 %, Fe_2O_3 < 1 %, K_2O >1 %, other impurities <0,5 %. This glass, when melted and mixed to the simulated or real corium melt, reduces its viscosity and thus favours the spreading process. In addition, the boron as strong neutron absorber would eliminate criticality problems in case of nuclear application.

Thin tiles of commercial ceramic separate sacrificial concrete and the low porosity layer at the bottom, to exclude blockage of the upper layer of low porosity concrete, when during preparation of the cooling device, the liquid sacrificial concrete layer is poured onto the device. When attacked by the hot melt, the tiles are expected to fail mechanically and give way to the coolant water flow.

Ceramic rings of MgO are placed on top of the coolant device to exclude attack of the outer protection tube. Figure 2-2 shows the cooling device installed in the test rig.

The initial diameter of the inner test volume is 690 mm. The height of the porous sidewalls is 380 mm and sufficient to contain all the metal melt, from which the main downward and sideward concrete erosion is expected. The height of the oxide melt extends over the cooling device into the area of ceramic rings.

Instrumentation in the cooling device consists of 75 thermocouples embedded in the different concrete layers (partly indicated by the levels A – E), and of light guides in bottom and side walls which act as safety instrumentation.

The maximum coolant water flow in case of complete opening of the fine porous concrete surface was estimated with 3 l/s with an effective water overpressure referred to the lower melt surface of 0.1 bar. This water pressure is maintained throughout the experiment by a water reservoir above the test rig.

4.1.2 Melt Generation

The following **Table 4-1** shows the composition of the thermite powder and the resulting melt composition.

Table 4-1: Composition of the thermite powder and of the resulting melts in CometPC-H5

Constituent	kg
Initial composition:	
Thermite powder R 70/SSH	552.9
CaO	193.5
Ni	53.6
total	800.0
Generated melt (initial T 1800°C):	
Oxide: 56.2 % Al_2O_3 + 43.8 % CaO	442.3
Metal: 85.0 % Fe + 15.0 % Ni	357.7
total	800.0

The thermite mixture was preheated over a period of 2 days to 250°C to increase the initial temperature of the thermite melt. The expected temperature of the melt at pouring is 1900°C. The generated melt is poured completely into the cooling device. The resulting initial heights are 148 mm for the metal melt and 350 mm for the oxide melt, without void by the percolating gases. The corresponding total melt height is 498 mm.

No simulated fission products were added to the melt.

4.2 Test Procedure

The conduct of the experiment was planned as listed in Table 4-2. The estimated time for start of flooding was based on prediction of downward propagation and is subject to uncertainties in the erosion process, such as local effects etc. The time for melt solidification is of course a rough estimate only.

In the early test phase until onset of bottom flooding, the net induction heating power is planned with 150 KW only, and will be increased to the typical 300 KW at onset of flooding. The lower power in the beginning is limited by the initially low coupling efficiency of the induction coil and shall avoid incoherent erosion of the sacrificial concrete by an inhomogeneous induction field.

Table 4-2: Planned conduct of the CometPC-H5 experiment

Time, s	Event
until –240	Facility prepared, argon inertisation completed, induction coil operating, coolant water supply connected with 0.1 bar overpressure
-90	Ignition of thermite powder, allow separation of metal and oxide phases
0	Start of melt pour (duration ~ 40 s), onset of dry erosion of sacrificial concrete layer, continuous decay heating with about 150 kW
≥ 180	activate flow meters in off-gas tube after decrease of first intense gas release
about 600	Onset of passive flooding from bottom layer expected after erosion of sacrificial concrete layer; heating power has increased by downward propagation of the melt to about 300 kW, operator controls decay power level to 300 kW until end of heated test. Observation of melt fragmentation, cooling, and solidification
about 2000	Complete melt solidification expected, further heating with 300 kW to observe stability of long-term cooling over further 1800 s
about 3800	End of heated test, decay power off
post test	Cool down and release of water from flooded and solidified melt, inspection and conservation of test vessel for further dismantling

The realized experimental conduct is provided in **Table 4-3**. After pour of the melt, dry concrete erosion took place until after 700 s passive water injection started from the bottom layer. This lead to fast cool down of the melt as expected under the conditions of bottom flooding. However, after 900 s the coolant flow steadily decreased. By short increase of the water pressure through operator action, a crust that blocked the coolant flow was broken and coolant flow continued until complete arrest and solidification of the melt. The experiment was ended after 3600 s by stop of induction heating.

The subsequent section describes the test sequence in more detail.

Table 4-3: Realized conduct of the CometPC-H5 experiment

Time, s	Event
until -90	Test preparation as planned, induction coil operating
-90	Ignition of thermite powder, thermite burn completed after 17 s, separation of metal and lighter oxide phases
0 →150	Pour of melt: 358 kg metal + 442 kg oxide melt with 1890°C, completed after 37 s. Onset of dry erosion of sacrificial concrete layer, initial downward erosion rate 0.16 mm/s, averaged over bottom surface. Simulated decay heat about 100 kW. Hydrogen flame at end of off-gas line until 225 s. Aerosol formation due to concrete erosion give diffuse view of the melt surface until about 225 s
150 →700	Dry concrete erosion continues with reduced rate according to heating rate. Maximal downward erosion in the centre is 0.09 mm/s. Heating power increases over 200 to 300 KW.
700	Passive onset of bottom flooding from centre of bottom layer. Coolant water flow-rate 1 l/s. Start of efficient melt cooling by melt fragmentation.
810	Surface of melt completely flooded, but fragmentation still ongoing
900	Porous surface crust dark, as quenched by top water layer. Peak cooling rate 2 MW. Bulk of melt still partly liquid in southern part. Thermocouples indicate stability of water-filled, porous concrete.
after 900	Coolant water flow from bottom starts to decrease linearly with time to virtually 0 at 1250 s. Probable reason: Blockage of flow channels by relocating residual liquid melt.
1253	Operator increases coolant water pressure from 0.1 to 2.0 bar within 11 s. Rupture of surface crust and vigorous ejection of melt into upper water layer over 16 s. Melt is readily quenched, resulting in a steam spike of 0,2 bar. Immediate reduction of water pressure to 0.1 bar. Continuous coolant flow of 1.2 l/s leads to water level of more than 100 cm.
up to 2000	stable cooling, temperatures in porous layers continuously below 100 °C
up to 3600	By operator action, stepwise reduction of heating power to reduce untypical high power density in metal and to account for efficient energy removal from solidified upper melt. Melt is stabilised and coolable. No further erosion and no attack of porous concrete layers. High efficiency of induction heating and its stability indicates complete solidification of the melt. Flooding from sidewall was not activated as melt is arrested before complete erosion of sidewalls. Porosity of melt sufficient to remove simulated decay heat by bottom flooding only.
3600	Planned end of decay heat simulation. End of test
post test	Accumulated coolant water drained out. Test vessel prepared for disassembly and further analysis

Melt generation and pour of the melt were performed as planned. Figure 4-2 shows the reaction period of the thermite (from –90 to –73 s) and the pour starting at time zero. Thermite burn was completed 17 s after the ignition (at -73 s, indicated by the end of oscillations of the weighing system), which is a short reaction time. The subsequent time of 73 s is sufficient to allow complete segregation of metal and oxide phases. Note that the thermite weight has a constant offset of about –75 kg.

Pour of all 800 kg melt to the test vessel, starting at time zero (definition of t = 0 s), is completed after 37 s. The clear change of the slop in Figure 4-2 at 12 s indicates the transition from heavier metal to the lighter oxide flow. It corresponds to the 385 kg metal weight and shows that metal and oxide melts are fully separated. The crucible hood is closed upon completion of the pour after 73 s, so that all gases are directed through the off-gas line.

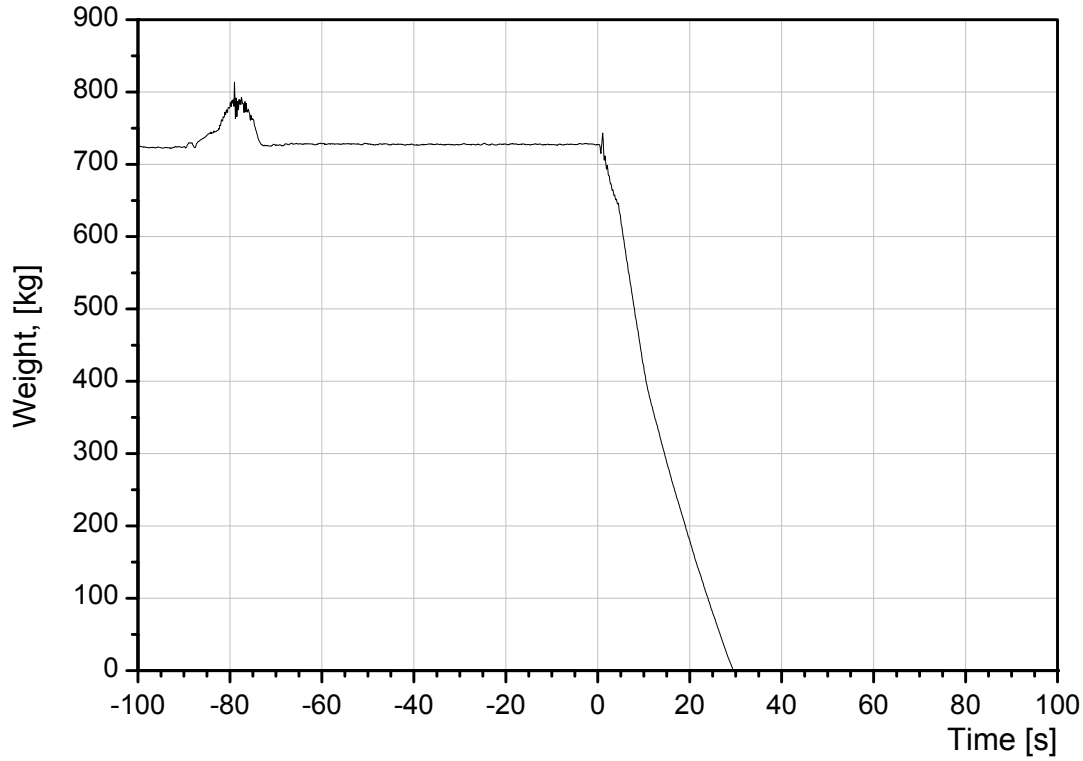

Figure 4-2 CometPC-H5: Weight of thermite vessel during thermite burn and melt release

The initial temperature of the melt as measured in the spout, is given in Figure 4-3. The W/Re thermocouple detects 1890°C during release of the metal and oxide melt between 8 and 14 s, in agreement with the expected 1900°C. The thermocouple fails by the thermochemical attack of the oxide melt at 14 s.

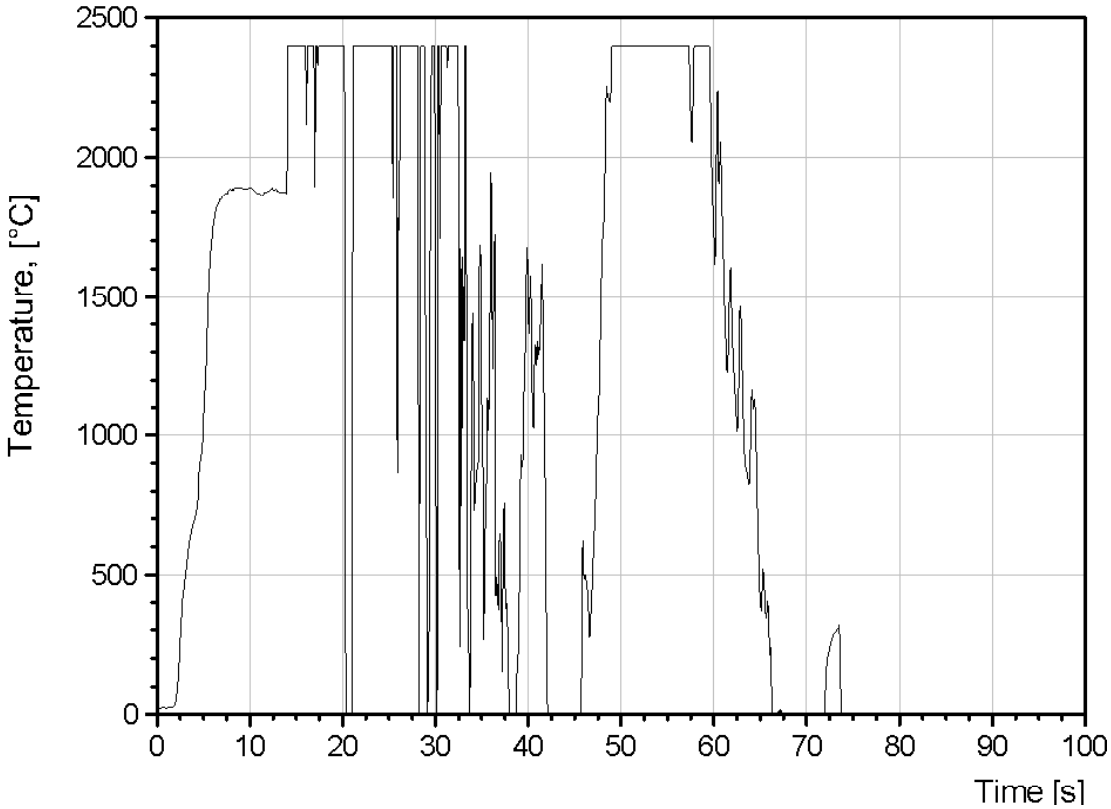

Figure 4-3 CometPC-H5: Initial temperature of melt measured in the spout

As derived from visual observations and the different measurements, the erosion and cooling process is characterized by the following phases:

8. From 0 – 150 s: Dry erosion of the sacrificial concrete layer with release of hydrogen and aerosols from decomposing concrete through the overheated melt with an average downward erosion rate of 0.16 mm/s. About 20 mm of sacrificial concrete eroded (see Figure 4-18). The temperature of the melt is reduced rapidly, as the energy, extracted by concrete erosion is higher than the simulated decay heat.
9. From 150 – 700 s: Balance of decay heat and concrete erosion. Average downward erosion rate reduced to about 0.09 mm/s. But erosion in centre and north-west of the bottom sacrificial concrete layer substantially higher than in southern part of the layer, resulting in variations of the erosion depth of about 20 mm. Thermocouples located in the sacrificial concrete layer at the sidewall, don't register arrival of the melt.
10. From 700 – 900 s: Melt cooling starts by passive water injection from the bottom. Coolant flow reaches about 1 l/s within 10 s after onset of flooding and stays at this high level until 900 s. Thermocouples and post-test analysis show that water ingression started in the centre and north of the centre of the bottom layer. Resulting steam release generates a porous melt, as viewed by the video camera from top. At 810 s, the melt is covered by boiling water that penetrated through the melt. At 900 s, the surface of the melt is dark, signifying the existence of a quenched surface crust. The temperature of the porous concrete layer are 15°C, which is the temperature of the coolant water. Ongoing oscillations of the inductive heating power indicate that the metal melt is still partly liquid. No volcanic eruptions occurred through the surface crust.

11. From 900 -1253 s: Inflow of coolant water reduces linearly with time and reaches 0.15 l/s only at 1253 s. This is possibly due to relocation of a metal or oxide melt fraction that blocks a previously open flow channel.
12. From 1253 – 1272 s: To avoid an uncontrolled course of the experiment, the operator increases the water pressure by connecting the coolant line to the general water supply of the building. The water pressure rises within 11 s from 0.1 to 2 bar, and at 1264 s part of the surface crust of the melt brakes up and about 30 kg of hot liquid melt is ejected into the overlaying water pool. This melt ejection occurs over a period of 16 s with decreasing intensity, and leads to vigorous boiling of the water layer and to strong steam release through the off-gas pipe. The operator reconnects the water supply to the supply tank and the water pressure returns to 0.1. The coolant water flow rate is now 1.14 l/s, that is 15 % above the previous value. The ejected melt forms a particle bed on top of the melt crust.
13. From 1272 – 2000 s: The situation is now stable. The melt is coolable, and the residual liquid melt further solidities, as indicated by the further reduction of the oscillations of inductive heating power and by some thermocouples near the melt front. Starting at 1800 s, the coolant inflow slowly decreases because of the rising water level above the melt, which reduces the effective water overpressure.
14. From 2000 - 3600 s: Decay heating is continued, but the operator reduces stepwise the total heating power from 300 KW to 150 KW, to heat the metal layer at the bottom with a power density, that is closer to the reactor situation after solidification of the upper oxide melt. The temperature in the porous concrete layer is below 100°C throughout the experiment. Inductive heating is terminated after 3600 s, that is 30 min after complete melt arrest and solidification in accordance with the test plan.

Lateral flooding did not start throughout the experiment, as the residual thickness of the lateral sacrificial concrete layer is still 4 cm. The overall lateral erosion of the sacrificial concrete at end of the experiment is therefore the same as downward erosion. Bottom flooding was so efficient that no additional sideward flooding was necessary.

It is evident that the increase of the coolant water pressure by the operator at 1253 s has an important influence on the course of the experiment. The consequences of this intervention are discussed in section 4.3.2 and 4.5.

The following sections discuss important experimental details of the test, as available from different measurements.

4.3 Detailed Test Results

4.3.1 Simulated Decay Power

Figures 4-4 through 4-6 show the characteristics of induction heating from start of melt pour (time 0) until 4000 s for the net power, the voltage supplied to the induction coil, and the efficiency of heating, which is defined as the net power to the melt divided by the total electric power delivered to the induction system. Heating efficiency is equivalent to the inductive coupling of the melt to the electromagnetic field.

The voltage of the induction coil is under control of the operator, who adjusts the voltage to achieve the net power input to the melt (decay power) according to the test plan. The operator uses on-line information about the total power and the net power to the melt.

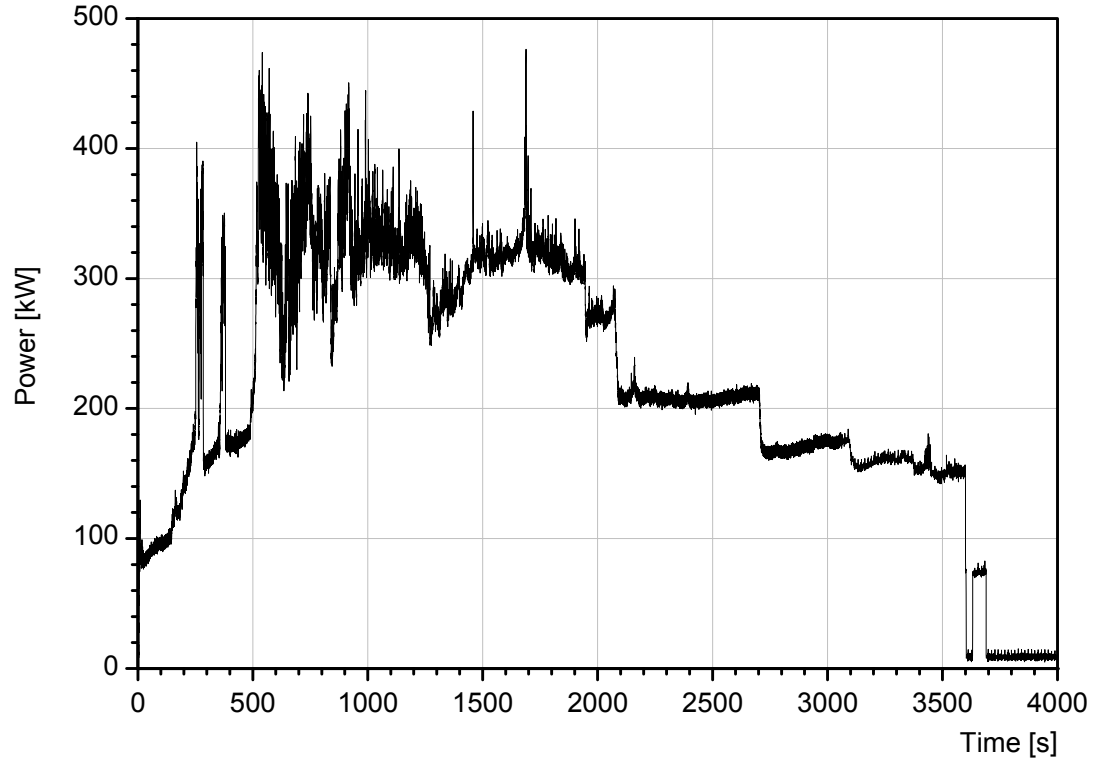

Figure 4-4 CometPC-H5:Simulated decay heat by induction heating of the melt (net power)

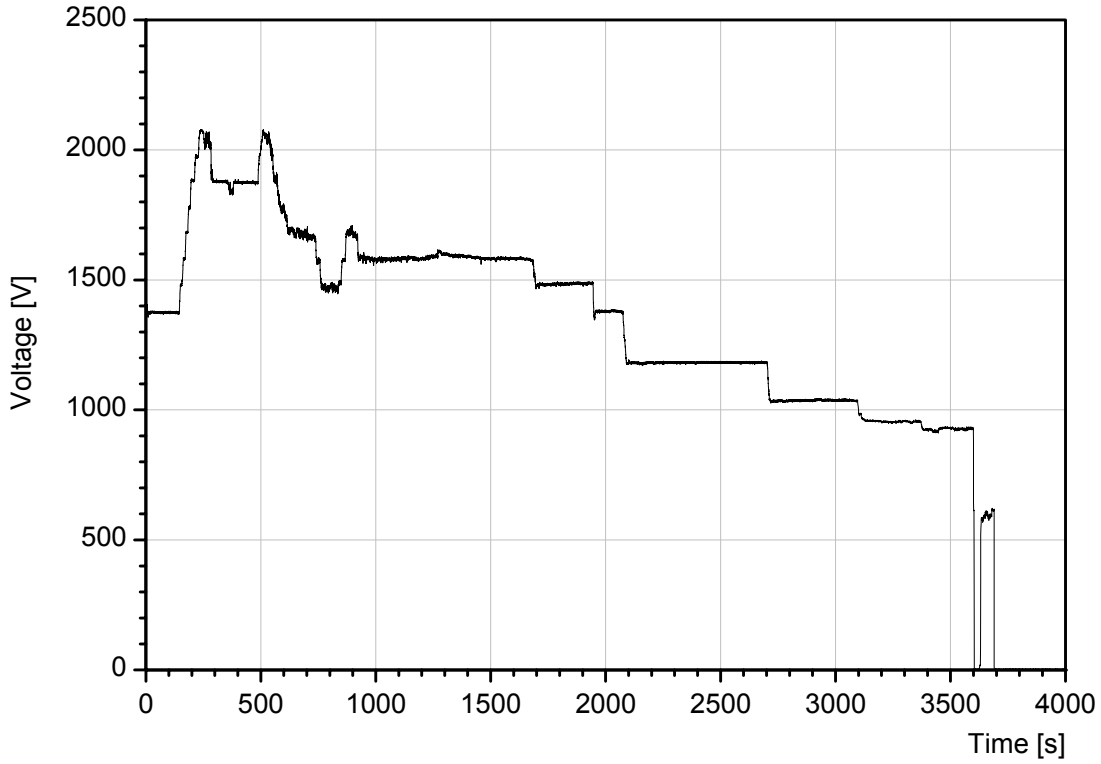

Figure 4-5 CometPC-H5: Voltage of induction coil

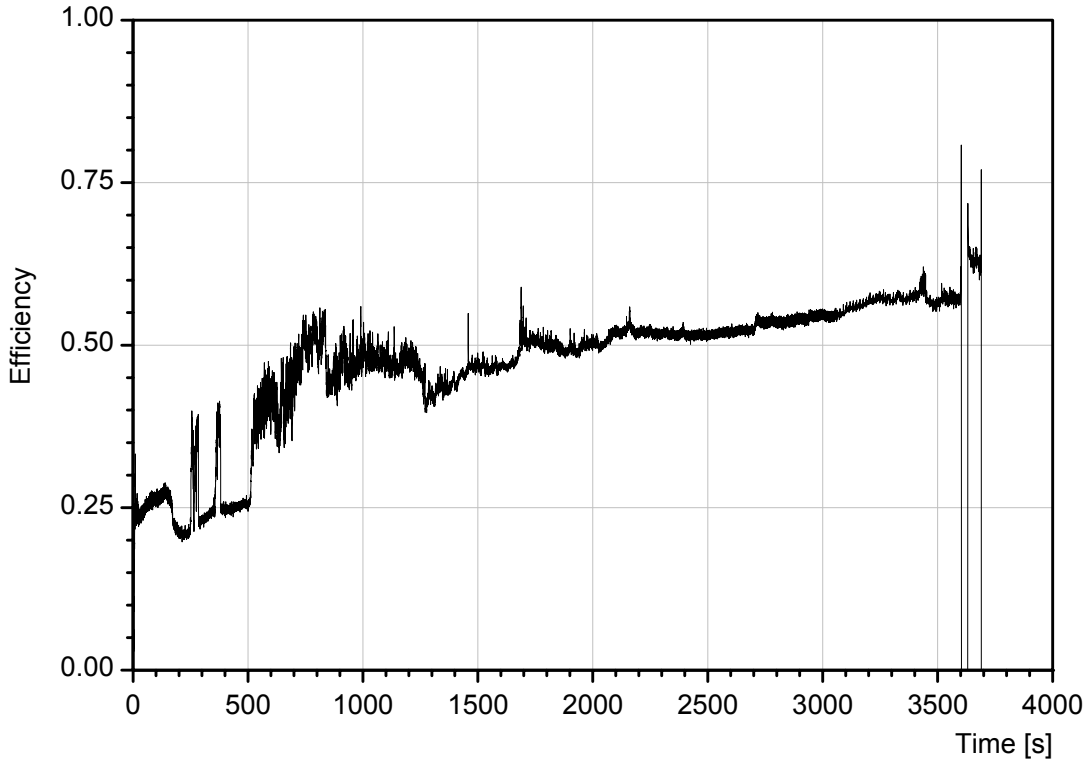

Figure 4-6 CometPC-H5: Efficiency of induction heating

At time zero, the induction coil is operated with a voltage of about 1.4 KV, which is expected to heat the melt with about 150 kW. The initial large distance of the melt to the induction coil and the smaller diameter of the melt (as compared to the previous experiment CoemtPC-H4) results, however, in a lower heating efficiency. Therefore, the operator tries to stabilize the power near 160 KW by increase of the inductor voltage. However, unexpected and rapid transient increase of the heating efficiency from 25 % to 35 % at 270 and 380 s make the control of net power difficult. The reason for the increase of efficiency may be sedimentation of the metal phase after the first intense gas release is reduced. At 500 s, the heating efficiency increases to a permanent elevated value of 35 % or higher. As a consequence, the net power increases to some 350 KW which is maintained by the operator slightly above 300 KW until 1900 s by some reduction of the induction voltage, which accounts for further, slow increase of the efficiency as the melt comes closer to the induction coil.

The strong oscillations which occur in power and heating efficiency especially in the period from 500 to 1000 s, are characteristic for the agitated metal melt. This is also visible for the passive onset of flooding from below, which occurs at 700 s. The continuous cooling process results in an increase of the heating efficiency to about 50 %, which is probably due to onset of melt solidification and transition of the steel crust into the ferromagnetic state. During the further course of the test until 1250 s, a certain reduction of the power oscillations does occur, but the prevailing oscillations indicate that parts of the metal melt are still liquid and not yet sufficiently cooled.

The injection of water initiated by the operator by increase of the water pressure at 1253 s, and the subsequent ejection of metallic and oxidic melt into the overlaying water pool results in fast reduction of the net power of some 50 KW. After this event, coolability is improved, indicated by further continuous increase of the heating efficiency due to transition of solidified

metal layer into the ferromagnetic state. In parallel, the power oscillations decrease with exception of two spikes that indicate some relocation process. At 1900 s, the situation is stable, and the operator reduces in several steps the net heating power to 270, 200, and 150 KW by lowering the induction voltage. At 3600 s, the power is switched off as planned, followed because of technical reasons by a short inductor test. In this late period of the experiment, heating efficiency is close to 60 %, which indicates that the metal temperature is below the Curie temperature of 750 °C.

4.3.2 Coolant Water Flow

Figure 4-7 through 4-10 show the coolant water flow to the bottom of the melt, the approximate water level in the crucible (measured in the isolation gap behind the MgO liner), and long-term and short-term water pressure in the supply lines.

Figure 4-7 clearly shows the onset of passive bottom flooding, which starts at 700 s in the centre of the bottom layer, as localized by thermocouple signals. The coolant flow quickly rises to about 1.2 litre water/s, which corresponds to the expected, efficient flooding rate. Sideward flooding does not occur throughout the experiment, as confirmed by the post test analysis of the sectioned crucible, which shows a residual thickness of the lateral sacrificial concrete of 3 to 4 cm. The flooding rate remains at about 1 litre/s until 900 s and results in a flooded melt surface at 810 s, but then drops gradually to virtually zero, which would have been achieved at 1300 s. This reduction and potential end of bottom flooding would have endangered the induction coil, if bottom erosion through the melt would start again. Therefore, by intervention of the operator, the coolant water supply is connected to the general water supply of the building, and the water pressure starts to rise at 1253 s (Figure 4-9 and 4-10). Within 11 s, the coolant pressure rises by 2 bar to 3.5 bar absolute pressure at 1253 s, at what time the melt crust, which blocks efficient water supply through the bottom surface of the cooling device, breaks up and allows restart of the coolant flow with the previous 1.3 litre/s (Figure 4-7). The coolant flow is reconnected by the operator to the water reservoir and water flow continues with this flow rate until 1800 s.

Thereafter, the water level above the melt surface rises rapidly, as is registered in the isolation gap behind the MgO liner (Figure 4-8). This significant increase of the water level in the crucible reduces the driving water pressure, and the water inflow reduces steadily as plotted in Figure 4-7. The ripple of the flow curve that is seen in Figure 4-7, is due to some oscillations of the level of the water supply tank related to the automatic refill action.

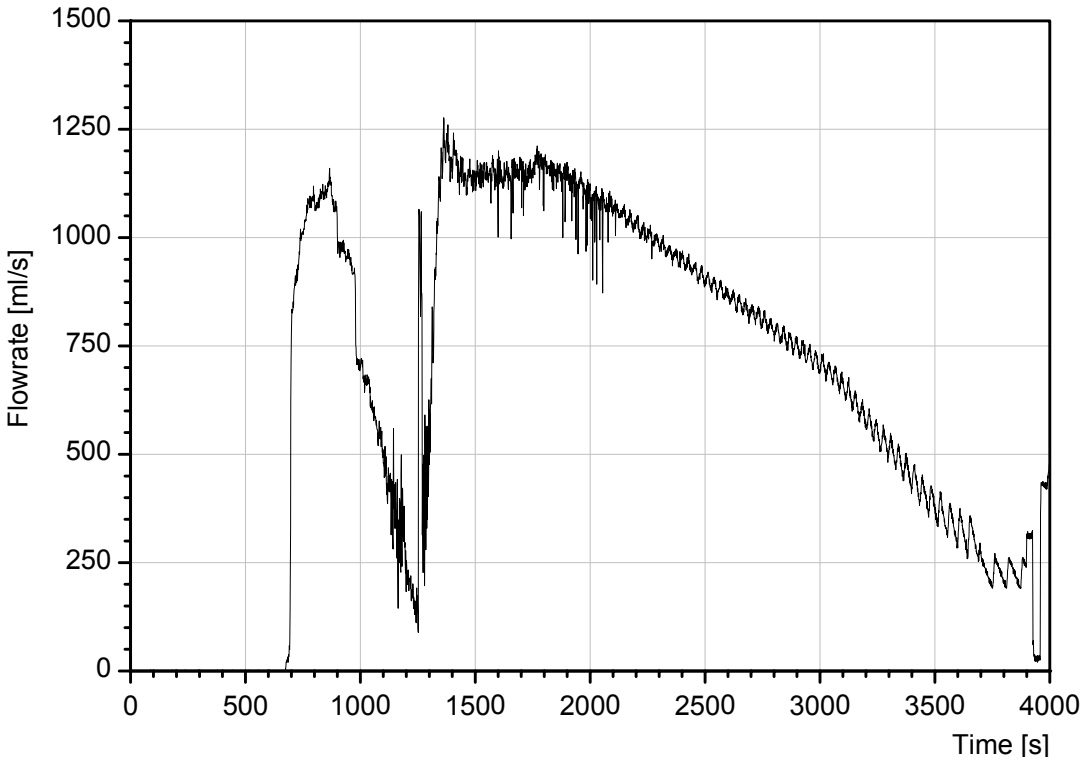

Figure 4-7 CometPC-H5:Total coolant water flow to the bottom of the melt

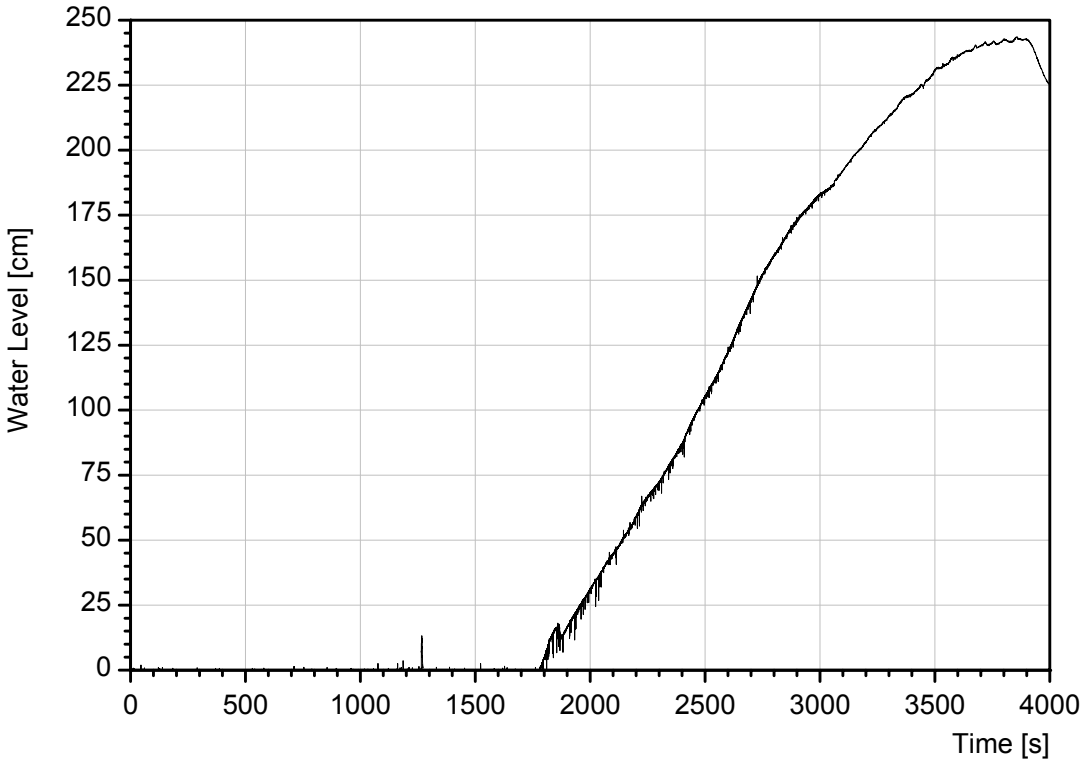

Figure 4-8 CometPC-H5: Approximate water level measured in the isolation gap

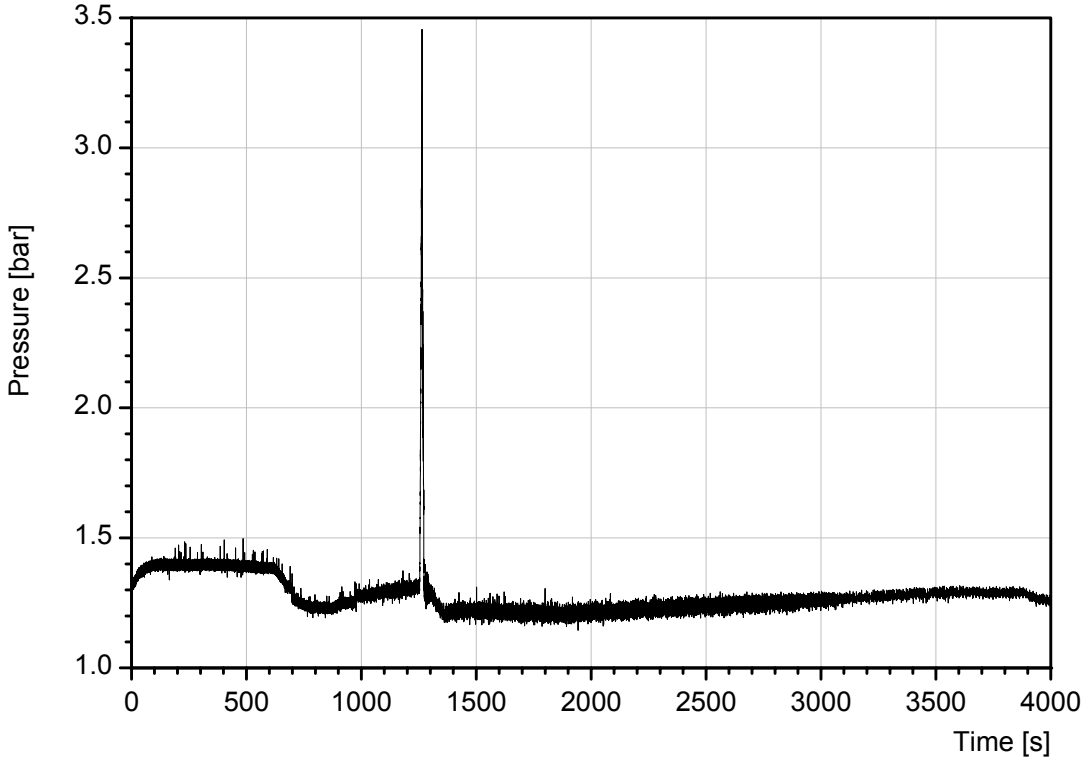

Figure 4-9 CometPC-H5: Coolant water pressure in supply lines

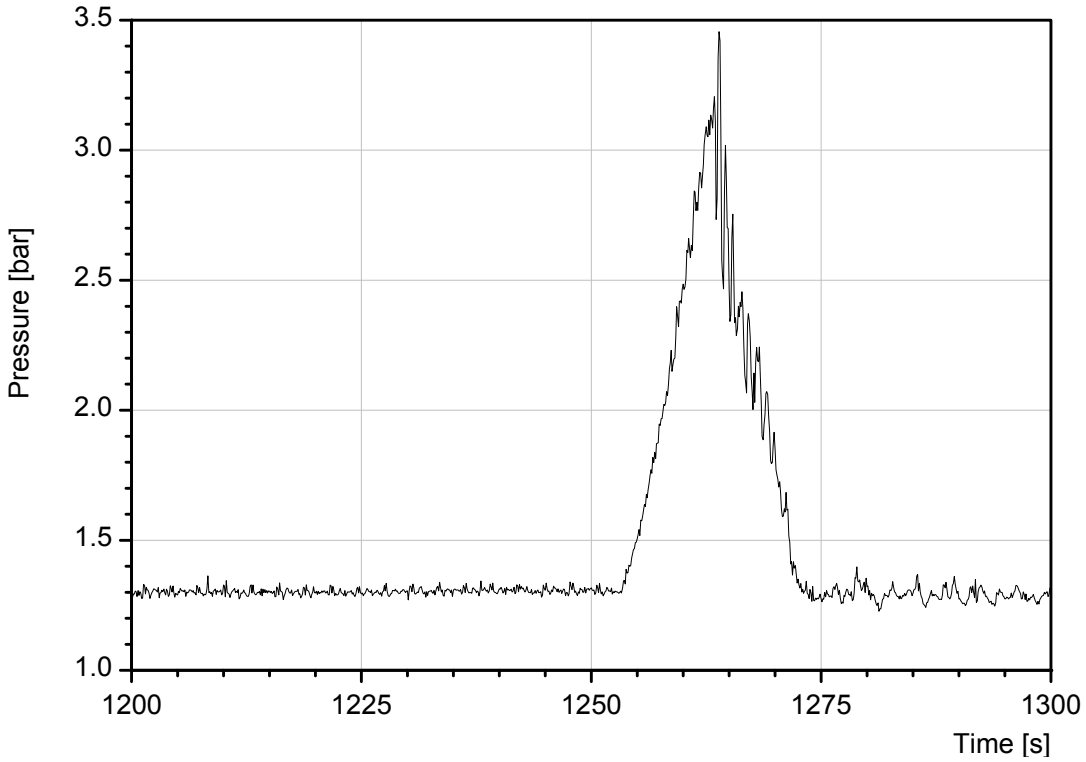

Figure 4-10 CometPC-H5: Water pressure in supply lines during pressure increase

The approximate water level in Figure 4-8 is measured in the isolation gap behind the MgO liner (see Figure 2.2) and therefore detects the water height in the central cavity with a certain delay, especially in the first test phase until about 2000 s, when leakage from the central crucible to the isolation gap is small. Afterwards, the measured trend agrees with the level in the central cavity and shows that the water level on top of the melt is more than 1 meter.

Figure 4-9 gives the absolute water pressure in the coolant supply lines near the water filled porous concrete layer over the total test phase. The absolute pressure of 1.4 bar before onset of flooding is defined by he height of the water supply tank, and corresponds to an effective overpressure related to the bottom of the liquid melt of 0.1 bar. With onset of flooding, pressure drop in the supply lines reduces the effective overpressure depending on the flow velocity. Clearly visible is the pronounced pressure rise when the operator connects the coolant line to the general water supply of the building over a short time period, as given in Figure 4-10 with a higher time resolution.

4.3.3 Heat removal by coolant evaporation

Figure 4-11gives the measured cooling power, which is determined in the off-gas line from the measurements of gas velocity by turbine flow meter and gas temperature by thermocouple. This heat flux is a good approximation of the heat flux that is extracted from the melt by evaporation of the bottom coolant flow.

Before 700 s, some small heat flux is calculated which results from gas release from the ongoing concrete erosion. This heat flux must of course not be attributed to any flooding process, as coolant flow did not yet start. Start of flooding at 700 s results in an immediate steam production, which extracts 1.5 to 2.0 MW from the melt until about 900 s. The subsequent decrease of the cooling rate is mainly due to the reduction of the coolant inflow, as the trend of the extracted power in Figure 4-11 and of the coolant flow in Figure 4.7 are very similar in this phase of the test. Comparison of coolant inflow and extracted power shows that about 50 to 70 % of the injected water is evaporated, the residual water covers the melt surface after 810 s. Integration of the extracted power from 700 to 1250 s yields an extracted energy of 624 MJ, which corresponds to the solidification of about 30 % of he initial melt mass[1]. This means that a substantial fraction of the melt is still liquid.

After 1250 s, when the extracted power has reduced close to the simulated decay heat, the increase of the coolant pressure leads to the break-up of the crust with substantial increase of the water inflow, and the expulsion of more than 100 kg of metal plus oxide melt into the overlaying water layer. This results in a pronounced steam spike with an energy flux of more than 4 MW. The high gas flow overloads the turbine flow meter, which gives no further valid data until end of the experiment.

[1] The enthalpy difference of the oxide from 1500 to 100°C is 1851 J/g, of the metal 987 J/g, calculated with GEMINI [2]

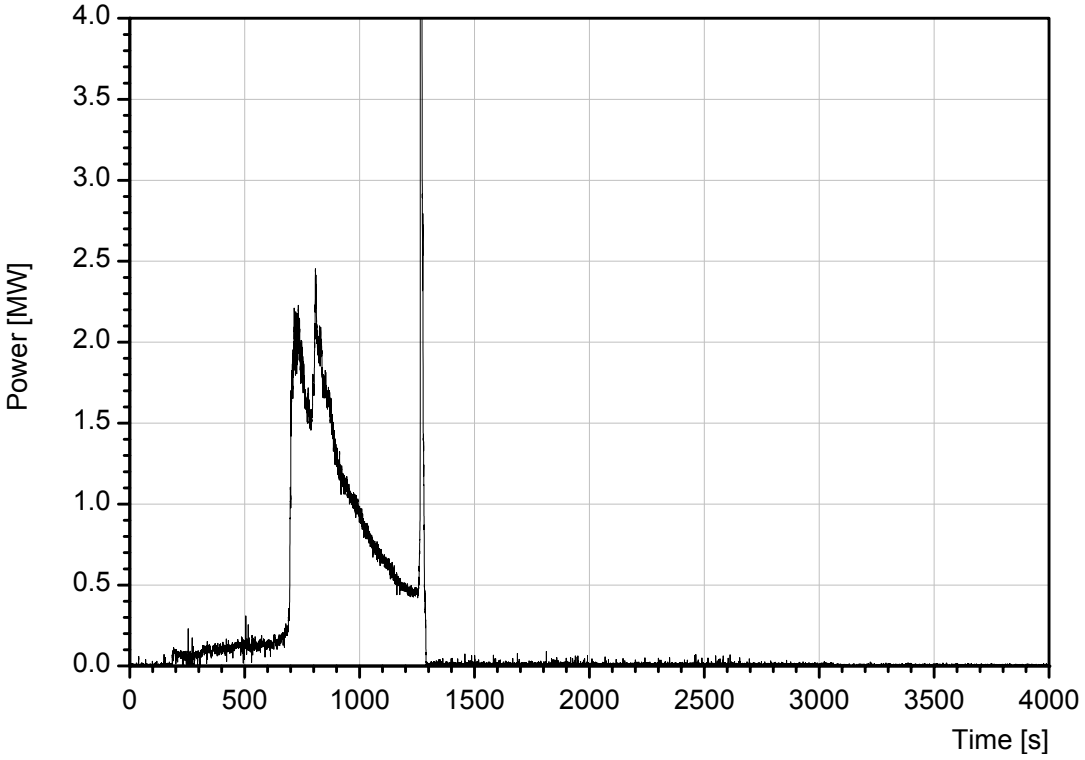

Figure 4-11 CometPC-H5: Power extracted by evaporation of coolant water (turbine system)

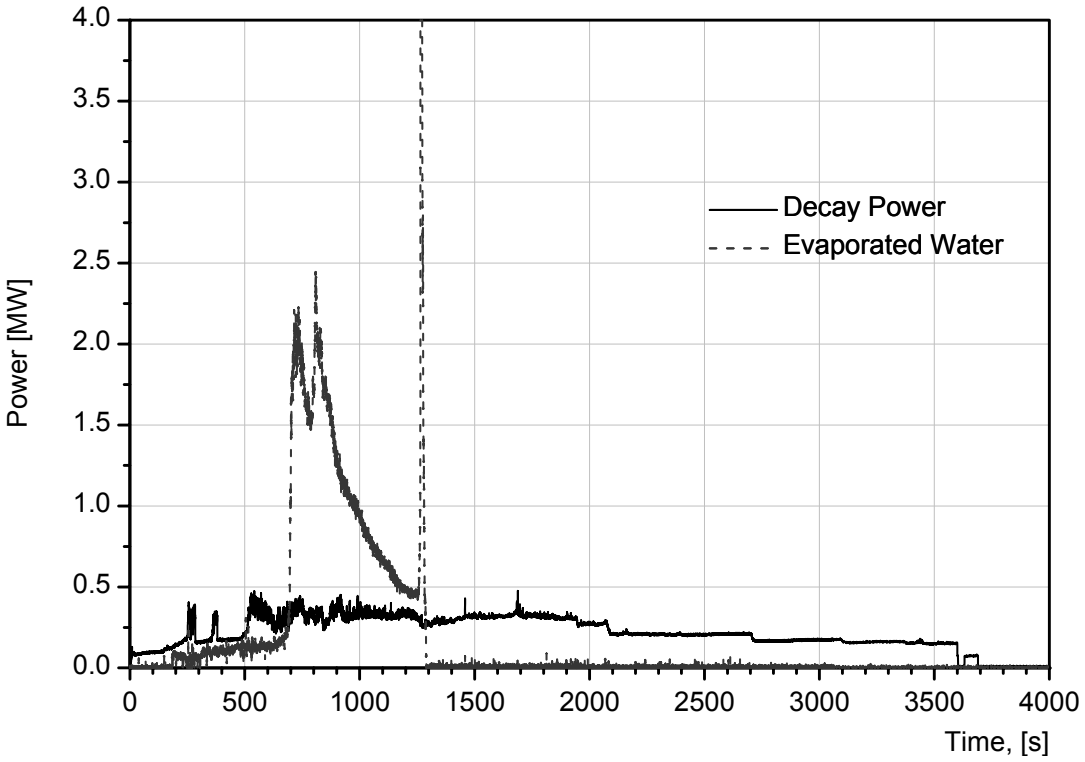

Figure 4-12 CometPC-H5: Simulated decay power and power extracted by evaporation

Figure 4-12 compares the simulated decay power in the melt and the power measured in the steam flow from Figure 4-11. After onset of bottom flooding, the extracted heat flux is higher then the simulated decay power. Nevertheless, the melt is only partly solidified after 1000 seconds, when inflow of the coolant water is blocked probably by some melt relocation. After 1300 s, no comparison is possible because of lacking data for the extracted heat flux. But because the melt is stabilized in the long term, the extracted heat flux must equal the simulated decay power.

4.3.4 Gas Release

This section describes the gas flow during the test, measured in the hood of the crucible and in the off-gas line, which connects the crucible with the open atmosphere.

The gas pressure in the hood is given in Figure 4-13, showing a practically constant atmospheric pressure, with the exception of a pressure spike of about 0.2 bar above the ground level. This spike is a result of the expulsion of the melt near 1250 s with the fast steam production from the quenching process.

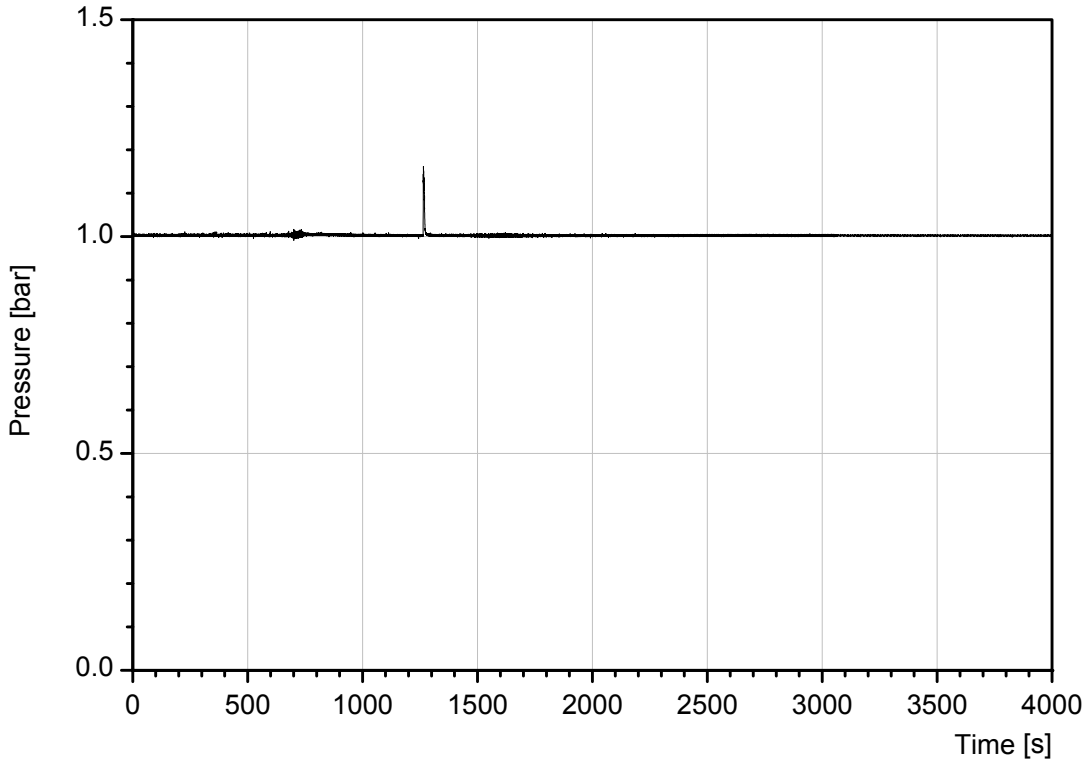

Figure 4-13 CometPC-H5: Gas pressure in the hood of the crucible

The off-gas temperature in the crucible hood is given in Figure 4-14, measured by a thermocouple protruding into the gas volume. This temperature is used to determine the enthalpy of the steam flow after onset of bottom flooding as discussed in section 4.3.3.

When the melt is poured into the crucible, the off-gas temperature rises up to 520°C, and then reduces to about 350°C during the first phase of dry concrete erosion. These temperatures are of course lower than at the melt surface , because the gases deposit part of their energy to the colder structures of the upper crucible. With onset of bottom flooding at 700 s, the gas temperature first drops to the boiling temperature of water. Subsequently the steam temperature rises to 180°C, and then falls back to 100°C, when the melt surface is covered by a water layer. The short temperature spike up to 620°C near 1250 s is due to quenching of the expelled melt . The long term gas temperatures below 100°C are due to the admixture of cold argon cover gas in the upper crucible, and produces some condensation.

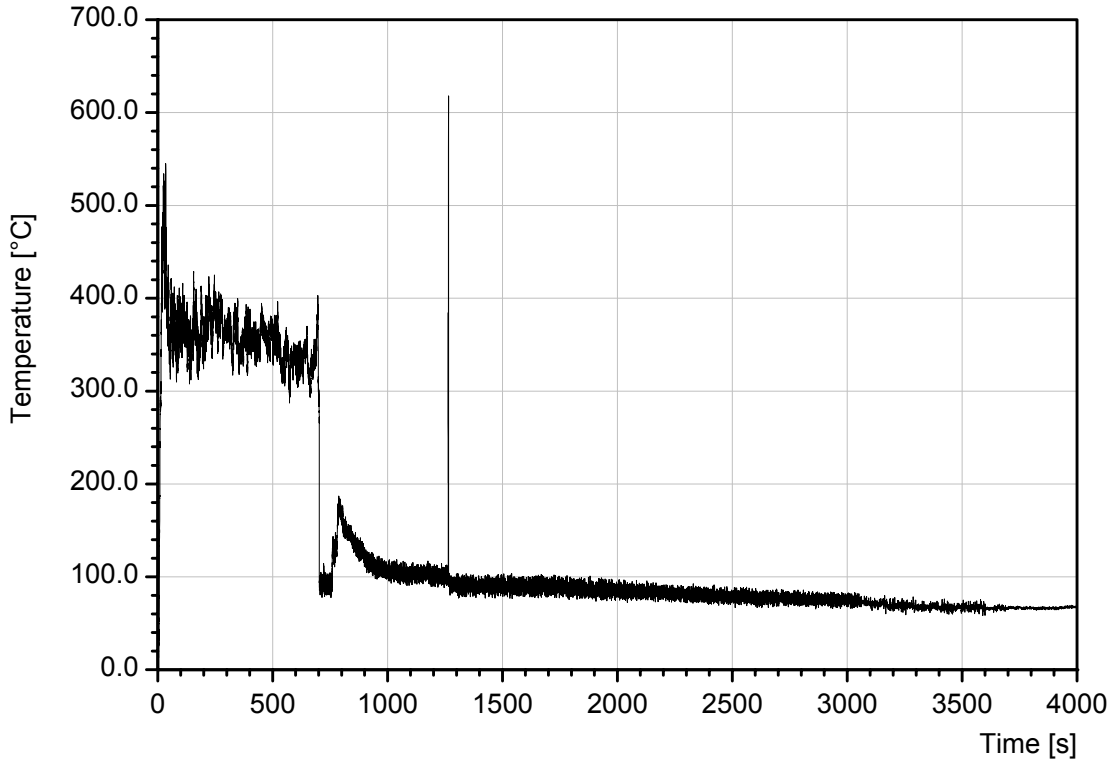

Figure 4-14 CometPC-H5: Gas temperature in the hood of the crucible

Gas composition was measured online by a quadrupole mass spectrometer that detects up to 8 chemical species. Figure 4-15 shows the results for the gases H_2, CH_4, CO, and CO_2. (The steam content could not be detected by this system, because of principal limitations of the spectrometer: As steam would damage the analysis system, steam flow in the analysis system was removed by condensation.) The constant argon cover gas flow is not shown in Figure 4-15, but was used as the reference to determine the release rates of the species based on their measured concentration. The mass spectrometer was calibrated before and after the test with 5 test gases of different compositions.

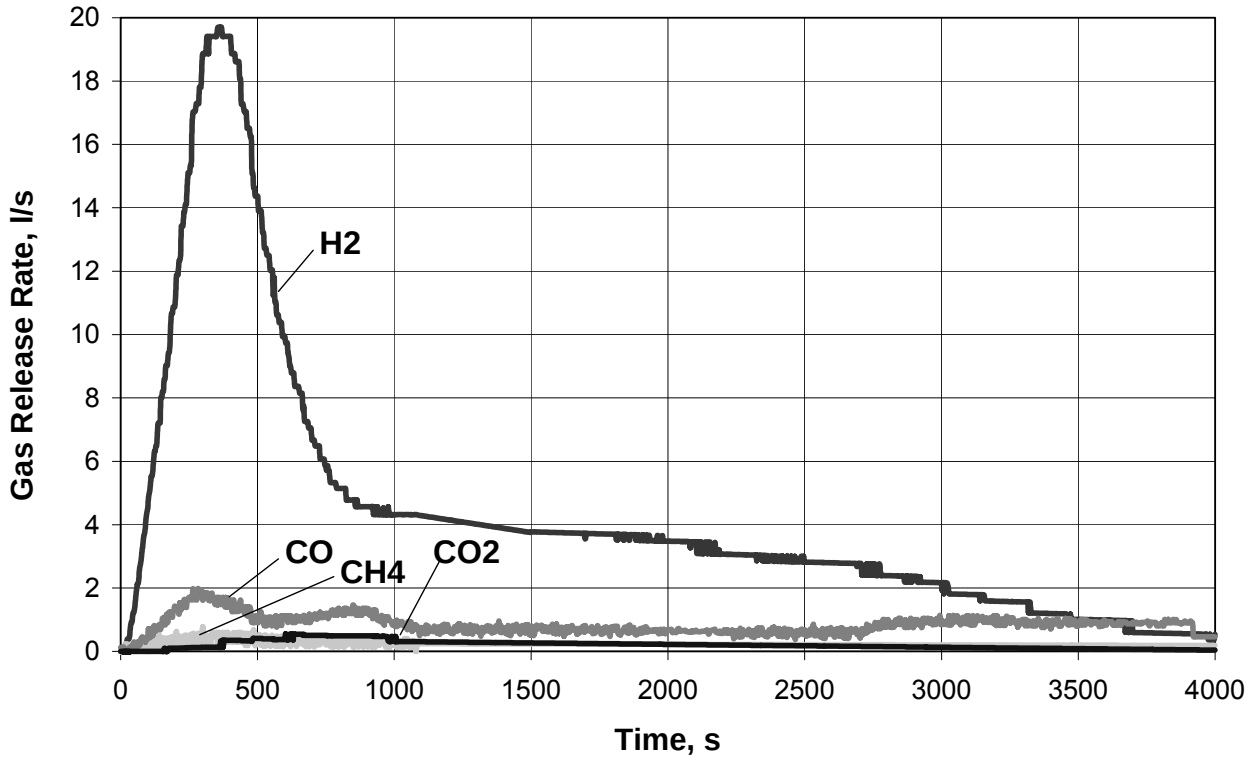

Figure 4-15 CometPC-H5: Release rates of H_2, CH_4, CO, and CO_2 in the off-gas, measurements beyond 1000 s only tentative

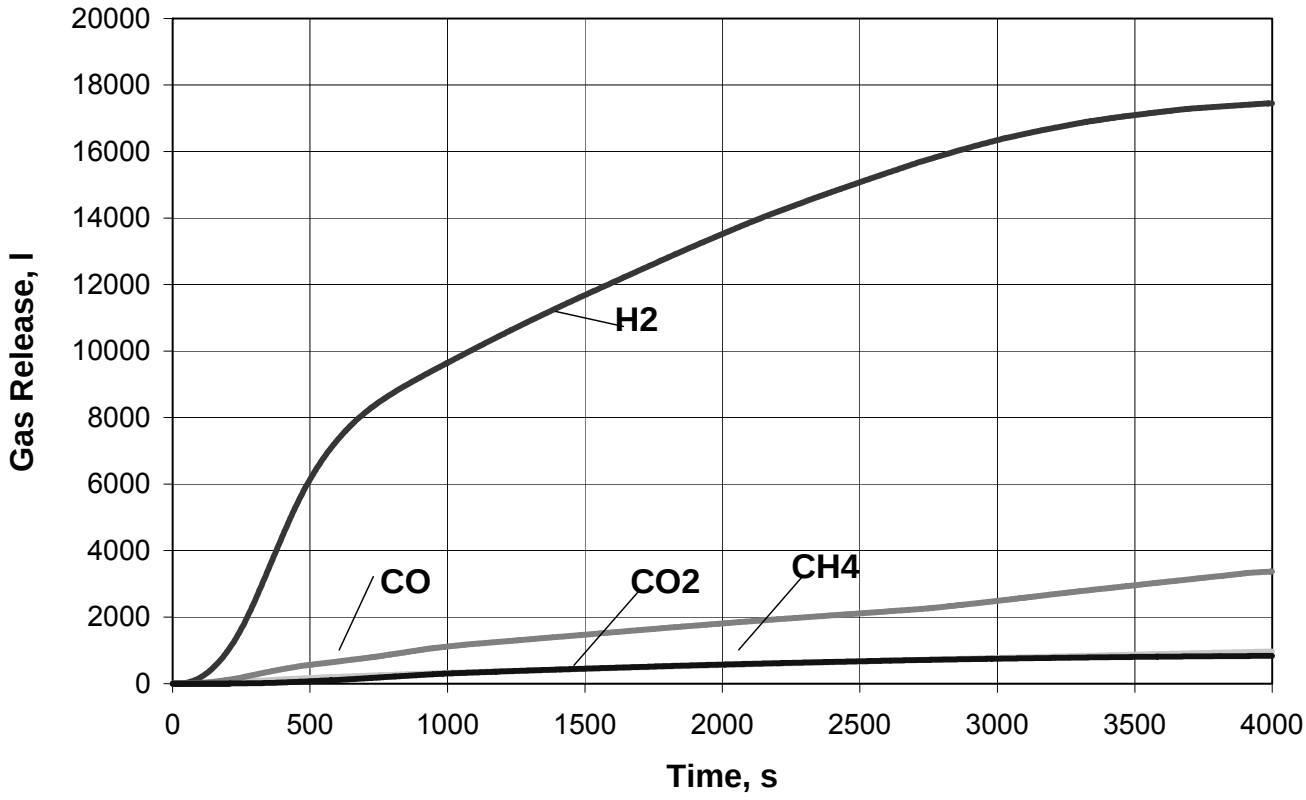

Figure 4-16 CometPC-H5: Integrated gas release of H2, CH4, CO, and CO2 in the off-gas, measurements beyond 1000 s only tentative

The release rates are given in litre/s at standard gas conditions: 1 l/s corresponds to 1/22.4 mole/s. Note, that due to the long response time of the gas analysis system, the time axis for the gas rates should be shifted by about 30 s to the left side to allow time correlation with processes in the crucible. Furthermore, because of substantial blockage of the detector gas line after 1000 s, the response time is substantially reduced and the detected gas composition is uncertain.

The measurements of the gas rates in Figure 4-15 show a clear hydrogen peak until 500 s, which occurs during dry erosion of the concrete as a result of the reduction of steam through the iron in the metal phase. In agreement with previous experiments with siliceous concrete, the release of CO is about 1/10 of the H_2 rate, whereas CO_2 and CH_4 rates are very small. The very small release of CH_4, if any, is an important information because of the potential formation of organic iodine in the reactor situation. The reduction of the gas rates after 400 s are due to the reduced erosion rate of the concrete, as erosion, after decrease of the initial melt overheat, is now determined by the simulated decay heat level.

No extra hydrogen peak is generated by onset of bottom flooding at 700 s. This may indicate that the temperature of the iron melt is so low that the chemical reaction rates are slow.

As the gas release rates after 1000 s are not reliable, they are not discussed here.

Figure 4-16 gives the integrated gas release as determined by integration of Figure 4-15. Again, data after 1000 s should be disregarded.

The aerosol concentration was measured in the off-gas by the absorption of a laser beam that passes the off-gas line. The extinction E is defined by the logarithmic ratio of the intensity I/I_0 of the laser beam before and after transmission through the off-gas tube

$$E = \ln (I/I_0)$$

and is in the present application a qualitative information of the aerosol density.

Figure 4-17 shows from 0 to 700 s aerosol release during the phase of dry concrete erosion. With onset of flooding, aerosol release is, however, drastically reduced, and is practically zero, when the coolant water has flooded the melt surface. This means that aerosol formation is reduced by formation of a crust surface, and that in addition aerosols are trapped in the water overlayer. The aerosol signal after 1250 s, when the melt was expelled into the water overlayer, is strongly influenced by steam droplets in the off-gas line, and must not be interpreted as relevant for particle emissions.

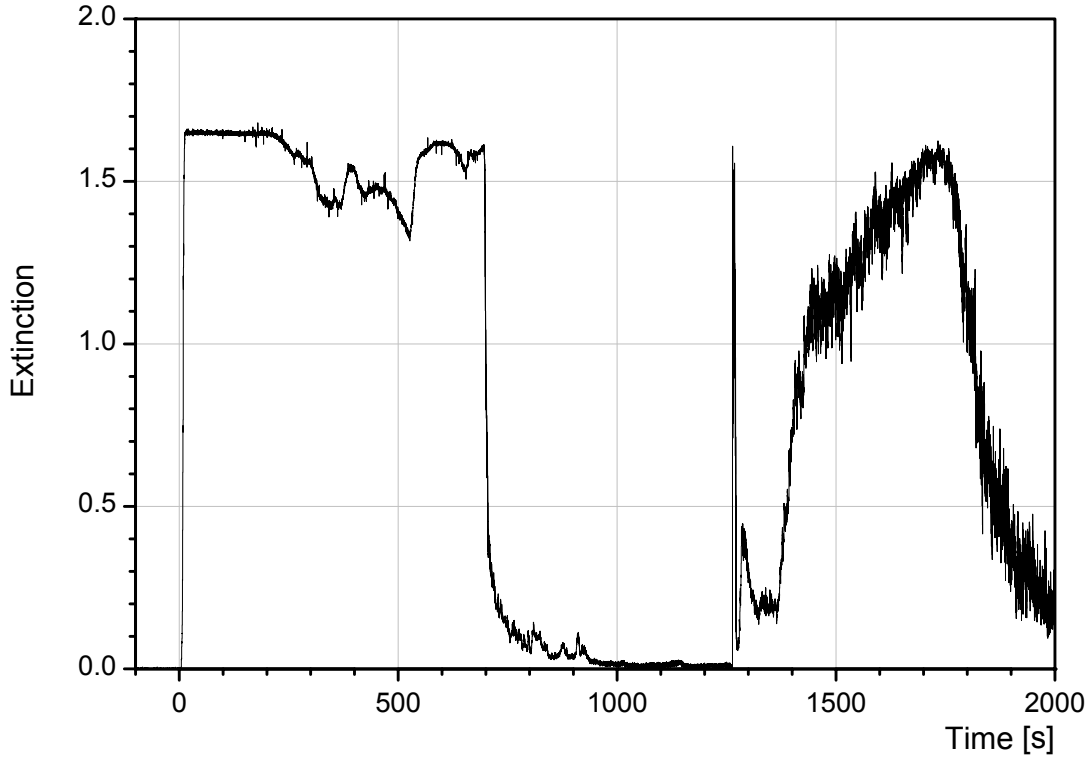

Figure 4-17 CometPC-H5: Extinction of laser beam by aerosols in the off-gas line

4.3.5 Concrete Erosion and Heat Fluxes

The downward erosion of the sacrificial concrete layer was determined from the failure time of a series of thermocouples, which were located in the centreline of the coolant device and in the middle of the 4 quadrants, named NW, SW, SE, and NE, respectively. The position of the thermocouples referred to the upper surface of the porous concrete layer (0 mm), is + 10, + 20, + 40, and + 60 mm, respectively. The top of the sacrificial concrete layer corresponds to + 80 mm. Thermocouples in the porous, water filled concrete layer are located at the height of – 5, – 20, and – 50 mm.

Figure 4-18 shows the measured downward erosion front in the sacrificial concrete versus time over the period from 0 to 1200 s. At 10 s, the erosion starts at the upper concrete surface (+ 80 mm). For the first 20 mm of concrete erosion, the typical detected erosion rate is 0.16 mm/s with only minor deviations of ± 25 % in the centre and the four sectors of the concrete surface. This erosion rate is in good agreement with the 0.20 mm/s detected in the preceding experiment CometPC-H4, and with 0.17 mm/s measured in experiment CometPC-H3 [1]. This initially high erosion velocity is predominantly due to the initial overheat of the melt and exceeds the rate, that corresponds to the simulated decay heat.

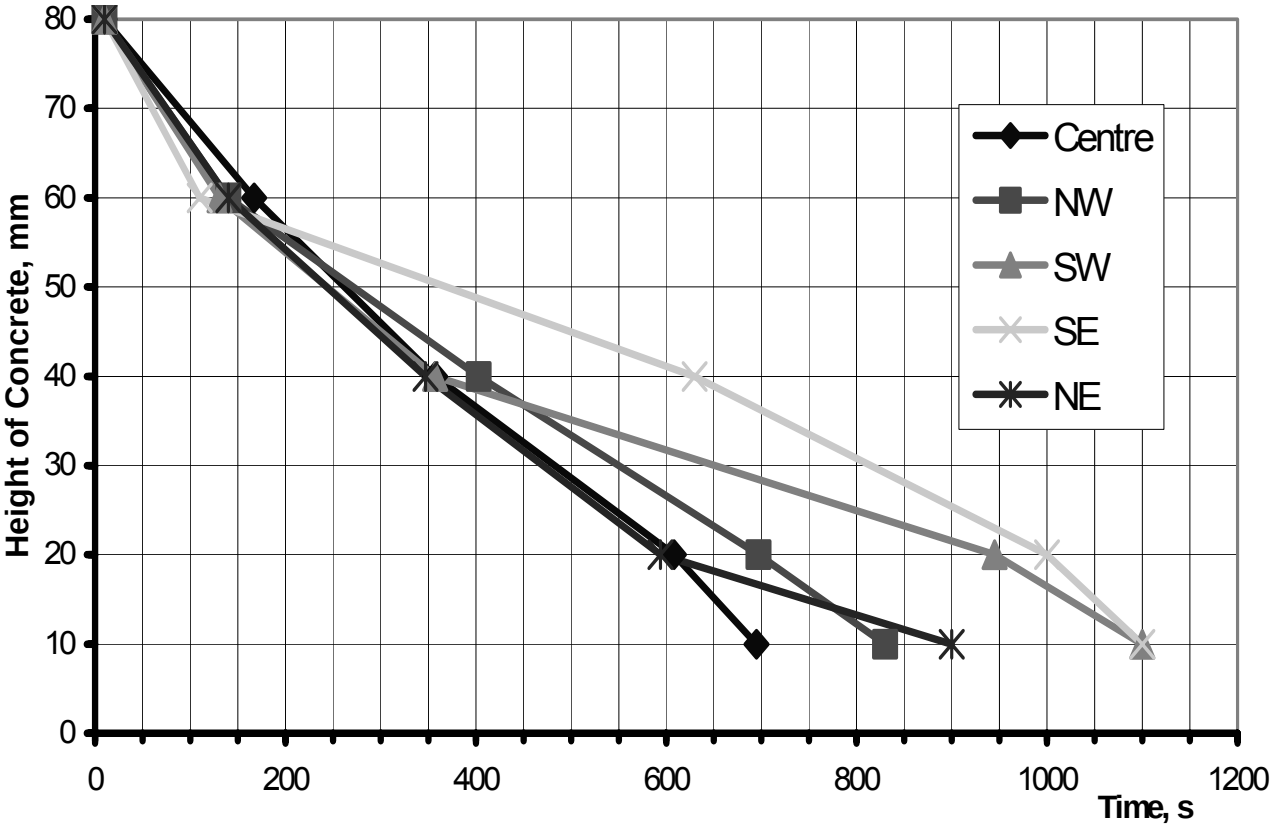

Figure 4-18 CometPC-H5: Erosion front of propagating melt in bottom concrete, based on thermocouple measurements

With decrease of the temperature of the melt, the erosion velocity reduces, but in an incoherent way. The maximum erosion rate occurs in the centre and northeast of the surface, with a nearly constant rate of 0.092 mm/s. The lowest erosion rate is observed in southeast and is 0.043 mm/s, which is only half the erosion rate. Extrapolation of the erosion curves in Figure 4-18 shows that water ingression indeed is expected near 700 to 800 s, when the zero level is reached. No further erosion into the porous concrete layer is detected during the further test period, as is also confirmed by the sectioned crucible in Figure 4-20. However, after onset of bottom flooding erosion in the sectors southwest and southeast continues until about 1200 s, when the melt reaches the porous concrete layer and is arrested.

For the sideward erosion, a time-resolved erosion rate can not be determined because of insufficient thermocouple instrumentation. One of 8 thermocouples that are located 110 mm behind the initial concrete surface of the cylindrical section and 10 mm above the zero level, detects 1200°C after 2050 s, followed by onset of local cooling. The average final lateral erosion is 8 to 9 cm as determined from the residual thickness of the lateral sacrificial concrete layer in Figure 4-20. Sideward erosion was indeed terminated only through cooling from the bottom, without any passive lateral water injection. It is therefore concluded that the time averaged sideward erosion rate is equal to are below the downward erosion rate.

The erosion velocity can be translated to the downward heat flux from the melt, using the properties of the concrete

$$Q_{down} = A \cdot \Delta h_{decomp} \cdot \rho \cdot v ,$$

where Q_{down} is the downward heat flux, A the eroded bottom surface (0.374 m^2), Δh_{decomp} the decomposition enthalpy of the sacrificial concrete (2.1 MJ/kg), ρ the density of concrete (2300 kg/m^3), and v the erosion velocity. For a complete energy balance, sideward and upward heat fluxes must also be considered.

For the average initial velocity of 0.16 mm/s until 200 s, the downward heat flux alone is 290 KW from equation (1), to which the unknown sideward heat flux must be added. This is of course higher than the simulated decay heat and results in a fast temperature drop of the melt in the early erosion period with the consequence of reduced erosion velocity later on. The downward heat fluxes after 200 s are 167 KW for 0.092 mm/s erosion speed, and 78 KW for 0.043 mm/s, which under consideration of lateral and upward heat fluxes, indicates a balance between erosion rate and simulated decay heat.

4.4 Post Test Analysis

The apparatus was carefully disassembled in order to document the debris configuration with respect to coolability. Figure 4-20 shows the surface of the solidified melt as removed from the apparatus. The uppermost layer is formed by a porous layer of loose particles, diameter 0.5 to 4 mm, which are partly solidified in the form of hollow half-spheres. This material is predominantly oxidic, but includes also metallic particles. The mass of this layer is about 30 kg and was ejected during the vigorous melt eruption after 1253 s over the period of 16 s. This layer was removed before sectioning the crucible in the vertical direction.

Figure 4-20 is a photograph of the vertical section through the centreline of the solidified melt in the direction east-west, as viewed from south or north, respectively. The photo shows that the melt solidified before complete erosion of the lateral, sacrificial concrete layer, of which a residual layer of 3 to 4 cm still exists. Therefore, the water filled, lateral porous ceramic layer was not contacted by the melt and no lateral water ingression did occur. Consequently, all cooling occurred by bottom flooding only.

Progression of the melt into the downward direction occurred down to the interface of the water filled, porous bottom layer of ceramic, where some of the loose ceramic tiles are still existing. These tiles are partly broken, but do not have tight contact with the sublayer, so that they allow the bottom water inflow. The porous ceramic layer was not attacked by the melt.

The metallic fraction of the initial 800 kg melt is solidified at the bottom of the cooling device. The metallic regulus is porous in the centre of the surface where water injection started. Porosity is however small in the outer regions of the diameter. Higher porosity is visible in the ceramic layer on top, and permeability for water is adequate.

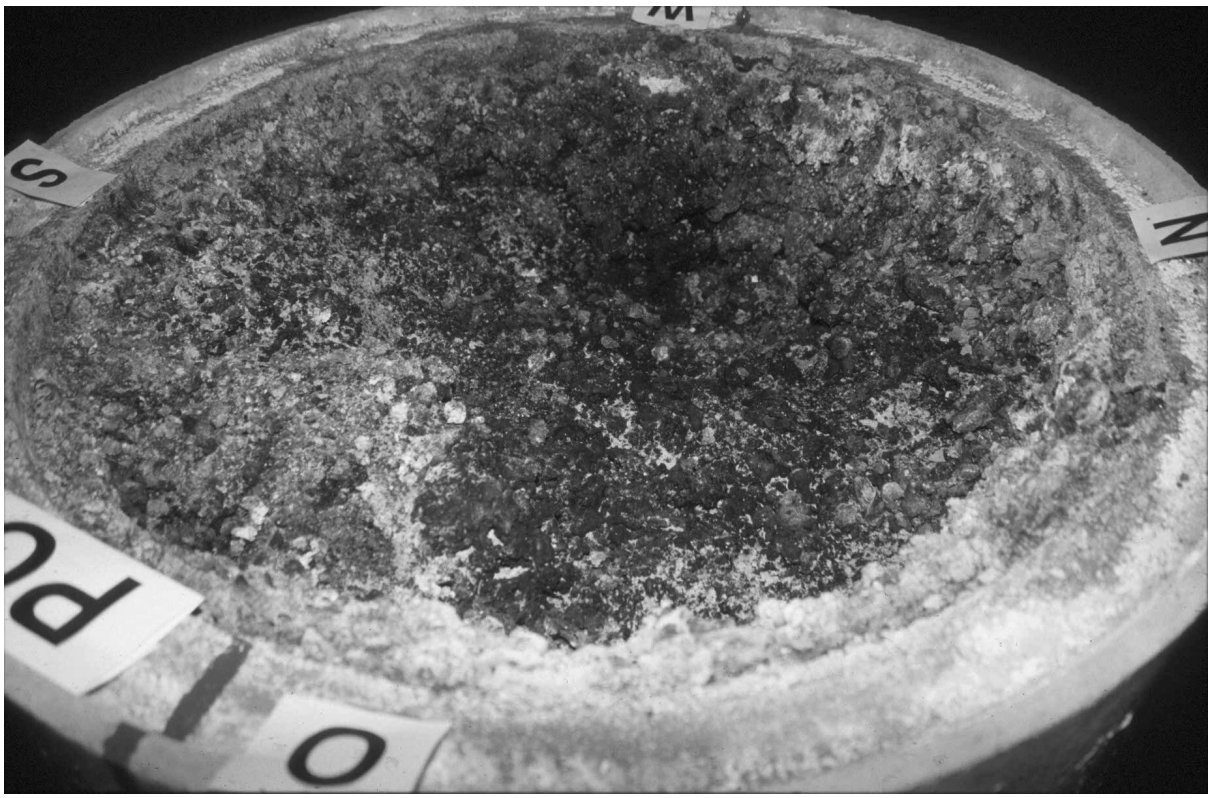

Figure 4-19 CometPC-H5: Top view of solidified melt with porous surface

The oxide layer in Figure 4–20 consists of 2 layers:

- The lower layer, mean thickness about 50 cm, with rough surface and pronounced peaks and valleys. This is the oxide melt as solidified after the first process of bottom flooding. This layer also includes one large cavern in the western part (Figure 4-20) that was generated during the strong melt eruption after increase of the water pressure. The cavern is about 170 mm wide and has an opening to the melt surface of some 70 mm diameter through which the melt was ejected. The porous structure in the other parts of this layer were formed by the moderate, long lasting steam-water flow from the bottom.

- Above this layer exists a porous layer of coarse material with high porosity, mostly particles of 10 to 40 mm diameter that are to a certain degree welded together. This layer is predominantly oxidic with a small metal content and was formed by the material that was ejected after increase of the coolant water after 1253 s. Its thickness is up to 200 mm. Because of its low mechanical strength, this layer was partly destroyed during sectioning of the crucible. It is still visible on the northern section of the crucible, but only little is retained on the southern part.

As mentioned above, the uppermost 3rd layer of loose material of finer particles were removed before sectioning of the crucible.

The outer crucible with the polypropylene shell and the layers of course and fine porous material are completely intact as their temperature did not exceed 100°C throughout the test.

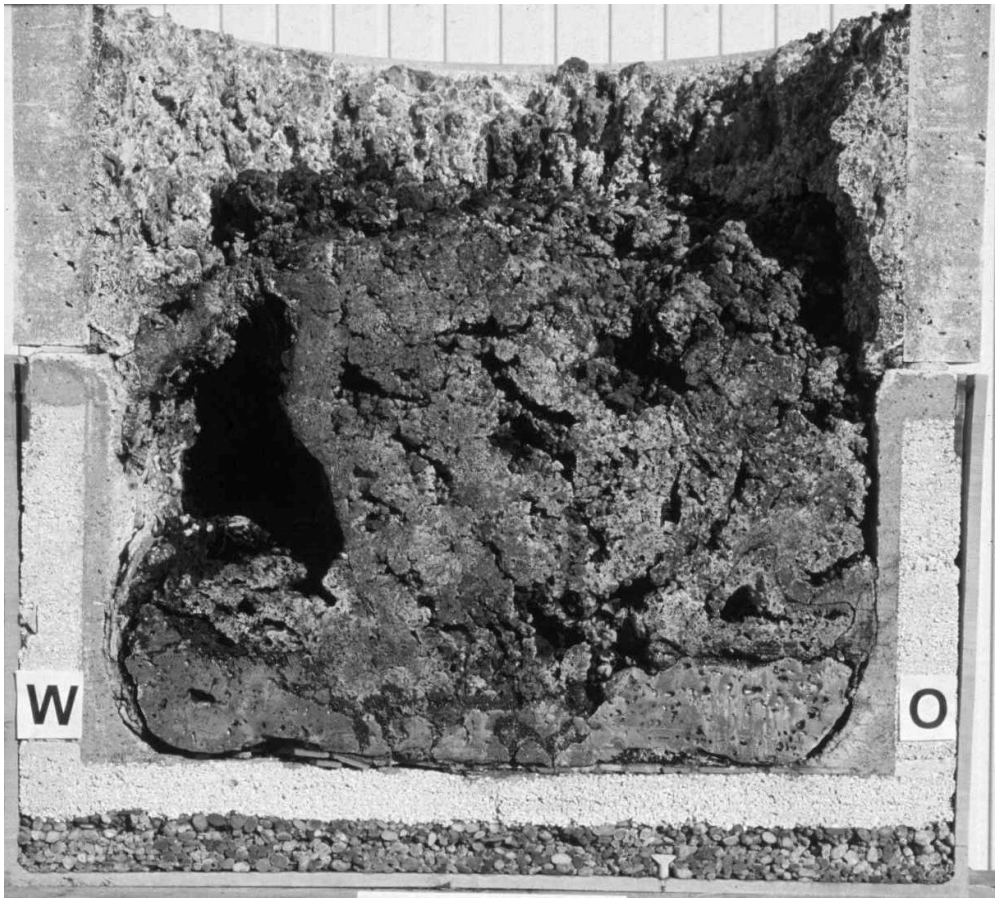

northern part

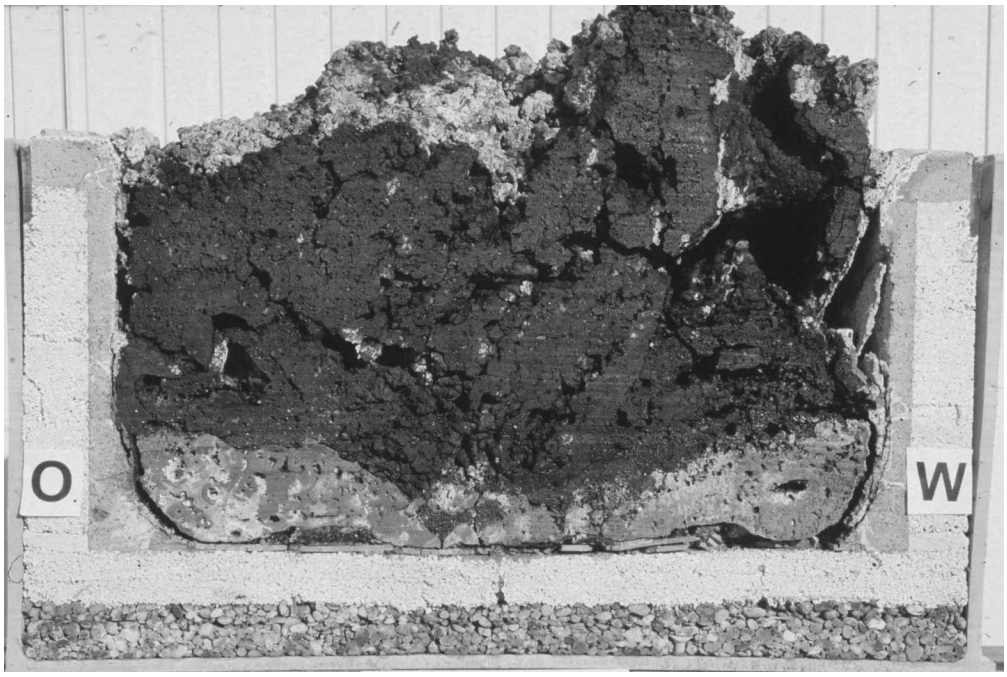

southern part

Figure 4-20 CometPC-H5: Solidified melt, sectioned in direction east-west

4.5 Conclusions for the actual test CometPC-H5

The experiment CometPC-H5 is the second 3-D cooling test and follows the set up of the CometPC-H4 experiment. The thickness of the sacrificial concrete layers at bottom and side were modified, so that flooding started from the bottom as expected.

The experiment is described by the following test phases: After poor of 800 kg melt and with sustained heating of 300 kW typical, dry concrete erosion gives similar downward and sideward erosion rates. The erosion of the bottom sacrificial concrete is, however, not homogeneous and is faster in the centre. Therefore, local onset of flooding from the bottom starts mainly in the centre of the bottom surface at 700 s with a water flow rate of about 1 l/s. This leads to large cool down of the melt and onset of porous solidification of the melt. The surface of the melt is flooded after 810 s, and the porous surface crust is dark (cold) at 900 s. The peak cooling rate was 2 MW, which is a factor 8 higher than the decay power.

However, as indicated by ongoing hydrogen release and oscillations of the net inductive heating power, the melt is still partly liquid especially in the southern part of the cooling surface. Thermocouples indicate further erosion of the residual sacrificial concrete layer, while the water-filled, porous layers at the bottom and sidewalls are stable and remain at low temperature. Starting from 900 s, the water inflow to the bottom of the melt (only bottom flooding is active) decreases steadily from 1 l/s to 0.1 l/s at 1250 s. This reduction may have been caused by a redistribution of some liquid melt fraction which may block the coolant flow channels. To exclude an unpredictable experimental development, the operator increases the pressure of the coolant water at 1253s. The water overpressure pressure rises from 0.1 bar by about 2 bar within 11 s. At this point in time, the pressure breaks up the melt and by a vigorous eruption, a significant part of the melt is ejected into the upper water layer. Fast quenching of the hot melt results in a transient steam pressure above the melt of 0.2 bar above ambient pressure. Upon this event, the water overpressure is immediately lowered to the former 0.1 bar, and the resulting continuous flooding rate is again close to 1 l/s. The melt is now coolable, and decay heating is continued until 1 hour. No further erosion is observed, the melt is stabilised and solid, and decay heat is safely removed.

The section through the solidified melt shows that the porous coolant layers were not attacked. The lateral, sacrificial concrete layer at the inner cylinder wall was not completely eroded, so that flooding from the side was not activated, which means that bottom flooding alone was sufficient to cool the melt. The porosity of the solidified melt is sufficiently high to allow removal of the decay heat.

The unexpected result of this experiment is, however, the drop of the coolant water flow after successful onset of cooling. It is not clear, how this experiment would have developed without intervention of the operator to increase the coolant pressure: Partial re-melting of the crust would probably have taken place, with the potential of formation of new porosities and flow paths, or with some attack of the porous, water filled bottom layer.

5 Conclusions for the Cooling Concept

The reported 2 experiments conclude the test series on bottom flooding through a porous concrete layer, and include investigations on lateral melt stabilisation. The experimental series investigated cooling of sustained heated melts of 600 to 800 kg with oxide and metal melt fractions. They give the following results:

- *Steam release*: During flooding of the melt, the evaporation of the coolant water, even in case of intensive cooling processes, is sufficiently moderate and does not result in transient pressure built-up above the melt. Energetic processes similar to steam explosions did not occur. This is valid for water injected through the porous concrete into the melt as well as for melts ejected into the overlaying water layer.

- *Stability of porous concrete:* The vertical, water filled porous concrete layer was not attacked by the melt from the side. Also, the horizontal porous concrete layer stopped the melt in most of the cases at the upper interface and showed excellent stability. However, in rare cases the porous bottom layer may be eroded locally, if supply of water to the lower side of the melt is impeded. This may occur for large melts in case that the coolant flow concentrates to a few flow paths through the melt only and bypasses certain areas in the porous concrete layer and in the melt. – On the other side, the nature of decay heat simulation in the experiments by induction heating results in a higher concentration of internal heat sources at the lower boundary, that is near the induction coil, which intensifies the attack of the concrete in the experiments in contrast to the reactor situation, where decay heat is homogeneously distributed throughout the melt.

- *Porosity of the melt*: In all experiments, the porosity of the melt which formed during the process of water injection and evaporation, was less homogeneous than in the original COMET concept with the array of injection nozzles [4], which to a certain extend prescribe a multitude of flow paths through the melt. The concentration of the coolant and steam flow through the melt to a few flow paths only is probably related to the fact that the porous concrete layer does not favour certain flow channels, but that the self organising flow pattern prefers less flow channels with wider flow areas because of their lower pressure loss.

- *Coolability*: In most of the experiments, coolability of the melt is achieved in spite of the inhomogeneities mentioned above. The consequence of the inhomogeneous coolant distribution is a slower cool down of the unfragmented portions of the melt, for which heat transfer by conduction becomes more important. Under unfavourable conditions, however, displacement of still liquid portions of the melt may lead to blockage of previously open coolant channels with a reduction of the coolant inflow. – However, similar to the argument given above, the concentration of decay heat near the induction coil makes cooling more difficult in the experiment, so that coolability may be achieved easier in the reactor situation.

- *Sideward flooding:* If for reactor application the sideward stabilisation of the melt shall be achieved by a vertical porous concrete layer, design of the cooling concept must assure

that flooding starts from the porous layer at the bottom by selection of appropriate thickness of the sacrificial concrete layers at bottom and side, respectively. Otherwise, early formation of a stable, upper surface crust as a consequence of premature lateral flooding may hinder the necessary fragmentation.

- *Consequence of surface flooding:* An additional result of the large-scale experiments is the observation that surface flooding alone does not stop melt propagation and concrete erosion. A consequence of surface flooding is formation of a stable surface crust, which establishes in spite of gas release from concrete. Eruptions of melt through the top crust soon come to an end and produce only minor melt fragmentation. Heat removal from the top of the melt is insufficient for relevant heights of the melt, and downward erosion by the melt continues.

The topics listed above require a conceptual improvement of the bottom-flooding concept, if a porous, water filled concrete layer shall be used. A more homogeneous penetration and fragmentation of the melt by water inflow should be achieved, similar to the original COMET concept [4], to facilitate heat extraction and solidification, and to exclude potential relocation of residual liquid melt fractions. Therefore, an increase of the coolant water pressure and a structural modification of the porous layer are presently considered.

6 Literature

[1] H. Alsmeyer, T. Cron, G. Merkel, S. Schmidt-Stiefel, W. Tromm, T. Wenz, Melt Cooling by Bottom Flooding: The Experiment CometPC-H3, SAM-ECOSTAR-D44, Forschungszentrum Karlsruhe – Wissenschaftliche Berichte, FZKA 6852, March 2003

[2] THERMODATA, 2000, GEMINI 2, Thermochemical equilibria calculation code - Complex multicomponent phases, THERMODATA, St. Martin d'Heres, France

[3] M.T. Farmer, B.W. Spencer, D.J. Kilsdonk, R.W. Aeschlimann, Status of Large Scale MACE Core Coolability Experiments, Proceedings of the OECD Workshop on Ex.Vessel Debris Coolability, Karlsruhe, November 15-18, 1999, Forschungszentrum Karlsruhe – Wissenschaftliche Berichte, FZKA 6475, May 2000

[4] H. Alsmeyer, W. Tromm, The COMET Concept for Cooling Core Melts: Evaluation of the Experimental Studies and Use in the EPR, FZKA 6186, October 1999